HAL open science

Coupling between two mesoscopic systems towards the measurement of noise

Thi Kim Thanh Nguyen

To cite this version:

Thi Kim Thanh Nguyen. Coupling between two mesoscopic systems towards the measurement of noise. Condensed Matter [cond-mat]. Université de la Méditerranée - Aix-Marseille II, 2007. English. NNT : . tel-00175563

HAL Id: tel-00175563

https://theses.hal.science/tel-00175563

Submitted on 28 Sep 2007

HAL is a multi-disciplinary open access archive for the deposit and dissemination of scientific research documents, whether they are published or not. The documents may come from teaching and research institutions in France or abroad, or from public or private research centers.

L'archive ouverte pluridisciplinaire **HAL**, est destinée au dépôt et à la diffusion de documents scientifiques de niveau recherche, publiés ou non, émanant des établissements d'enseignement et de recherche français ou étrangers, des laboratoires publics ou privés.

Université de la Méditerranée-aix-marseille II
centre de physique théorique
institut de physique et d'electronique d'hanoi

Thèse
pour obtenir le grade de
docteur de l'Université de la Méditerranée
présenté par

NGUYEN Thi Kim Thanh
spécialité: Physique Théorique

Titre:

Coupling between two mesoscopic systems towards the measurement of noise

Directeur de Thèse : Thierry MARTIN
Co-directeur de Thèse : NGUYEN Ai Viet

soutenue le 7 Septembre 2007 devant le jury composé de:

M.	Fabio PISTOLESI	Président
M.	Dominique MAILLY	Rapporteur
M.	Benoit DOUCOT	Rapporteur
Mme.	Adeline CRÉPIEUX	
M.	Thierry MARTIN	
M.	Thibaut JONCKHEERE	Invité

Centre de Physique Théorique - Marseille

Abstract: The central topic of this thesis is the physics of noise: the Fourier transform of the current-current correlation function in time. We examine situations where the noise generated by a given mesoscopic circuit affects the behavior of another mesoscopic circuit. In the first part of this study, the noise source is unknown, and the mesoscopic circuit which is capacitively coupled to it acts as a detector of high frequency noise. In our case, the detector consists of a normal metal-superconductor junction where electron transport occurs via quasiparticle tunneling, or more interestingly, via Andreev reflection processes. The theory of dynamical Coulomb blockade is employed in order to compute the dc current which flows into the detector circuit, providing information on high frequency noise. In the second part of this thesis, the noise source is known: it consists of a Hall bar with a quantum point contact, for which anomalous current voltage and noise characteristics are established when the Hall bar is placed in the fractional quantum Hall regime. A quantum dot connected to leads, which is placed next to this point contact, acquires a finite linewidth when the current fluctuates, and acts as a detector of charge noise. We compute the dephasing rate in the weak and strong backscattering regime, describing both case of unscreened and screened Coulomb interaction between the Hall bar and the quantum dot.

INTERACTION ENTRE DEUX CIRCUITS MESOSCOPIQUES POUR LA MESURE DU BRUIT

Résumé: Le point central de cette thèse est la physique du bruit: la transformée de Fourier de la function de correlation temporelle courant-courant. Nous examinons des situations dans lesquelles le bruit généré par un circuit mésoscopique donné affecte le comportement d'un autre circuit mésoscopique. Dans une première partie, la source de bruit est inconnue, et le circuit mésoscopique qui lui est couplé de manière capacitive se comporte comme un détecteur de bruit à haute fréquence. Dans notre cas, le détecteur est constitué d'une jonction métal normal-supraconducteur, òu le transport électronique est du au transfert de quasiparticules, ou, de manière plus intéressante, est du à la réflexion d'Andreev. La théorie du blocage de Coulomb dynamique est utilisée pour calculer le courant continu qui passe dans le circuit de détection, procurant ainsi une information sur le bruit à haute fréquence. Dans la deuxième partie de cette thèse, la source de bruit est connue : elle provient d'une barre de Hall avec un contact ponctuel, dont les caractéristiques de courant-tension et de bruit sont bien établies dans le régime de l'effet Hall quantique fractionnaire. Un point quantique connecté à des bornes source et drain, qui est placé au voisinage du contact ponctuel, acquière une largeur de raie finie lorsque le courant fluctue, et se comporte comme un détecteur de bruit de charge. Nous calculons le taux de déphasage du point quantique dans le régime de faible et de fort rétrodiffusion, tout en décrivant l'effet de l'écrantage faible ou fort de l'interaction Coulombienne entre la barre de Hall et le point quantique.

Speciality: Theoretical nano-physics.

Keywords: quantum noise, noise measurement, dynamical Coulomb blockade theory, Andreev reflection, fractional quantum Hall effect, Luttinger liquid, Keldysh formalism, decoherence, dephasing rate.

Mots clés: bruit quantique, mesure du bruit, théorie du blocage de Coulomb dynamique, réflexion d'Andreev, effet Hall quantique fractionnaire, liquide de Luttinger, formalisme Keldysh, décohérence, taux de déphasage.

Centre de physique Théorique, Université de la Méditerranée, Luminy case 907, 13288 Marseille cedex 09

Acknowledgements

First of all, I would like to thank the members of the jury: Prof. Dominique Mailly and Prof. Benoit Doucot for accepting to be the referees of my thesis, as well as Prof. Fabio Pistolesi and Prof. Adeline Crépieux for accepting to join the jury and Prof. Thibaut Jonkheere for accepting to be the invitee.

The work of this thesis has been realized in collaboration between the Centre de Physique Théorique, Université de la Méditerranée, Marseille and the Institute of Physics and Electronics, Vietnam Academy of Science and Technology under the supervision of Prof. Thierry Martin and Prof. Nguyen Ai Viet. I would first like to thank Prof. Martin. The first time I understood basic knowledge about nano-physics such as noise was in his lectures at the eighth Vietnam School of Physics. During my Ph.D. program, under his guidance, I have learned much not only in Physics but also in the way to study Physics. I benefited a lot from his enthusiasm and his expertise. I am deeply thankful for everything I learned from him. I would also like to thank Prof. Viet, my co-advisor in Vietnam. He has shared with me unselfishly his knowledge in Physics and professional skill during the time I was working in Vietnam.

During my thesis work, the atmosphere of "the Nanophysics team of the CPT" has deeply influenced my research in Physics. I also highly appreciate the collaboration of Adeline and Thibaut. I have learned much from the useful discussions with them. I am grateful to my advisor and my collaborators for helping me solve problems, for patient discussions, for the preparation of the thesis manuscript, and the defense presentation and especially, for their help in my personal life during my time in France.

I would also like to show my great gratitude to Prof. Patrick Aurenche, who always gives advice to me whenever I am in difficult situations as a wise father does.

I need to thank the directors as well as the staffs of both Theoretical Physics Centers in Marseille and Hanoi for good working conditions and friendly atmosphere.

I was supported in part by the Minister of Foreign Affairs, "Rencontres du Vietnam" organisme through on Odon Vallet fellowship, and the Centre de Physique Théorique. I am deeply thankful to Prof. Odon Vallet and Prof. Tran Thanh Van.

I must not forget the other postdocs and Ph.D. students in Centre de Physique Théorique. The three years I spent with them are really a pleasant time to remember. I thank them with my heart.

I owe a lot of gratitude to my family. I dedicate this thesis to my mother in heaven and my family in Vietnam.

Contents

1 Introduction **1**
1.1 Mesoscopic physics . . . 1
1.2 Motivation . . . 2
1.2.1 Part one: Capacitive measurement of noise at high frequencies . . . 2
1.2.2 Part two: Dephasing of a quantum dot level in the presence of a fluctuating current . . . 3
1.3 Thesis outline . . . 4

I Capacitive measurement of noise at high frequencies **6**

2 Noise in mesoscopic physics **7**
2.1 Introduction to noise . . . 7
2.1.1 General current fluctuations . . . 7
2.1.2 Thermal noise . . . 8
2.1.3 Classical and quantum shot noise . . . 9
2.1.4 Quantum noise at high frequencies . . . 10
2.2 The scattering approach of noise in a two-terminal conductor . . . 11
2.2.1 Average current . . . 11
2.2.2 Expression for noise . . . 14
2.3 Finite frequency noise in quantum point contact . . . 15
2.3.1 Quantum point contacts . . . 15
2.3.2 Finite frequency noise . . . 16
2.3.3 Excess noise . . . 16

3 Noise detection **18**
3.1 Dynamical Coulomb blockade . . . 18
3.1.1 Electron tunneling through a tunnel junction . . . 18
3.1.2 Hamiltonian of a tunnel junction embedded in an electromagnetic environment . . . 19
3.1.3 Calculation of tunneling rates in the tunnel junction . . . 20
3.1.4 Phase-phase correlation and distribution functions . . . 21
3.1.5 Tunneling rate . . . 22
3.2 Detection of high-frequency quantum noise in mesoscopic conductors by double quantum dot junction . . . 23
3.2.1 The inelastic current . . . 23
3.2.2 Quantum point contact as a source of noise . . . 24
3.3 Noise detection in experiments . . . 25
3.3.1 Noise reduction measurements . . . 25

3.3.2 Full counting statistics of current fluctuations 26
3.3.3 On-chip detection of quantum noise 27

4 Andreev reflection **30**
4.1 Introduction 30
4.2 Transition from metallic to tunneling regimes in superconducting micro-constrictions 31
4.2.1 The Bogolubov-de Gennes equation 32
4.2.2 Transmission and reflections of particles at the NS interface 33
4.2.3 The conductance of a normal metal-superconductor junction 35

5 Photo-assisted Andreev reflection as a probe of quantum noise **37**
5.1 Introduction 37
5.1.1 Detector consisting of a single NS junction 38
5.1.2 Detector consisting of a NS junction separated by a quantum dot . 39
5.2 Tunneling current through the NS junction 40
5.2.1 Model Hamiltonian 40
5.2.2 Tunneling current 41
5.2.3 Single electron tunneling 42
5.2.4 Two electrons tunneling as two quasiparticles 44
5.2.5 Two electron tunneling as a Cooper pair: Andreev reflection 46
5.2.6 Quantum point contact as a source of noise 47
5.3 Tunneling current through a NDS junction 51
5.3.1 Model Hamiltonian 51
5.3.2 General formula for the photo-assisted Andreev current 52
5.3.3 Application to a quantum point contact 56
5.4 Conclusion 59
5.5 Appendix 60
5.5.1 Appendix A 60
5.5.2 Appendix B 61
5.5.3 Appendix C 62
5.5.4 Appendix D 62
5.5.5 Appendix E 63
5.5.6 Appendix F 64

II Dephasing of a quantum dot level in the presence of a fluctuating current **67**

6 Introduction to the quantum Hall effect **68**
6.1 Hall effect 68
6.1.1 The classical Hall effect 68
6.1.2 Integer quantum Hall effect 68
6.1.3 Fractional quantum Hall effect 69
6.2 Edge states 71
6.2.1 The integer quantum Hall edge states 72
6.2.2 The fractional quantum Hall edge states 73
6.3 Luttinger liquid theory 74
6.3.1 Non-chiral Luttinger liquid theory 74

6.3.2 Chiral Luttinger liquid in the fractional quantum Hall effect 76
6.4 Transport between two quantum Hall edges 78
6.4.1 Keldysh digest for tunneling 78
6.4.2 Backscattering current 80
6.4.3 Backscattering current noise 82
6.4.4 The direct observation of a fractional charge 83

7 Dephasing in a quantum dot 85
7.1 Phase measurement in a quantum dot via a double-slit interference 85
7.2 Dephasing in quantum dot due to coupling with a quantum point contact . 86

8 Quantum dot dephasing by fractional quantum Hall edge states 90
8.1 Introduction 90
8.2 Model setup and Hamiltonian 91
8.3 Dephasing rate 92
8.3.1 Dephasing rate for the case of weak and strong backscattering and strong screening 93
8.3.2 General expression of dephasing rate for arbitrary backscattering . . 96
8.3.3 Dephasing rate in the case of arbitrary screening 99
8.4 Conclusion 100

Conclusion 101

Bibliography 104

Curriculum Vitae 111

List of publications 112

Chapter 1

Introduction

1.1 Mesoscopic physics

Electrons carry the current in most commonly used conductors. Electrons are elementary particles that have a discrete charge and a spin. In quantum physics, depending on their energy, the temperature conditions and the length scales involved, electrons can propagate in conductors as waves which are characterized by the Fermi wavelength. However, the particle and wave properties of individual electrons are hardly important in usual electrical wires supplying electricity, say, to light fixtures in a room. The wire width is about 10 million times the Fermi wave length of an electron. In this case, electrons flow through wires like a liquid does.

The ability to transmit current of a piece of wire as a conductor can be characterized by its conductivity or its conductance. The conductance, which is, as we shall see, a useful concept for this study, is defined as the current passing through the wire divided by the voltage bias applied between the wire ends. In classical or incoherent regime, where the wave picture does not apply, the conductance is directly proportional to the wire width, and inversely proportional to its length. The proportionality coefficient, or conductivity, characterizes the material the wire is made of, but not the shape of the wire. However, what happens with this simple scaling law for the conductance when we make a wire thinner and shorter? It turns out that the scaling law breaks down when the wire size is small enough to allow coherent propagation of an electron across it. A new field of physics studying such conductors, which are small enough to allow for coherent electron propagation, but which still consist of a huge number of atoms, is called mesoscopic physics. Mesoscopic physics has been a rapidly growing field in solid state physics for more than two decades [1, 2, 3, 4, 5, 6, 7, 8].

Let us give a few more precisions about the mesoscopic regime. We consider conductors whose size have to be compared to other characteristic length scales: the Fermi wavelength, which is related to the kinetic energy of the electrons, the elastic mean free path, which is the average distance that an electron travels before its initial momentum is destroyed, and the phase relaxation length – the distance that an electron travels before its initial phase is destroyed. This phase relaxation length is typically related to processes which change the initial electron energy or the phase of the wave function, such as electron-phonon collisions, electron-electron collisions, and spin flip scattering due to magnetic impurities. For a solid these lengths can vary wildly depending on the material and the temperature, they can range from a nanometer to tens of microns. What decides the transport regime is how they compare. The phase coherence length is always assumed to be the largest length

scale in mesoscopic physics. For instance, if the size of the sample is smaller than the elastic mean free path, the transport is called ballistic. If this mean free path is smaller than the sample size, but larger than the Fermi wave length, we have a quantum diffusive regime, and so on...

Note that quantum effects can also occur at the macroscopic scale, as is the case for superconductivity (as in the Josephson effect [9]), in the early signatures of weak localization in thin films [10] or in the quantized Hall effect [11]. Nevertheless the major part of mesoscopic physics deals with the submicrometer range and with low temperatures. One of the most famous phenomena to characterize phase coherence is the Aharanov-Bohm effect [12]. Another high ranking experiment of mesoscopic physics is the quantization of the electrical resistance in a quantum point contact [13] (which we shall use later on). Finally, we also mention, as an important concept of mesoscopic physics, the Coulomb blockade in small electrical islands [14] and quantum dots [15], which behave like artificial atoms (another point of our study).

1.2 Motivation

Conductance studies are widely used to obtain information about electronic transport properties, by measuring the current (average amount of charge transferred in a unit of time) for an applied voltage bias. At the same time, the fluctuations in time of a measured quantity can provide important information that is not presented in the time averaged value. Noise is defined as the Fourier transform of current-current correlation function. In mesoscopic systems, quantum noise detection is a powerful tool to get information not accessible by transport experiments [16]. It can provide information on the statistics of carriers (bosons or fermions), their charges, and correlations may be related to interaction effects. And the measurements of some other physical quantities such as the dephasing rate of quantum dot level also invoke the noise. This is the reason that noise measurements attract attentions of both theoretical and experimental nano-physicists.

The unifying theme of this thesis is the study of two coupled mesoscopic systems, typically in situation where the behavior of one of these influences the other one. In most cases, one will be considered as the noise source, and the other will be considered as the detector.

1.2.1 Part one: Capacitive measurement of noise at high frequencies

The field of quantum noise in mesoscopic physics has been intensively developing for more than a decade. Most experiments focused on measuring the noise at low frequencies (kHz range) where shot noise dominates [17]. The shot noise spectrum is white with a power density directly proportional to the average current and symmetric in terms of frequencies.

However, how to study noise in the high frequency regime? In this case, it is important to consider the quantum system (mesoscopic device circuit) together with the surrounding environment (another mesoscopic system called the detector circuit), and the energy exchange between two circuits. In Ref. [18], the authors consider a time averaged measurement of finite frequency current noise using a resonant circuit, which can be an ordinary LC element, as a model for the detector, i.e., an inductive element coupled to the quantum wire, a capacitor whose charge is the quantity to be measured as a response,

and the resistance of the circuit. In this work, a mixture of the two unsymmetrized noise correlators is measured. This point has been reemphasized in Ref. [19].

In Ref. [20], a detection circuit, which was capacitively coupled to the mesoscopic circuit to be measured, was proposed as a high frequency noise detector (GHz range). This basic idea was implemented experimentally recently [21, 22] using a superconductor-insulator-superconductor (SIS) junction as a detector, measuring in this case the finite frequency noise characteristics of a Josephson junction, or a Super-Poissonian noise of a carbon nanotube/quantum dot [23].

The purpose of the first project is thus to analyze a similar situation, except that the SIS junction is replaced by a normal metal-superconductor circuit, which may also be inserted by a quantum dot, transferring two electrons using Andreev reflection between a normal lead and a superconductor. The measurement of a DC current in the detector can thus provide information on the absorption and the emission components of the current noise correlator.

1.2.2 Part two: Dephasing of a quantum dot level in the presence of a fluctuating current

Mesoscopic systems can be used to study the interplay between interference and dephasing of electrons [24]. Nano-scale fabrication and low temperature measuring techniques, which minimize unintentional dephasing, enable the observation of variety of coherent effects of electrons such as an induced Aharonov-Bohm phase, weak localization, resonant tunneling and conductance quantization [7].

Recently, a set of elegant Aharonov-Bohm ring experiments was performed to detect the phase shift of electrons passing through a quantum dot built in one arm of the ring [25, 26, 27]. The observation of phase coherence in transport through a quantum dot presents an opportunity to study the origins of decoherence in mesoscopic structures. These experiments, however, did not control the rate of dephasing. An Aharonov-Bohm ring with a quantum dot in one of its arms offers the ability not only to measure dephasing rates, but also to directly control these rates by modifying the environment of the quantum system. This proposal has been done by Y. Levinson [28] and I. L. Aleiner and coworkers [29] independently where the environment is a quantum point contact located close or coupled capacitively to the quantum dot.

The aim of this second project is to study the dephasing rate of an electron state in a quantum dot, due to charge fluctuations in a nearby voltage-biased point contact in the fractional quantum Hall regime, which can be described by Luttinger liquid theory. Quantum point contact transmission can then be described by tunneling between edge states [30]. In this strongly correlated electron regime, edge states represent collective excitations of the quantum Hall fluid: depending on the pinching of the quantum point contact, it is either FQHE quasiparticles or electrons which tunnel. It is particularly interesting because the current-voltage and the noise characteristics deviate strongly from the case of normal conductors [31, 32, 33]: for the weak backscattering case, the current at zero temperature may increase when the voltage bias is lowered, while in the strong backscattering case the $I(V)$ is highly non linear. It is thus important to address the issue of dephasing from a Luttinger liquid.

1.3 Thesis outline

The first part presents results on the detection of quantum noise at high frequencies by using the on-chip detector circuit including the normal metal – superconductor junction. This part is organized as follow:

Chapter 2: We introduce the concept of noise in mesoscopic physics, the sources of noise. We also introduce the scattering approach to obtain the expression of noise in a two-terminal conductor, then apply for the quantum point contact, a simple mesoscopic conductor we use to study noise.

Chapter 3: We discuss the single electron tunneling in a ultra-small tunnel junction, which is known as dynamical Coulomb blockade. This theory is a basis for detecting noise in a mesoscopic device by coupling it capacitively to a junction in a nearby detector circuit, which is also discussed in this chapter. Some experiments of noise detection are pointed out in the last section.

Chapter 4: Andreev reflection is briefly introduced, together with the transmission and reflection of particles at the normal metal-superconductor interface, where the Bogolubov-de Gennes theory is applied.

Chapter 5: We propose a way to measure high frequency quantum noise. A detector is proposed, which consists of a normal lead–superconductor circuit, which is capacitively coupled to a mesoscopic circuit where noise is to be measured. We discuss two detector circuits: a single normal metal – superconductor tunnel junction and a normal metal separated from a superconductor by a quantum dot operating in the Coulomb blockade regime. A substantial DC current flows in the detector circuit when an appropriate photon is provided or absorbed by the mesoscopic circuit, which plays the role of an environment for the junction to which it couples. Results for the current can be cast in all cases in the form of a frequency integral of the excess noise of the environment weighted by a kernel which is specific to the transport process (quasiparticle tunneling, Andreev reflection,...) which is considered. We apply these ideas to the measurement of the excess noise of a quantum point contact and we provide numerical estimates of the detector current.

In the second part, we study the dephasing in a quantum dot which is coupled capacitively with a quantum point contact in the fractional quantum Hall effect regime. This part is organized as follow:

Chapter 6: This chapter presents the history of the Hall effect, the quantum Hall effect as well as both integer and fractional quantum Hall edge states. We also introduce the Luttinger liquid and the chiral Luttinger liquid which describes well the fractional quantum Hall edge states. Studying non-equilibrium transport between two quantum Hall edges motivates us to review the Keldysh formation. The backscattering current noise is proportional to the backscattering current as the Schottky formula which allows us to observe directly fractional charge.

Chapter 7: In this chapter, we introduce the phase measurement in a quantum dot via a double-slit interference. Then, we introduce the problem of decoherence of electron propagation through the quantum dot due to the effect of environment. The environment can be a normal quantum point contact, which is coupled to or in the proximity of quantum dot.

Chapter 8: We consider the dephasing rate of an electron level in a quantum dot, placed next to a fluctuating edge current in the fractional quantum Hall effect. Using perturbation theory, we show that this rate has an anomalous dependence on the bias

voltage applied to the neighboring quantum point contact, which originates from the Luttinger liquid physics which describes the Hall fluid. General expressions are obtained using a screened Coulomb interaction. The dephasing rate is strictly proportional to the zero frequency backscattering current noise, which allows to describe exactly the weak to strong backscattering crossover using the Bethe-Ansatz solution.

In the conclusion, we resume our work in this thesis.

Notice that in this thesis, I omit the Planck constant ($\hbar = 1$) in the calculation, but it is restored in the numerical results.

Part I

Capacitive measurement of noise at high frequencies

Chapter 2

Noise in mesoscopic physics

2.1 Introduction to noise

In dc current setups, when a constant voltage is applied to a conductor, a stationary current is typically established. However, with a more sophisticated measurement, we discover that it fluctuates in time around the average value (Figure 2.1). One of the ways to characterize the fluctuations of this stationary current is to compute the current – current correlation function and to calculate its Fourier transform, which is called the noise.

The fundamental reason for fluctuations to occur is the fact that electronic transport is a stochastic process: incoming/outgoing states of electrons are specified by an occupation probability, and the transmission trough the sample is also probabilistic.

2.1.1 General current fluctuations

The current $I(t)$ flowing through a device exhibits fluctuations $\Delta I = I(t) - \langle I \rangle$ in time around the average $\langle I \rangle$. The noise is defined as the mean square fluctuations of ΔI per unit frequency bandwidth, i.e. the spectral density of the fluctuations. Experimentally the fluctuations are measured within a finite frequency bandwidth determined by a band-pass filter restricting frequencies to an interval $[\omega - \Delta\omega/2, \omega + \Delta\omega/2]$. Mathematically, we express the fluctuations in this interval as follows [34]:

$$\Delta I_{band}(t) = \frac{1}{2\pi} \int_{\omega-\Delta\omega/2}^{\omega+\Delta\omega/2} d\omega [\Delta I(\omega) e^{-i\omega t} + \Delta I^{\star}(\omega) e^{i\omega t}] \ , \tag{2.1}$$

where $\Delta I(\omega)$ is the Fourier transform of $\Delta I(t)$. For $\Delta\omega \ll \omega$ the mean squared fluctuations $\langle (\Delta I)^2 \rangle$ are proportional to the width of the frequency interval $\Delta f = \Delta\omega/2\pi$. Therefore, we obtain for the spectral density

$$S_I(\omega) = \left\langle (\Delta I_{band})^2 \right\rangle / \Delta f \ . \tag{2.2}$$

To derive the frequency-dependence of Eq. (2.2), we need to know on which time scale the fluctuations take place. This is described by the correlation function that connects the fluctuations at two different instants t and $t + t'$: $C(t) = \langle \Delta I(t + t') \Delta I(t') \rangle$. From the Weiner - Khintchine theorem we know that the spectral density is exactly twice the Fourier transform of the correlation function [35]

$$S_I(\omega) = 2 \int_{-\infty}^{\infty} dt \langle \Delta I(t + t') \Delta I(t') \rangle e^{i\omega t} \ . \tag{2.3}$$

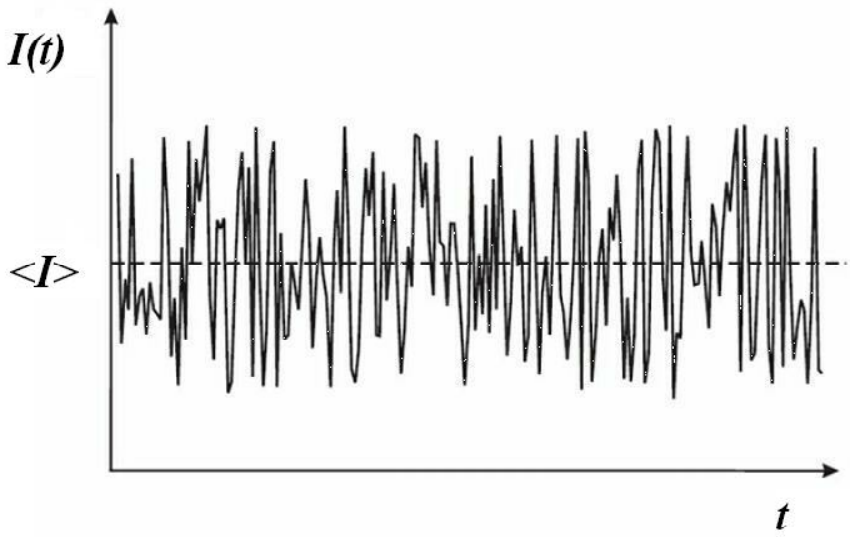

Figure 2.1: The current as a function of time through a mesoscopic device, the fluctuations around the average value and their frequency are characterized by the noise.

Usually physical systems have a certain relaxation time τ, after which all correlations are lost. Therefore, the correlation function tends to zero for $t \gg \tau$. Normally in an electric transport experiment the sampling rate is much slower than any characteristic relaxation time. This does not mean that the fluctuations vanish or cancel out. They are still present as a white background noise.

In the classical limit, the current – current correlation is real and symmetric: $C(-t) = C(t)$, then the noise spectral density is symmetric: $S_I(-\omega) = S_I(\omega)$. So we can define the symmetrized spectrum $S_I^{sym}(\omega) = (S_I(\omega) + S_I(-\omega))/2$ for positive frequencies ω, which is detected in standard, low frequency noise measurements. However, in the quantum limit, the spectrum is no longer symmetric $S_I(-\omega) \neq S_I(\omega)$ and this classical description is not valid anymore.

The fundamental sources of noise (thermal noise, shot noise, and a mixture of both) depend on the relation between three energy scales: the thermal energy $k_B\theta$ [1], the energy associated with the frequency of interest ω, and the energy eV provided by the device voltage. Three limit cases of noise are discussed immediately in this section. On the other hand, there exists 1/f noise, which is caused by slow changes in the device resistance and they are found in most conducting materials. 1/f noise dominates at very low frequencies ($<$ 10 – 100 kHz) and is strongly suppressed as frequency is increased, so that in this thesis, it is not addressed since noise measurements are considered at high frequencies. When frequency in the range from 100 kHz to 1 - 10 MHz, the white noise exists (such as thermal noise, shot noise), and at frequencies above 1 GHz, we find finite frequency noise.

2.1.2 Thermal noise

At non-zero temperature, thermal fluctuations contribute considerably to the noise, even in the absence of the bias current (i.e. in equilibrium). These thermal fluctuations are called thermal noise and also known as Johnson-Nyquist noise because they were first reported experimentally by J. B. Johnson [36] and analyzed theoretically by H. Nyquist

[1] To avoid the confusion of temperature symbol with transmission probability symbol, we use θ to denote temperature.

[37]. In the limit $k_B\theta \gg eV, \omega$, thermal noise dominates over other types of noise. The magnitude of the noise power is proportional to the conductance G of the system, which is an illustration of the fluctuation-dissipation theorem:

$$S_I = 4k_B\theta G \ , \tag{2.4}$$

where $G = 1/R$ with R is resistance. We note that the expression in Eq. (2.4) is valid in both the classical and the quantum regime. In the latter case, we have simply to replace G by the conductance quantum in Landauer's formula $G = 2e^2T/h$, where T is the transmission probability (for single channel case).

Thermal noise is also called white noise – the spectral density is independent of f.

2.1.3 Classical and quantum shot noise

Shot noise in an electrical conductor is a non-equilibrium (bias voltage $V \neq 0$) noise originated from the discreteness of the charges of electrical current. Shot noise is a dominant contribution in the noise when $eV \gg k_B\theta, \omega$. Shot noise was first described by Schottky [38] who studied the charge fluctuation phenomena in a vacuum tube diode.

If we assume that the electrons pass completely independent through a conductor, then the number of quanta N in a time interval T_0 fluctuates and can be described by Poissonian statistics. The average number is given by the mean current $\langle N\rangle = \langle I\rangle T_0/e$ and the mean square derivation is $\langle(\Delta N)^2\rangle = \langle N\rangle$, which is used to calculate the current fluctuations at zero frequency

$$\begin{aligned} \langle(\Delta I)^2\rangle &= \frac{e^2\langle(\Delta N)^2\rangle}{T_0^2} \\ &= \frac{e\langle I\rangle}{T_0} \ . \end{aligned} \tag{2.5}$$

From Eq. (2.3), we can determine the universal shot noise expression in the zero-temperature limit

$$S_I^{Poisson} = 2e\langle I\rangle \ . \tag{2.6}$$

The shot noise power is twice the product of the charge quantum and the mean current flowing through a device. This effect can be observed in vacuum tubes or in tunnel junctions where the charge quanta are transferred independent of each other. This shot noise is called Poissonian noise and Eq. (2.6) is known as Schottky formula. This result is modified in quantum transport due to the fact that electrons are fermionic particles which obey the Pauli principle. In this case, if we consider incident electrons on a potential barrier which are randomly either transmitted with probability T or reflected with probability $R = 1 - T$ (this is the reason that shot noise is also called partition noise), so the frequency independent shot noise spectral density is [39]

$$S_I = 2e\langle I\rangle(1 - T) \ . \tag{2.7}$$

It is useful to define the Fano factor as the ratio between the independent frequency shot noise divided by the Poisson noise

$$F \equiv \frac{S_I}{2e\langle I\rangle} \ , \tag{2.8}$$

which is equal to $1-T$ in the present case. In the limit of very low transmission ($T \ll 1$), we recover the Poissonian noise.

Interestingly, correlation phenomena like the Pauli principle or Coulomb interaction can substantially suppress shot noise in mesoscopic systems. For systems in which current is not carried in units of electron charge, the general formula for the shot noise is $S_I = F2q\langle I\rangle$, where the electron charge e is replaced by an effective charge q. Shot noise measurements performed in the fractional quantum Hall regime allowed the observation of the fractional charge corresponding to the quasi-particles [40, 41, 42], and shot noise is enhanced by a factor 2, in a NS-junction because of the Andreev-reflection [43]. Therefore, a shot noise measurement gives additional information about the electrical transport which is not accessible via conductance measurements. Shot noise measurement also can be used to distinguish between classical and quantum scattering in a chaotic cavity [44], it gives information about the electron scattering processes in a diffusive wire [45] or in a system in Coulomb blockade regime. On the other hand, shot noise measurements can be used to probe particle statistics. Bosons emitted by a thermal source tend to bunch resulting in a super-Poissonian statistics [46], while a fermionic thermal source emits particles separately (anti-bunching) leading to sub-Poissonian statistics [47]. This fact constitutes a very important tool for testing entanglement in the context of quantum computation.

In macroscopic systems, shot noise is not present because current fluctuations are averaged out by electrons transferred through multiple transport channels.

2.1.4 Quantum noise at high frequencies

In the high frequency limit ($\omega \gg k_B\theta, eV$), zero-point fluctuations in the device introduce an asymmetry in the spectrum $S(\omega) \neq S(-\omega)$. In the definition of noise (Eq. (2.3)), $I(t)$ is replaced by the time dependent current operator in the Heisenberg picture $\hat{I}(t) = \exp(i\hat{H}t)\hat{I}\exp(-i\hat{H}t)$ with $\hat{H}$ being the time independent Hamiltonian of the system. The spectral density is now defined as

$$S_I(\omega) = 2\int_{-\infty}^{\infty} dt\langle\Delta\hat{I}(t)\Delta\hat{I}(0)\rangle e^{i\omega t} \ . \tag{2.9}$$

If we know the initial (ground) states $|i\rangle$ and the final (intermediate) states $|f\rangle$, we obtain

$$S_I(\omega) = 4\pi\sum_{i,f}|\langle f|\hat{I}|i\rangle|^2 P(i)\delta(E_f - E_i - \omega) \ , \tag{2.10}$$

with $P(i)$ is the probability distribution for initial states. In order to interpret physically $S_I(\omega)$ we assume the noise source system is coupled to a detector. We find that $S_I(\omega)$ is proportional to the energy transfer rate between the system and the detector. If $E_f > E_i$ ($\omega = E_f - E_i > 0$), energy is transferred from the detector to the system. That means positive frequencies correspond to an absorption energy process from the environment, while negative frequencies correspond to an emission process. The reason of the asymmetry in the spectrum is the presence of zero-point fluctuations. If the system is in equilibrium at zero temperature, no energy is available for emission so that $S_I(-\omega) = 0$, but the system can always absorb energy and therefore $S_I(\omega) \neq 0$. The asymmetry is important also at finite voltage V and temperature θ if the condition $\omega \gg eV, k_B\theta$ still valid.

In equilibrium, at finite temperature θ, the power density obeys the detailed balance relation [48]

$$S_I(\omega) = e^{\omega/k_B\theta}S_I(-\omega) \ . \tag{2.11}$$

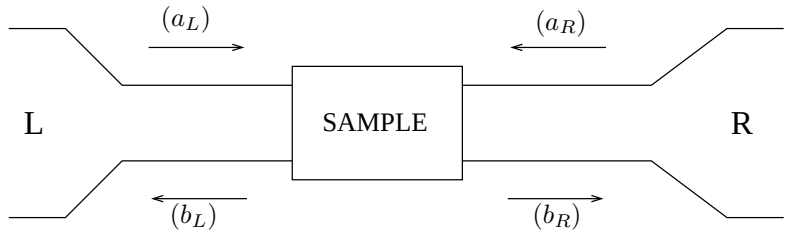

Figure 2.2: The model of a conductor connected to two terminals and several transverse channels. If the left/right lead has $N_{L/R}$ channels then $(a_{L/R})$, $(b_{L/R})$ have $N_{L/R}$ dimensions.

In the limit of low frequency $\omega \ll k_B\theta$, we recover the classical case $S_I(\omega) = S_I(-\omega)$.

In principle, it is possible to measure separately the two sides of the spectrum, but a special detector, which can discern between emission and absorption processes, is needed [18, 19, 20, 21, 49]. To be convenient, hereafter, in this thesis, I use the notation $I(t)$ instead of $\hat{I}(t)$ for current operator. We also introduce other definition of unsymmetrized noise spectral density

$$S^+(\omega) = 2\int_{-\infty}^{\infty} dt e^{i\omega t}\langle \Delta I(0)\Delta I(t)\rangle \ , \tag{2.12}$$

$$S^-(\omega) = 2\int_{-\infty}^{\infty} dt e^{i\omega t}\langle \Delta I(t)\Delta I(0)\rangle \ , \tag{2.13}$$

which relates to the $S_I(\omega)$ by $S^+(-\omega) = S_I(\omega)$, $S^-(\omega) \equiv S_I(\omega)$. With these definitions, it is quite simple to remark that in $S^+(\omega)$ $(S^-(\omega))$, positive (negative) frequencies correspond to an emission rate from the mesoscopic device, while negative (positive) frequencies correspond to an absorption rate.

2.2 The scattering approach of noise in a two-terminal conductor

The idea of the scattering approach (also referred as the Landauer approach) is to relate transport properties of the system (in particular, current fluctuations) to its scattering properties, which are assumed to be known from a quantum mechanical calculation. This approach was generalized to multi-channel, multi-terminal conductors [50].

In this section, we consider a conductor connected to two terminals as left (L) and right (R) where each lead has $N_{L/R}$ channels (see Figure 2.2). The reservoirs are assumed so large that they can be characterized by a temperature $\theta_{L/R}$ and a chemical potential $\mu_{L/R}$.

2.2.1 Average current

This is a standard result which can be found in Refs. [51, 52]. We introduce now operators $a^\dagger_{L/R,\alpha}(E)$ and $a_{L/R,\alpha}(E)$ which create and annihilate electrons with energy E in the channel α in the left lead (L) or right lead (R), which are incident upon the sample. In the same way, the creation $b^\dagger_{L/R,\alpha}(E)$ and annihilation $b_{L/R,\alpha}(E)$ operators describe electrons in the outgoing states. Because we assume that the scattering matrix is independent of the spin states of the electrons, we ignore the spin index in these operators. These operators

obey anticommutation relations such as

$$\begin{aligned}
\{a^\dagger_{L,\alpha}(E), a_{L,\alpha'}(E')\}_+ &= \delta_{\alpha\alpha'}\delta(E-E') \ , \\
\{a_{L,\alpha}(E), a_{L,\alpha'}(E')\}_+ &= 0 \ , \\
\{a^\dagger_{L,\alpha}(E), a^\dagger_{L,\alpha'}(E')\}_+ &= 0 \ .
\end{aligned}$$

The operators a and b are related via the scattering matrix s as

$$\begin{pmatrix} b_{L1} \\ \cdots \\ b_{LN_L} \\ b_{R1} \\ \cdots \\ b_{RN_R} \end{pmatrix} = s \begin{pmatrix} a_{L1} \\ \cdots \\ a_{LN_L} \\ a_{R1} \\ \cdots \\ a_{RN_R} \end{pmatrix} \ . \tag{2.14}$$

The scattering matrix s has dimensions $(N_L + N_R) \times (N_L + N_R)$. It relates all reflection processes at the left reservoir, all transmission processes from the right reservoir to the left one, and vice versa. It has the block structure

$$\begin{pmatrix} r & t' \\ t & r' \end{pmatrix} \tag{2.15}$$

where the square diagonal blocks r (size $N_L \times N_L$) and r' (size $N_R \times N_R$) describe electron reflection processes, while the off-diagonal, rectangular blocks t (size $N_R \times N_L$) and t' (size $N_L \times N_R$) describe the electron transmission through the sample.

The current operator can be considered in the left lead as

$$I(x,t) = \frac{e}{2mi} \sum_\sigma \int dydz \left(\psi^\dagger_L(\mathbf{r},t) \frac{\partial \psi_L(\mathbf{r},t)}{\partial x} - \frac{\partial \psi^\dagger_L(\mathbf{r},t)}{\partial x} \psi_L(\mathbf{r},t) \right) \ , \tag{2.16}$$

where x, y, and z are the coordinates in the left lead, $\psi^\dagger_L$ and ψ_L are the fermion creation and annihilation field operator. The annihilation field operator is expressed in terms of the scattering properties of the sample as

$$\psi_L(\mathbf{r},t) \ = \ \frac{1}{\sqrt{2\pi}} \int dE e^{-iEt} \sum_{\alpha=1}^{N_L(E)} \frac{\chi_{L\alpha}(y,z)}{\sqrt{\upsilon_{L\alpha}(E)}} \left[a_{L\alpha}(E) e^{ik_{L\alpha}x} + b_{L\alpha}(E) e^{-ik_{L\alpha}x} \right] \ . \tag{2.17}$$

In Eq. (2.17), $\chi_{L\alpha}(y,z)$ is the transverse wave function in the left lead channel α, which is normalized as $\int dydz \chi_{L\alpha}(y,z)\chi^*_{L\alpha'}(y,z) = \delta_{\alpha,\alpha'}$, the velocity of carriers $\upsilon_{L\alpha}(E) = k_{L\alpha}/m$, and $k_{L\alpha} = \sqrt{2m(E - E_{L\alpha})}$, with the notice that we separate the energy E of electrons into the transverse energy $E_{L\alpha}$ corresponding to the motion of electrons in the α-th transverse channel (across the lead), and the longitudinal energy corresponding to the motion of electrons along the lead. The summation in Eq. (2.17) only includes channels with real $k_{L\alpha}$. Substituting the fermion operators relation in Eq. (2.14) for the current operator, we have

$$I(t) = \frac{e}{2\pi} \int dE \int dE' \sum_{nn'} \sum_{\alpha\alpha'} e^{i(E-E')t} a^\dagger_{n\alpha}(E) A^{\alpha\alpha'}_{nn'}(L;E,E') a_{n'\alpha'}(E') \ , \tag{2.18}$$

where $A^{\alpha\alpha'}_{nn'}(L;E,E')$ is the current matrix element, which depends on position in general,

$$\begin{aligned}
A^{\alpha\alpha'}_{nn'}(L;E,E') =& \sum_{\beta} \frac{1}{\sqrt{k_{L\beta}(E)k_{L\beta}(E')}} \{[k_{L\beta}(E)+k_{L\beta}(E')] \\
&\times\Big[e^{-i[k_{L\beta}(E)-k_{L\beta}(E')]x}\delta_{\beta\alpha}\delta_{\beta\alpha'}\delta_{nL}\delta_{n'L} - e^{i[k_{L\beta}(E)-k_{L\beta}(E')]x}s^{\dagger}_{Ln;\alpha\beta}(E)s_{Ln';\beta\alpha'}(E')\Big] \\
&+[k_{L\beta}(E)-k_{L\beta}(E')] \\
&\times\Big[e^{-i[k_{L\beta}(E)+k_{L\beta}(E')]x}\delta_{\beta\alpha}\delta_{nL}s_{Ln';\beta\alpha'}(E') - e^{i[k_{L\beta}(E)+k_{L\beta}(E')]x}s^{\dagger}_{Ln;\alpha\beta}(E)\delta_{\beta\alpha'}\delta_{n'L}\Big]\Big\} .
\end{aligned} \tag{2.19}$$

However, here we discuss some assumptions and anticipate a few results.

• As our model does not take into account inelastic processes, we get a delta function of energy when we compute the average current and noise at zero frequency. As a result the average stationary current is constant and the zero frequency noise does not depend on where it is measured.

• In practical situations, the bias eV is assumed to be much smaller than the chemical potential of the leads. Because most relevant momenta happen in the vicinity of the chemical potential within a few eV, this implies that the momenta $k_{L\beta}(E)$ and $k_{L\beta}(E')$ are rather close. In this case, the second big term in formula of $A^{\alpha\alpha'}_{nn'}(L;E,E')$ oscillates rapidly with a wavelength π/k_F. These k_F oscillations can thus be neglected in this condition. This assumption will be applied to calculate both average current and noise.

Hereafter in this thesis, we will work in this assumptions, then we will have

$$A^{\alpha\alpha'}_{nn'}(L;E,E') = \delta_{\alpha\alpha'}\delta_{nL}\delta_{n'L} - \sum_{\beta} s^{\dagger}_{Ln;\alpha\beta}(E)s_{Ln';\beta\alpha'}(E') \ . \tag{2.20}$$

In order to compute the average current, it is necessary to consider the statistical average for a system at thermal equilibrium

$$\langle a^{\dagger}_{n\alpha}(E)a_{n'\alpha'}(E')\rangle = f_n(E)\delta(E-E')\delta_{n,n'}\delta_{\alpha\alpha'} \ , \tag{2.21}$$

with $f_n(E)$ is the Fermi-Dirac/Bose-Einstein distribution function associated with lead n whose chemical potential is μ_n: $f_n(E) = 1/[\exp((E-\mu_n)/k_B\theta_n) \pm 1]$. Taking into account the unitary of the scattering matrix, from Eq. (2.18), we obtain

$$\langle I\rangle = \frac{e}{2\pi}\int dE \mathrm{Tr}[t^{\dagger}(E)t(E)][f_L(E)-f_R(E)] \ , \tag{2.22}$$

with t is the off-diagonal block of the scattering matrix (2.15), $t_{\alpha\alpha'} = s_{RL;\alpha\alpha'}$. The matrix $t^{\dagger}t$ can be diagonalized, and has a real set of eigenvalues (transmission probabilities) T_α. So that the average current can be written as

$$\langle I\rangle = \frac{e}{2\pi}\sum_{\alpha}\int dE T_\alpha(E)[f_L(E)-f_R(E)] \ . \tag{2.23}$$

This equation of average current would has been generalized for many channels and many terminals [52].

2.2.2 Expression for noise

The noise is defined in terms of current operators as

$$S^+(\omega) = \lim_{T\to+\infty} \frac{2}{T} \int_{-T/2}^{T/2} dt \int_{-\infty}^{\infty} dt' e^{i\omega t'} [\langle I(t)I(t+t')\rangle - \langle I\rangle\langle I\rangle] \ . \tag{2.24}$$

The calculation of noise involves products $I(t)I(t+t')$ of two current operators. It therefore involves grand canonical averages of four fermion operators, which can be computed with Wick's theorem

$$\begin{aligned}
&\langle a^\dagger_{n_1\alpha_1}(E_1,t) a_{n_2\alpha_2}(E_2,t) a^\dagger_{n_3\alpha_3}(E_3,t+t') a_{n_4\alpha_4}(E_4,t+t')\rangle \\
&= f_{n_1}(E_1) f_{n_3}(E_3) \delta_{n_1n_2}\delta_{\alpha_1\alpha_2}\delta_{n_3n_4}\delta_{\alpha_3\alpha_4}\delta(E_1-E_2)\delta(E_3-E_4) \\
&+ f_{n_1}(E_1)[1\mp f_{n_2}(E_2)]\delta_{n_1n_4}\delta_{\alpha_1\alpha_4}\delta_{n_2n_3}\delta_{\alpha_2\alpha_3}\delta(E_1-E_4)\delta(E_2-E_3)e^{-i(E_1-E_2)t'} \ .
\end{aligned} \tag{2.25}$$

The first term presents the product of the average currents. In the expression for the noise, only the irreducible current operator contributes, and the integral over time gives a delta function in energy (one of the integrals drops out). The noise (considered in the left lead) is obtained as

$$\begin{aligned}
S^+(\omega) \ = \ & \frac{2e^2}{\pi} \int dE \sum_{\alpha\alpha'} \Big\{ A^{\alpha\alpha'}_{LL}(L;E,E+\omega) A^{\alpha'\alpha}_{LL}(L;E+\omega,E) f_L(E)[1\mp f_L(E+\omega)] \\
& + A^{\alpha\alpha'}_{LR}(L;E,E+\omega) A^{\alpha'\alpha}_{RL}(L;E+\omega,E) f_L(E)[1\mp f_R(E+\omega)] \\
& + A^{\alpha\alpha'}_{RL}(L;E,E+\omega) A^{\alpha'\alpha}_{LR}(L;E+\omega,E) f_R(E)[1\mp f_L(E+\omega)] \\
& + A^{\alpha\alpha'}_{RR}(L;E,E+\omega) A^{\alpha'\alpha}_{RR}(L;E+\omega,E) f_R(E)[1\mp f_R(E+\omega)] \Big\} \ .
\end{aligned} \tag{2.26}$$

where $A^{\alpha\alpha'}_{nn'}(L;E,E')$ is expressed in Eq. (2.20). Assuming that $s_{nn';\alpha\beta}(E)$ is independent of energy, we have

$$\begin{aligned}
S^+(\omega) \ = \ & \frac{2e^2}{\pi} \int dE \Big\{ \sum_\alpha T_\alpha^2 \left(f_L(E)[1\mp f_L(E+\omega)] + f_R(E)[1\mp f_R(E+\omega)] \right) \\
& + \sum_\alpha T_\alpha(1-T_\alpha) \left(f_L(E)[1\mp f_R(E+\omega)] + f_R(E)[1\mp f_L(E+\omega)] \right) \Big\} \ .
\end{aligned} \tag{2.27}$$

The noise at $\omega = 0$ is obtained without assuming $s_{nn';\alpha\beta}(E)$ is independent of energy as

$$\begin{aligned}
S^+(\omega=0) \ = \ & \frac{2e^2}{\pi} \sum_{\alpha=1}^{N_L} \int dE \left\{ T_\alpha(E)[f_L(1\mp f_L) + f_R(1\mp f_R)] \right. \\
& \left. \pm T_\alpha(E)(1-T_\alpha(E))(f_L-f_R)^2 \right\} \ .
\end{aligned} \tag{2.28}$$

This formula is also obtained for fermions by using the wave packet approach [53]. In the absence of bias or at high temperature θ ($|\mu_L - \mu_R| << k_B\theta$), the two first terms dominate. Using the relation $f_i(1-f_i) = -k_B\theta\partial f_i/\partial E$, we recover the Johnson Nyquist formula [36, 37] for thermal equilibrium noise [54]

$$S^+(\omega=0) = 2\frac{2e^2(\sum_\alpha T_\alpha)}{\pi} k_B\theta = 4Gk_B\theta \ , \tag{2.29}$$

where $G = e^2 \sum_\alpha T_\alpha/\pi$ is the Landauer conductance of the mesoscopic circuit. In the opposite limit the bias larger than the temperature, ($|\mu_L - \mu_R| >> k_B\theta$), we get a shot noise (which is also called reduced shot noise or quantum shot noise)

$$S^+(\omega = 0) = 2eF\langle I\rangle \ , \tag{2.30}$$

with F is the Fano factor with transmission is energy independent or in the linear regime

$$F = \frac{\sum_\alpha T_\alpha(1 - T_\alpha)}{\sum_\alpha T_\alpha} \ . \tag{2.31}$$

The same results were discussed by Landauer and Martin [53, 55] appealing to wave packets.

In the practically important case, when the scale of the energy dependence of transmission coefficients $T_\alpha(E)$ is much larger than both the temperature and applied voltage, the quantities in Eq. (2.28) may be replaced by their values taken at the Fermi energy. Then we obtain

$$S^+(\omega = 0) = \frac{2e^2}{\pi}\left[2k_B\theta \sum_\alpha T_\alpha^2 + eV \coth\left(\frac{eV}{2k_B\theta}\right)\sum_\alpha T_\alpha(1 - T_\alpha)\right] \ , \tag{2.32}$$

In the case all the transmission coefficients are small compared to 1, terms proportional to T_α^2 are neglected, then

$$S^+(\omega = 0) = 2e\langle I\rangle \coth\left(\frac{eV}{2k_B\theta}\right) \ . \tag{2.33}$$

This formula describes the shot noise-thermal noise crossover.

2.3 Finite frequency noise in quantum point contact

2.3.1 Quantum point contacts

A point contact is usually defined as a constriction between two metallic reservoirs. The conductance of quantum point contact displays a stepwise increase as a function of the gate voltage [13].

There are different ways of fabricating a point contact. It can be realized for instance in a break-junction by pulling apart a piece of conductor until it breaks. In a more controlled way, point contacts are formed in 2-dimensional electron gases, e.g. in GaAs/AlGaAs hetero-structures. By applying a voltage to suitably-shaped gate electrodes, the electron gas can be locally depleted and a point contact can be defined locally. Another means of creating a point contact is by positioning an STM-tip close to the surface of a conductor.

All the sizes of the constriction are assumed to be shorter than the mean free path due to any type of scattering, and thus transport through the point contact is ballistic. In a quantum point contact, the width of the constriction is comparable to the Fermi wavelength. Quantum point contact is a simple conductor which is used to test our noise measurement setup.

2.3.2 Finite frequency noise

Concerning the finite frequency noise, performing the integral of E in Eq. (2.27) with the notice that $\int_{-\infty}^{\infty} dE f(E)[1-f(E+x)] = x/(1-e^{-\beta x})$, we obtain the nonsymmetrized noise spectrum for electron system as [20]

$$\begin{aligned} S^{+}(\omega) &= -\frac{2e^2}{\pi}\sum_{\alpha}^{N_L} T_\alpha^2 \frac{2\omega}{1-e^{\beta\omega}} \\ &\quad -\frac{2e^2}{\pi}\sum_{\alpha}^{N_L} T_\alpha(1-T_\alpha)\left[\frac{eV+\omega}{1-e^{\beta(eV+\omega)}} + \frac{\omega-eV}{1-e^{\beta(\omega-eV)}}\right] , \end{aligned} \tag{2.34}$$

where N_L is the number of channel, V is the applied voltage. Eq. (2.34) is not symmetric for positive and negative frequencies.

In equilibrium ($V=0$), we recover the fluctuation-dissipation theorem at finite frequencies [56]

$$S^{+}(\omega) = 2G\frac{2(-\omega)}{1-e^{\beta\omega}} , \tag{2.35}$$

In the zero temperature limiting case, we recover the quantum noise, which is discussed in Ref. [20] and shown in Eq. (3.28) in the next chapter of this thesis. If the reservoirs have one channel, the results are illustrated as [57, 58]

$$S^{+}(\omega) = \begin{cases} (2e^2/\pi)T(1-T)(eV-\omega)\Theta(eV-\omega)\,, & \text{if } \omega \geq 0, \\ (2e^2/\pi)[-2T^2\omega - T(1-T)(eV+\omega)\Theta(-eV-\omega) + T(1-T)(eV-\omega)]\,, & \text{if } \omega < 0\,, \end{cases} \tag{2.36}$$

where $\Theta(x)$ is the Heaviside function and T is the transmission probability. In fact, we obtain Eq. (2.36) by using the relation $S^{+}(\omega) = S_I(-\omega)$. The plot of $S^{+}(\omega)$ is shown in the upper panel in Figure 2.3.

2.3.3 Excess noise

Measuring the non-symmetrized noise means being able to distinguish between emission ($\omega > 0$, energy flows to the detector) and absorption ($\omega < 0$, energy flows from the detector) of the device under test. However, experimentally it is difficult to distinguish unambiguously between symmetrized and non-symmetrized noise, partly because what is often measured is the excess noise.

Often, two such measurements are performed on the same system: the first while it is driven out of equilibrium (e.g., by applying a dc voltage) and the second in equilibrium (the voltage source is turn off). The excess noise is defined as the difference in the noise between the first and the second measurement:

$$S_{M,excess}(\omega) = S_{M,noneq}(\omega) - S_{M,eq}(\omega). \tag{2.37}$$

In most cases mesoscopic samples are driven out of equilibrium by an external dc voltage V, so that

$$S_{M,excess}(\omega) = S_M(\omega, V \neq 0) - S_M(\omega, V = 0). \tag{2.38}$$

The excess noise is useful when we are interested in looking into the change in the system which are due to driving out of equilibrium. It is also useful when a particular setup

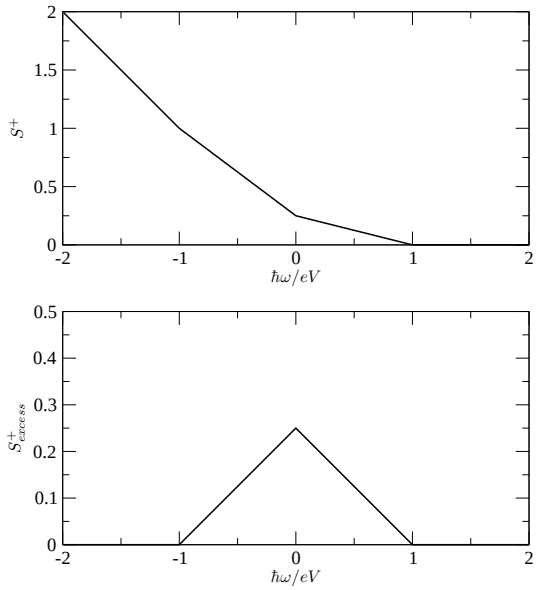

Figure 2.3: The quantum noise spectral density of quantum point contact S^+ as a function of frequency $\hbar\omega/eV$ (in units of $4e^3V/h$) with $T = 0.5$ is ploted in the upper panel. The excess noise $S^+_{excess}(\omega)$ (in units of $4e^3V/h$, $T = 0.5$) is ploted in the lower one.

affects the measurement by introducing an additional noise which is independent of the sample state, so by taking the difference between the two noise powers we can get rid of the instrumentation-dependent noise power.

Now, we apply Eq. (2.38) to calculate the excess noise of quantum point contact at zero temperature corresponding to its spectrum of noise S^+ in Eq. (2.36):

$$S^+_{excess}(\omega) = (2e^2/\pi)T(1-T)(eV - |\omega|)\Theta(eV - |\omega|) \ . \tag{2.39}$$

The spectral density of excess noise bears most of its weight near zero frequencies, but the noise decreases linearly to zero over a range $[0, \pm eV]$ for both positive and negative frequencies, and vanishes beyond the points $\omega = eV$ (see the lower panel in Figure 2.3). The excess noise therefore contains a singularity: its derivative diverges at this point. We find that the spectral density of the excess non-symmetrized noise $S^+_{excess}(\omega)$ is an even function of the frequency ($S^+_{excess}(\omega) = S^+_{excess}(-\omega)$). Consequently, the excess symmetrized noise $S^{sym}_{excess}(\omega) = S^+_{excess}(\omega) + S^+_{excess}(-\omega)$ differs only by a factor two (measured in Ref. [21]) from the excess non-symmetrized noise. Thus excess noise experiments in the quantum regime can usually indifferently be explained by using non-symmetrized or symmetrized noise expression. So, to know precisely what quantity is measured in such experiments where the excess non-symmetrized noise is symmetric, we need a good understanding of the detection process.

Chapter 3

Noise detection

Finite frequency noise is the subject of a debate. What is actually measured in finite frequency noise measurements? As we have discussed in the section of quantum noise, it is important to specify a measurement procedure in order to decide which noise correlator is measured. Recently, theoretical efforts have been made to describe the high frequency noise measurement process based on the dynamical Coulomb blockade theory.

In this chapter, I first discuss the single electron tunneling in a ultra-small tunnel junction, which are known as dynamical Coulomb blockade. This theory is a basis for detecting noise in a mesoscopic device by coupling it capacitively to a junction in a nearby detector circuit, which is also discussed in this chapter. Some experiments of noise detection are pointed out in the last section.

3.1 Dynamical Coulomb blockade

Coulomb blockade is the increased resistance at small bias voltages of an electronic device comprising at least one low-capacitance tunnel junction. Coulomb blockade was first observed and understood within the framework of single electron tunneling in small capacitance metallic tunnel junctions with a large number of weakly transmitting channels.

3.1.1 Electron tunneling through a tunnel junction

A tunnel junction, in its simplest form can be described for example, as a thin insulator barrier between two normal conducting electrodes (see Figure 3.1). According to the law of classical electrodynamics, no current can flow through an insulating barrier. According to the law of quantum mechanics, however, there is a non-vanishing probability for an electron on one side of the barrier to reach the other side. When a bias voltage is applied, this means that there will be a current flow.

Due to the discreteness of electrical charge, current flows through a tunnel junction is a series of events in which exactly one electron passes (tunnels) through the barrier. At zero temperature a tunneling process leading from Q to $Q - e$ is only possible if the difference of charging energies before and after the tunneling process is positive

$$\Delta E = \frac{Q^2}{2C} - \frac{(Q-e)^2}{2C} > 0 \ . \tag{3.1}$$

This condition is satisfied if $Q > e/2$ (or the voltage across the junction $U > U_c = e/2C$). If we assume that starting at a charge $|Q| < e/2$, the junction is charged by the ideal

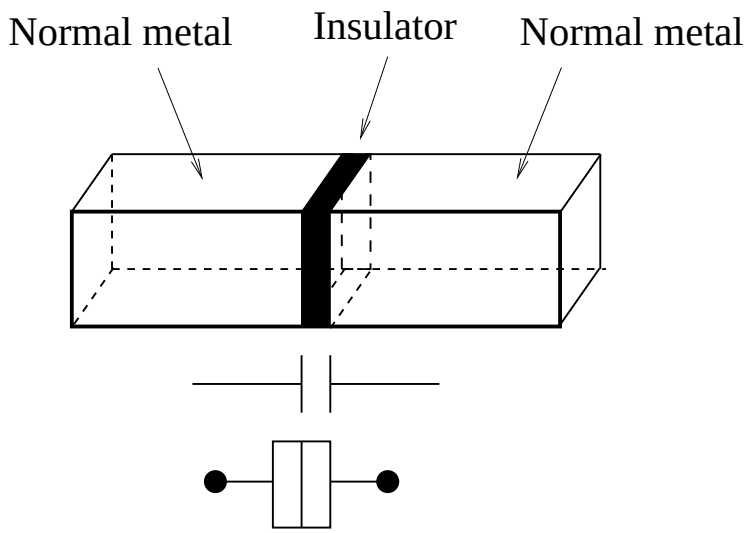

Figure 3.1: Schematic drawing of a metal tunnel junction and the symbol for an ultra-small normal metal tunnel junction.

external current I. When $|Q| > e/2$ an electron may tunnel thereby decreasing the charge on the junction below the threshold $e/2$. This process occurs with a frequency $f = I/e$ and is called single electron tunneling oscillation [59, 60]. We may also use an ideal voltage source and feed a current to the junction through a large resistor. Its resistance is assumed to be smaller than the tunneling resistance of the junction but large enough to inhibit a fast recharging of the capacitor after a tunneling event. There will be no current if the external voltage is smaller than $e/2C$. So we find that at zero temperature, the average current in the current-voltage characteristic is shifted in voltage by $e/2C$. This shift in the current-voltage characteristic is called the Coulomb gap and the phenomenon of suppression of the current below U_c is referred to as Coulomb blockade.

The Coulomb blockade is also observable when the temperature is low enough so that the charging energy (the energy $E_c = e^2/2C$, that is required to charge the junction with one elementary charge) is larger than the thermal energy of the charge carrier $k_B\theta$. For capacitances below 10^{-15}F, the temperature must be below about 1K.

In fact, the single junction cannot be decoupled from the rest of the world or replacing its surroundings by ideal current or voltage sources. We have to consider the junction embedded in the electrical circuit [61, 62, 63]. Dynamical Coulomb blockade is a quantum effect which appears when a quantum coherent conductor is connected in series with an electromagnetic impedance [64].

3.1.2 Hamiltonian of a tunnel junction embedded in an electromagnetic environment

We follow Ingold and Nazarov [64] deriving the expression of tunneling rate through a junction. The quasi-particles in the two metal electrodes are described by the Hamiltonian

$$H_{qp} = \sum_{k\sigma} \epsilon_k c^\dagger_{k\sigma} c_{k\sigma} + \sum_{q\sigma} \epsilon_q c^\dagger_{q\sigma} c_{q\sigma} \ , \tag{3.2}$$

where ϵ_k and ϵ_q are the energies of quasi-particles with wave vector k and q while σ denotes their spin. The first and the second sum correspond to the left and right electrode, respectively.

Tunneling is introduced by the Hamiltonian [62, 65, 66]

$$H_T = \sum_{kq\sigma} T_{kq} c^\dagger_{q\sigma} c_{k\sigma} e^{-i\phi} + h.c. \ , \tag{3.3}$$

with ϕ is the phase $\phi(t) = e\int_{-\infty}^{t} dt' U(t')$ where $U = Q/C$ is the voltage across the junction. With the purpose of studying the effect of environment to the changing of charge on the junction electrodes by the operator $e^{-i\phi}$, we consider only the fluctuations around the mean value determined by the external voltage V. That induces us to consider $\tilde{\phi}(t) = \phi(t) - eVt$ and $\tilde{Q} = Q - CV$. Introducing $\tilde{\phi}$ into H_T, we perform a time-dependent unitary transformation $\tilde{H} = U^\dagger H U - iU^\dagger \partial U/\partial t$ with

$$U = \prod_{k\sigma} \exp\left[ieVtc^\dagger_{k\sigma} c_{k\sigma}\right] \ . \tag{3.4}$$

The new tunneling Hamiltonian then reads

$$\tilde{H}_T = \sum_{kq\sigma} T_{kq} c^\dagger_{q\sigma} c_{k\sigma} e^{-i\tilde{\phi}} + h.c. \tag{3.5}$$

and the new Hamiltonian of the electrodes is

$$\tilde{H}_{qp} = \sum_{k\sigma} (\epsilon_k + eV) c^\dagger_{k\sigma} c_{k\sigma} + \sum_{q\sigma} \epsilon_q c^\dagger_{q\sigma} c_{q\sigma} \ , \tag{3.6}$$

with eV shifted energy levels between the leads.

In the following, we will use the tunneling Hamiltonian in the form (3.5), and now the total Hamiltonian of the system is

$$H = \tilde{H}_{qp} + H_{env} + \tilde{H}_T \ , \tag{3.7}$$

where H_{env} describing the environment. In our case, the environment is represented by the device where we would like to measure noise and the junction is used as a detector.

3.1.3 Calculation of tunneling rates in the tunnel junction

Before calculating the tunneling rates through the junction by using perturbation theory, we make two important assumptions. First, the tunneling resistance R_T is large compared to the resistance quantum $R_K = 2\pi/e^2$. This implies that the states on the two electrodes only mix very weakly so that the Hamiltonian (3.6) is a good description of the quasi-particles in the electrodes. We then may consider the tunneling Hamiltonian $\tilde{H}_T$ as a perturbation. The second assumption is charge equilibrium being established before a tunneling event occurs so that the states to be used in the perturbation theoretical calculation are equilibrium states.

The tunneling rate is given by the Fermi golden rule

$$\Gamma_{i\to f} = 2\pi |\langle f|\tilde{H}_T|i\rangle|^2 \delta(E_i - E_f) \ . \tag{3.8}$$

This is the rate of transitions between the initial state $|i\rangle$ and the final state $|f\rangle$. Specifically, we set $|i\rangle = |E\rangle|R\rangle$ and $|f\rangle = |E'\rangle|R'\rangle$ where $|E\rangle$, $|E'\rangle$ are quasi-particle states of

respective energy E, E', and $|R\rangle$, $|R'\rangle$ are reservoir states (charge states) with energies E_R, E'_R. The matrix element in (3.8) then becomes

$$\langle f|\tilde{H}_T|i\rangle = \langle E'|H_T^e|E\rangle\langle R'|e^{-i\tilde{\phi}}|R\rangle + \langle E'|H_T^{e\,\dagger}|E\rangle\langle R'|e^{i\tilde{\phi}}|R\rangle \ , \tag{3.9}$$

with $H_T^e = \sum_{kq\sigma} T_{kq} c_{q\sigma}^\dagger c_{k\sigma}$ acts in the quasiparticle space. The term $\langle E'|T_{kq} c_{q\sigma}^\dagger c_{k\sigma}|E\rangle$ gives the non-zero contribution only when the initial and final states are of the form $|E\rangle = |..., 1_{k\sigma}, ..., 0_{q\sigma}, ...\rangle$ and $|E'\rangle = |..., 0_{k\sigma}, ..., 1_{q\sigma}, ...\rangle$ respectively. This means that in the initial state an electron is occupying the state (k, σ) in the left electrode, whereas the state (q, σ) is unoccupied in the right electrode, leading to $P_\beta(E)$ as a combination of $f(\epsilon_k)[1 - f(\epsilon_q)]$.

If the applied voltage eV is much smaller than the Fermi energy, we may assume that all quasi-particle states involved have energies close to the Fermi energy. Taking the tunneling matrix element to be approximately independent of ϵ_k, ϵ_q, we may replace $\sum_{k,q,\sigma} |T_{kq}|^2$ by an averaged matrix element $|T|^2$, which accounts for the density of states at the Fermi energy. All constant terms are collected in the tunneling resistance R_T. The total rate for electron tunneling from left to right is

$$\begin{aligned}\Gamma_\rightarrow(V) &= \frac{1}{e^2 R_T}\int_{-\infty}^{\infty} dE dE' f(E)[1 - f(E')] \\ &\quad \times \sum_{R,R'} |\langle R'|e^{-i\tilde{\phi}}|R\rangle|^2 P_\beta(R)\delta(\epsilon_k + eV + E_R - \epsilon_q - E'_R) \ . \end{aligned} \tag{3.10}$$

Now we trace out the environment states. The probability of finding the initial reservoir state $|R\rangle$ is $P_\beta(R) = \langle R|\rho_\beta|R\rangle$ with the equilibrium density matrix $\rho_\beta = Z_\beta^{-1}\exp(-\beta H_{env})$. Here $Z_\beta = \mathrm{Tr}\{\exp(-\beta H_{env})\}$ is the partition function of the environment.

Rewriting the delta function in (3.10) in term of its Fourier transform and using the Heisenberg presentation, we obtain

$$\begin{aligned}\Gamma_\rightarrow(V) &= \frac{1}{e^2 R_T}\int_{-\infty}^{\infty} dE dE' \int_{-\infty}^{\infty}\frac{dt}{2\pi}\exp\left(i(E - E' + eV)t\right) f(E)[1 - f(E')] \\ &\quad \times \sum_{R,R'} P_\beta(R)\langle R|e^{i\tilde{\phi}(t)}|R'\rangle\langle R'|e^{-i\tilde{\phi}(0)}|R\rangle \ . \end{aligned} \tag{3.11}$$

3.1.4 Phase-phase correlation and distribution functions

We define the equilibrium correlation function

$$\begin{aligned}\langle e^{i\tilde{\phi}(t)} e^{-i\tilde{\phi}(0)}\rangle &= \sum_R P_\beta(R)\langle R|e^{i\tilde{\phi}(t)} e^{-i\tilde{\phi}(0)}|R\rangle \\ &= \frac{1}{Z_\beta}\sum_R \langle R|e^{i\tilde{\phi}(t)} e^{-i\tilde{\phi}(0)} e^{-\beta H_{env}}|R\rangle \ , \end{aligned} \tag{3.12}$$

so that we get

$$\begin{aligned}\Gamma_\rightarrow(V) &= \frac{1}{e^2 R_T}\int_{-\infty}^{\infty} dE dE' f(E)[1 - f(E')] \\ &\quad \times \int_{-\infty}^{\infty}\frac{dt}{2\pi}\exp\left(i(E - E' + eV)t\right)\langle e^{i\tilde{\phi}(t)} e^{-i\tilde{\phi}(0)}\rangle \ . \end{aligned} \tag{3.13}$$

If the noise is Gaussian, the correlation function defined in (3.12) can be simplified by applying the generalized Wick theorem as (also see Appendix A [Eqs. (5.54) and (5.57)])

$$\langle e^{i\tilde{\phi}(t)} e^{-i\tilde{\phi}(0)} \rangle = \exp(\langle [\tilde{\phi}(t) - \tilde{\phi}(0)] \tilde{\phi}(0) \rangle) \ . \tag{3.14}$$

For latter convenience we introduce the abbreviation called phase–phase correlation function:

$$J(t) = \langle [\tilde{\phi}(t) - \tilde{\phi}(0)] \tilde{\phi}(0) \rangle \ , \tag{3.15}$$

and the Fourier transform of the correlation function (3.14):

$$P(E) = \frac{1}{2\pi} \int_{-\infty}^{\infty} dt \exp\left[J(t) + iEt\right] \ , \tag{3.16}$$

which is called the distribution function.

The integral over energy of $P(E)$ is normalized to 1, which confirms $P(E)$ as a probability density

$$\int_{-\infty}^{\infty} P(E) dE = e^{J(0)} = 1 \ . \tag{3.17}$$

Another property of $P(E)$ is the so-called detailed balance symmetry

$$P(-E) = e^{-\beta E} P(E) \ , \tag{3.18}$$

which means that the probability to excite the environment is larger than the probability to absorb energy from the environment by a Boltzmann factor. Consequently, no energy can be absorbed from the environment at zero temperature, and $P(E)$ then vanishes for negative energies.

3.1.5 Tunneling rate

Using the definition of $P(E)$, we can rewrite the forward tunneling rate in (3.13) as

$$\Gamma_{\rightarrow}(V) = \frac{1}{e^2 R_T} \int_{-\infty}^{\infty} dE dE' f(E)[1 - f(E' + eV)] P(E - E') \ . \tag{3.19}$$

The expression (3.19) takes into account the possibility of energy exchange between the tunneling electron and the environment. We may interpret $P(E)$ as the possibility to emit the energy E to the external circuit. Correspondingly, $P(E)$ for negative energies describes the absorption of energy by the tunneling electron. Integrating over variable E', we obtain the final formula for forward tunneling rate being

$$\Gamma_{\rightarrow}(V) = \frac{1}{e^2 R_T} \int_{-\infty}^{\infty} dE \frac{E}{1 - \exp(-\beta E)} P(eV - E) \ . \tag{3.20}$$

Similarly, we calculate the backward tunneling rate. However, it is rather obvious from the symmetry of a voltage biased single junction as

$$\Gamma_{\leftarrow}(V) = \Gamma_{\rightarrow}(-V) \ . \tag{3.21}$$

In conclusion, the consideration of current–voltage characteristic of a single tunnel junction reduces to the determination of $P(E)$ or the phase correlation function $J(t)$. In the next section, we will present an example for special impedance which relates the fluctuations of the voltage across the junction and the current fluctuations in a nearby mesoscopic device [20].

3.2 Detection of high-frequency quantum noise in mesoscopic conductors by double quantum dot junction

In Ref. [20], the authors propose a measurement setup for detecting quantum noise over a wide frequency range using a tunable two-level system as a detector. The detector consists of a double quantum dot (DQD) which is capacitively coupled to the leads of a nearby mesoscopic conductor. The scheme of the system is shown in Figure 3.2.

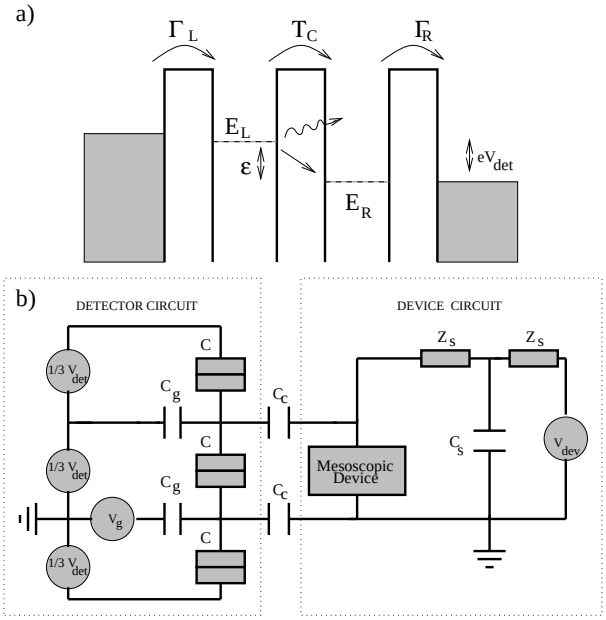

Figure 3.2: a) Energy diagram of a DQD in the regime of high bias voltage. b) Circuit for capacitively coupling the DQD to a second mesoscopic device [20].

3.2.1 The inelastic current

A double quantum dot is a fully controllable two level system with the separation between levels $\epsilon = E_L - E_R$ controlled by gate voltage, a dc inelastic current can circulate in the detection circuit only if the frequency $\omega = \epsilon$ is provided by the mesoscopic device. The tunnel rate between the dots is assumed much smaller than the tunnel rates across the left and right barriers so that the inelastic current is given by

$$I_{inel}(\epsilon) = eT_c^2 P(\epsilon) \ , \tag{3.22}$$

where T_c is the tunnel coupling between the dots. The formula (3.15) can be rewritten as $J(t) = \langle[\delta\tilde{\phi}(t) - \delta\tilde{\phi}(0)]\delta\tilde{\phi}(0)\rangle$, where now the fluctuating phase $\delta\tilde{\phi}(t)$ relates to the fluctuating voltage across the DQD junction $\delta V_{DQD}(t) = V(t) - \langle V(t)\rangle$ by the relation $\delta\tilde{\phi}(t) = e\int_{-\infty}^{t} dt'\delta V_{DQD}(t')$. We calculate the first part in the phase correlator and take into account the definition for the non-symmetrized power spectral density of the voltage fluctuations across the junction

$$S_V(\omega) = 2\int_{-\infty}^{\infty} dt e^{i\omega t}\langle\delta V_{DQD}(t)\delta V_{DQD}(0)\rangle \ , \tag{3.23}$$

then we obtain

$$\langle \delta\tilde{\phi}(t)\delta\tilde{\phi}(0)\rangle = \frac{e^2}{2}\int_{-\infty}^{t} dt' \int_{-\infty}^{0} dt'' \int_{-\infty}^{\infty} d\omega e^{-i\omega(t'-t'')} S_V(\omega) \ . \tag{3.24}$$

Performing the integrals over the time t' and t'', and noting that the fluctuations of the voltage across the DQD junction relate to the current fluctuations through the mesoscopic device as $S_V(\omega) = |Z(\omega)|^2 S_I(\omega)$, with $Z(\omega)$ is the transimpedance connecting detector and device circuits and $S_I(\omega) = 2\int_{-\infty}^{\infty} dt e^{i\omega t}\langle \Delta I(t)\Delta I(0)\rangle$ appears in a non-symmetrized form, we have

$$J(t) = \frac{\pi}{R_K}\int_{-\infty}^{\infty} d\omega \frac{|Z(\omega)|^2}{\omega^2} S_I(\omega)(e^{-i\omega t} - 1) \ , \tag{3.25}$$

with $R_K = 2\pi/e^2$ is the quantum of resistance.

In the limit of small fluctuations of voltage across the junction, $J(t)$ is not diverging for long times, we expand $e^{J(t)} \simeq 1 + J(t)$ in Eq. (3.16) and derive

$$P(\epsilon) \simeq \left\{1 - \frac{\pi}{R_K}\int_{-\infty}^{\infty} d\omega \frac{|Z(\omega)|^2}{\omega^2} S_I(\omega)\right\}\delta(\epsilon) + \frac{\pi}{R_K}\frac{|Z(\epsilon)|^2}{\epsilon^2} S_I(\epsilon) \ . \tag{3.26}$$

The first part renormalizes the elastic current when $\epsilon = 0$. In fact, by controlling the gate voltage in the detector circuit to control $\epsilon \neq 0$, we do not consider further this term. If the impedance Z_S is small enough ($Z_S = 0.1R_K$), the coupling of the noise into the detector is sufficiently effective but the transimpedance is approximatively independent of frequency: $|Z(\omega)|^2 \simeq |Z(0)|^2 \equiv \kappa^2 R_K^2$. The last formula we obtain for the inelastic current through the DQD is

$$I_{inel}(\epsilon) \simeq 2\pi^2\kappa^2 \frac{T_c^2}{e}\frac{S_I(\epsilon)}{\epsilon^2} \ . \tag{3.27}$$

We find that the current fluctuations at frequency ω result in the inelastic current at level difference $\epsilon = \omega$. That means we can study the properties of current noise in the mesoscopic device by investigating the inelastic current of detector.

This interesting theoretical idea has so far eluded experimental verification, possibly because in the double dot system, additional (unwanted) sources of inelastic scattering render a precise noise measurement quite difficult. It is therefore necessary to look for detection circuits which are less vulnerable to dissipation, as is the case of superconducting circuits, because of the presence of the superconducting gap.

3.2.2 Quantum point contact as a source of noise

As an application, we study the current noise spectrum of a quantum point contact. In Ref. [20], noise of quantum point contact (see Eq. (2.34) in chapter 2) is considered as a function of renormalized frequency $\nu = \omega/|eV_{dev}|$ (for simplicity, we take $eV_{dev} > 0$), with $N = 2$ and different values of the total transmission $T = \sum_\alpha^N T_\alpha$

$$S_I(\omega) = \frac{2e^3 V_{dev}}{\pi}\begin{cases} 2T\nu & \text{if } \nu > 1 \ , \\ \sum_\alpha T_\alpha(1-T_\alpha)(1+\nu) + \sum_\alpha T_\alpha^2 2\nu & \text{if } 0 < \nu < 1 \ , \\ \sum_\alpha T_\alpha(1-T_\alpha)(1+\nu) & \text{if } -1 < \nu < 0 \ , \\ 0 & \text{if } \nu < -1 \ , \end{cases} \tag{3.28}$$

$I_{inel}(\nu)$ with values of the total transmission are plotted in Figure 3.3. The asymmetry of noise determines the main feature of $I_{inel}(\nu)$. In the absorption side, for open channels

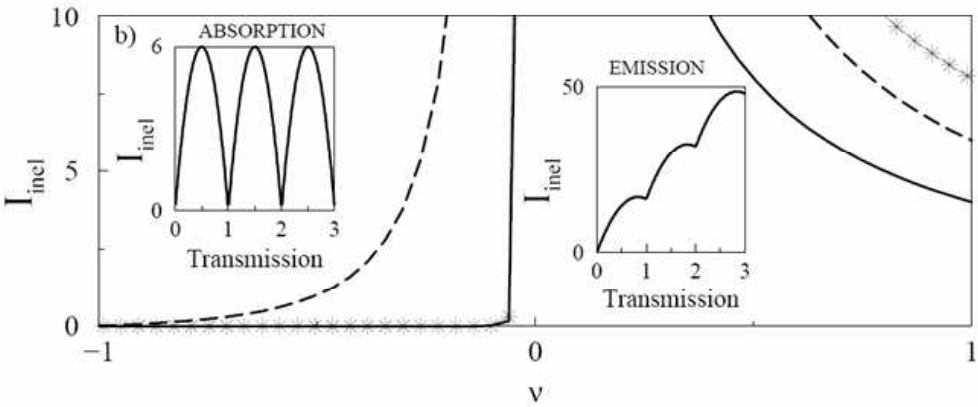

Figure 3.3: $I_{inel}(\nu)$ (in units of $16\pi^2\kappa^2T_c^2/hV_{dev}$) for some values of the total transmission $T = 1, 1.5, 2$ corresponding to the continuous line, the dashed line and the line with stars. Insets: transmission dependence of I_{inel} for a fixed value of the frequency; $\nu = -0.25$ for absorption and $\nu = 0.25$ for emission [20].

(which have T_α close to 1, in this case $T = 1$ and $T = 2$), the non-equilibrium part of the noise is zero and no energy can be absorbed by detector, while for non-open channels the non-equilibrium noise is finite and the detector can absorb energy even at zero temperature. Emission is possible for both open and non-open channels due to zero-point fluctuations so the inelastic current for $\nu > 0$ is always finite.

The inelastic current depending on the transmission is shown in the insets to Figure3.3 with a fixed value of the frequency. In the absorption case, $I_{inel}(\nu)$ oscillates as a function of T (left inset) whereas it is an increasing function with plateau-like features in the emission case (right inset).

In conclusion, the inelastic current through a DQD at low temperature can be a probe of noise in a nearby mesoscopic conductor. The asymmetry between absorption and emission processes gives a clear measurement of the non-equilibrium quantum noise.

3.3 Noise detection in experiments

We know that noise is not only an unwanted signal. It contains a wealth of information not presented in averaged observable quantities. The most important question is how we actually detect the noise? In principle, we can measure time-resolved, that is continuously obtain values of the fluctuating quantity and later do statistics on the data, calculating for instance the noise power. It also is the basic definition of the noise. However, noise measurements in experiment are done alternatively following the sources of noise.

3.3.1 Noise reduction measurements

The shot noise is usually tested following the Schottky formula (Eq. (2.6)) at zero temperature or following the crossover as in Eq. (2.33) at non-zero temperature. The first experimental shot noise measurements in semiconductor quantum point contacts were done by Reznikov *et al.* [67] and Kumar *et al.* [68]. For a single channel sample, the noise has a peak for transmission 1/2, and subsequent oscillations are observed as the number

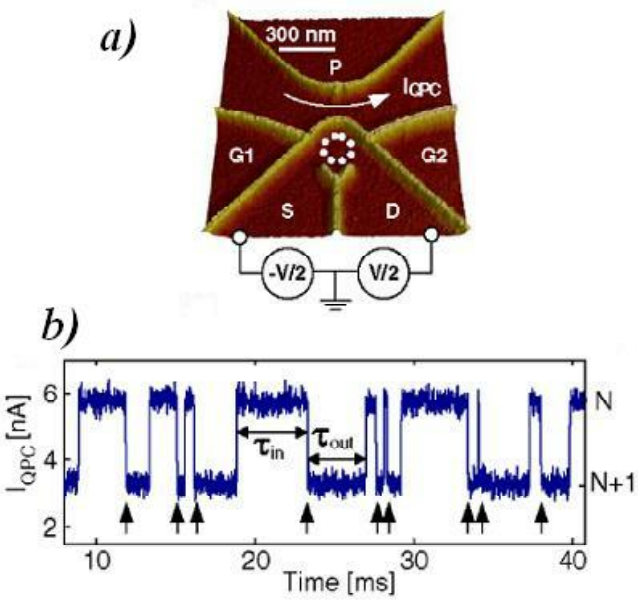

Figure 3.4: a) Atomic force micrograph of the sample consisting of a quantum dot connected to two contacts S and D and a nearby quantum point contact. G1, G2, and P are related gates allowing the tuning of the tunnel coupling to S, the coupling to D, and the conductance of the quantum point contact. G1 and G2 are also used to tune the number of electrons in the quantum dot. A symmetric bias voltage V is applied between S and D. b) Time trace of the current measured through the quantum point contact (for more details, see Ref. [74]).

of channels increases [67]. The noise reduction factor is found to be in excellent agreement with theoretical expectations, evolving from nearly unity at low electronic wave transmission to nearly zero on a conductance plateau [68]. The $1-T$ reduction of shot noise is most explicit in point contact experiment and break junctions experiment because we can tune the system in order to have the controlled opening of the first few conduction channels. However, it can be also observed in various mesoscopic systems, other than ballistic such as double barrier structures, diffusive conductors, or chaotic cavities.

The shot noise measurements were also focused on the quantum Hall regime [40, 41, 42] where the carriers can be not electrons but quasiparticles (in the weak backscattering limit). The fractional charges $e/3$, $e/5$ were observed at incompressible Landau level filling (see also at intermediate filling [69]). These works will be discussed latter on in this thesis. The hot-electron shot noise in a metallic resistor was observed by Steinbach *et al.* [70] and the shot noise in a diffusive mesoscopic conductor is measured in the high frequency regime by Schoelkopf *et al.* [71], who also studied noise in photo-assisted phase-coherent mesoscopic transport [72].

3.3.2 Full counting statistics of current fluctuations

An alternative way to investigate current fluctuations, introduced by Levitov *et al.* [73], is known as full counting statistics. This method relies on the evaluation of the probability distribution function of the number of electrons transferred through a conductor within a given time period (intuitively, it is counting electrons passing one by one). In Ref.[74], based on the real-time detection of single electron tunneling through a quantum dot using a quantum point contact as a charge detector, the authors can directly measure the distribution function of current fluctuations in the quantum dot. The sample of the system,

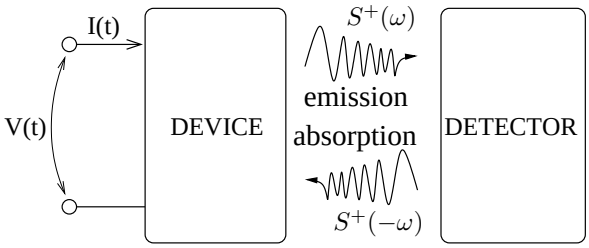

Figure 3.5: Quantum device and a detector as its environment. The current $I(t)$ fluctuating in time gives rise to different types of noise. Energy exchange between the device and the detector (emission or absorption).

fabricated on a GaAs-GaAlAs heterostructure containing a two-dimensional electron gas 34nm below the surface, is shown in Figure 3.4 a). From the time trace of the current measured through the quantum point contact corresponding to fluctuations of the charge of the dot between N and $N+1$ electrons, we can count the number of electrons entering the quantum dot from the source contact during a given time, then obtain the statistical distribution (see Figure 3.4 b)). With this method, we can measure current, shot noise (the second moment), and the higher moments.

3.3.3 On-chip detection of quantum noise

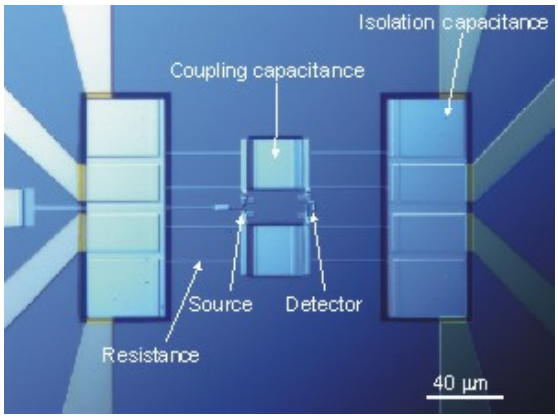

Figure 3.6: Optical image of a sample used to detect high-frequency current fluctuations of mesoscopic devices. The source is capacitively coupled on-chip to the detector via coupling capacitances. Source and detector are isolated from the external environment at high-frequency by resistance and isolation capacitance [22].

However, this might be difficult to achieve if the typical time of fluctuations is very small requiring an extremely fast detector. That is one of the reasons why experiments on noise in quantum transport have remained a tricky subject. Noise measurements at high frequencies benefit of an better sensitivity and allow the study of correlation induced in transport or to access the internal energy scale of the system. In this case, it

is important to consider the quantum system (the device) together with the surrounding environment (the detector) and the energy exchange between them as sketched in Figure 3.5. Any kind of processes involving emission of energy from the device to the environment are depicted by the upper arrow and contribute to $S^+(\omega)$, while processes associated with absorption of energy from the environment are indicated by the lower arrow and contribute to $S^+(-\omega)$ (see Eqs. (2.12) and (2.13) for definitions). In experiments on mesoscopic systems, high-frequency noise is usually measured by coupling capacitively with a detection circuit, which is developed from the basic idea of Ref.[20]. The detection principle is based on the noise-induced photo-assisted tunneling of quasiparticles between the two superconducting electrodes of a superconductor-insulator-superconductor (SIS) junction. This allows frequency resolved measurements between few GHz and a few 100 GHz, depending on the superconducting gap. This kinds of experiment are performed in the Quantum Transport group in Delft University and the Mesoscopic Physics group in the Laboratory of Solid Physique at Paris-South University, Orsay. The sample used to detect high-frequency current noise of mesoscopic devices are shown in Figure 3.6.

A good sensitivity is achieved by having both the device and the detector inserted in an on-chip circuitry. In the Ref. [21], the mesoscopic device is another SIS junction due to the AC Josephson effect where the non-symmetrized noise with frequency from 5 to 90 GHz is measured (up to 100 GHz, depending on the superconducting material). At higher bias shot noise was measured due to the quasiparticle current. The emission part of the noise is first measured using a sub-gap biased detector. The same scheme is used to detect the current fluctuations arising from coherent charge oscillations in a two-level system, a superconducting charge qubit. A narrow band peak is observed in the spectral noise density at the frequency of the coherent charge oscillations. Indeed, as the detector is

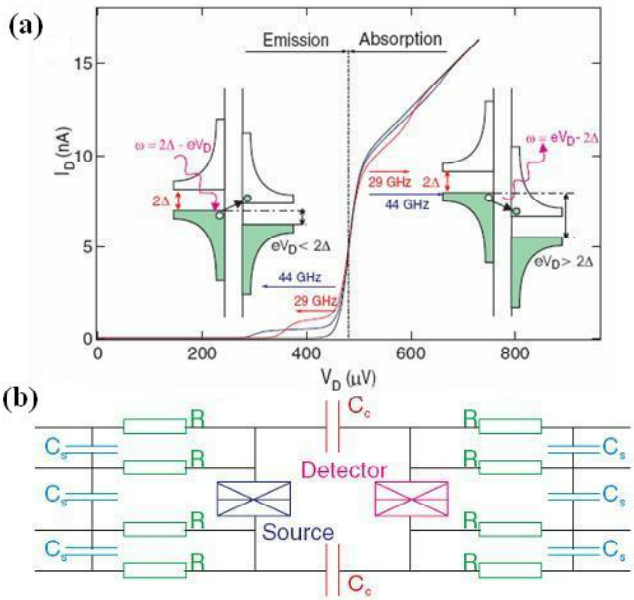

Figure 3.7: (a) $I(V)$ of the detector under monochromatic irradiation (black curve without irradiation), with frequency indicated on the figure and high enough amplitude to have a visible PAT current, and schematic pictures of the tunneling process involved in the PAT current through the detector. Left : $|V_D| < 2\Delta/e$, only emission by the source can lead to PAT. Right : $|V_D| > 2\Delta/e$ the detector is mainly sensitive to absorption by the source. (b) Equivalent circuit of the sample [22].

itself a mesoscopic device, the device under study and the detector need to be considered on the same level. In Ref. [22], the photo-assisted tunneling quasiparticle current through the detector due to the high frequency current fluctuations of the source, in the regime $eV_D, \omega \gg k_B\theta$, is

$$\begin{aligned} I_{PAT}(V_D) &= I_{QP}(V_D) - I_{QP,0}(V_D) \\ &= \int_0^{+\infty} d\omega \left(\frac{e}{\omega}\right)^2 S_V(-\omega) I_{QP,0}\left(V_D + \frac{\omega}{e}\right) \\ &\quad + \int_0^{eV_D} d\omega \left(\frac{e}{\omega}\right)^2 S_V(\omega) I_{QP,0}\left(V_D - \frac{\omega}{e}\right) \\ &\quad - \int_{-\infty}^{+\infty} d\omega \left(\frac{e}{\omega}\right)^2 S_V(\omega) I_{QP,0}\left(V_D\right) \ , \end{aligned} \tag{3.29}$$

with $S_V(\omega)$ the non-symmetrized spectral density of excess voltage fluctuations at frequency ω across the detector and $I_{QP,0}(V_D)$ the $I(V)$ characteristic of the detector when the source is not polarized, V_D the detector voltage. $S_V(\omega)$ is related to the current fluctuations of the source $S_I(\omega, V_S)$ through the transimpedance $Z(\omega)$ determined by the on-chip circuitry $[S_V(\omega) = |Z(\omega)|^2 S_I(\omega, V_S)]$. The different terms of Eq. (3.29) contribute only when the argument of $I_{QP,0}$ is higher than $2\Delta/e$ (i.e. $I_{QP,0} \neq 0$). This defines two regimes of detection. When $|eV_D| < 2\Delta$ only the first term in Eq. (3.29) contributes: we are then measuring the emission of the source (Figure 3.7 (a), left). When $|eV_D| > 2\Delta$, all the terms contribute but with a stronger weight for the absorption by the source (Figure 3.7 (a), right).

It has been shown that by measuring the photo-assisted tunneling current of a superconducting junction we are able to measure separately, and with comparable sensitivities, the contribution of emission and absorption to the non-symmetrized current fluctuations of the source. For this particular detection scheme, the symmetrized current fluctuations are not relevant, because they mix emission and absorption. The current fluctuations due to quasiparticle tunneling in a Josephson junction present a strong asymmetry between emission and absorption, with singularities in emission or absorption depending on the bias condition.

The SIS on-chip detection scheme is also used to detect noise generated by a quantum dot formed in a single wall carbon nanotube [23]. Measurement of shot noise over a full Coulomb diamond is reported with excited states and inelastic cotunneling clearly visible. Super-Poissonian noise is detected in the case of inelastic cotunneling.

On the other hand, the experimental realization of a quantum dot operating as a high-frequency noise detector is presented in Ref. [75]. Current fluctuations produced in a nearby quantum point contact ionize the quantum dot and induce transport through excited states. The resulting transient current through the quantum dot represents the detector signal. Investigating its dependence on the quantum point contact transmission and voltage bias, the authors observe and explain a quantum threshold feature and a saturation in the detector signal. This experimental and theoretical study is relevant in understanding the back-action of a quantum point contact used as a charge detector.

Chapter 4

Andreev reflection

Before mesoscopic physics was born, superconductors already displayed a variety of phase coherent phenomena, such as the Josephson effect. In recent years, scientists have been interested in the problem: what would happen if a normal metal lead was put in contact with a superconductor. For example, in the Figure 3.1, if one of two normal-conducting electrodes is replaced by a superconducting electrode, we have a normal metal-superconductor junction (NS junction). Much experimental and theoretical work on NS junctions has been done recently since such junctions have advantages for certain practical applications.

In this chapter, the basic transition properties of NS junction, specially the Andreev reflection will be introduced. This will be useful for the readers following the next chapter, because we will describe a noise detector which exploits Andreev reflection.

4.1 Introduction

Andreev reflection is a special type of particle scattering which occurs at interfaces between superconductors or normal metal-superconductor interfaces. In such a reflection process an electron incident on the interface is retro-reflected and converted into a hole and vice versa. The differences between normal reflection and Andreev reflection are illustrated in Figure 4.1. This phenomenon is found by Alexander F. Andreev in 1963 [76].

The basic knowledge of Andreev reflection is usually described on an interface between a normal metal and a s-wave conventional superconductor with the interface is assumed to be transparent.

We know that superconductor has an energy gap of width 2Δ in the density of states at the Fermi energy (called μ_S). Hence, there are no single particle states at those energies. A normal metal, however, has all electron states filled up to the Fermi energy (called μ_L). Connecting these two materials there will be electrons moving from the normal metal towards the superconductor only if $\mu_L - \mu_S > \Delta$ following the normal reflection. Single particle transmissions are therefore forbidden when $\mu_L - \mu_S < \Delta$. However, higher-order two-particle process is possible. By transferring two electrons at the same time, the incident and another one, a Cooper pair can be formed in the superconductor. In view of a single particle picture, the second additional electron corresponds to a reflected hole in the normal metal.

The properties of the Andreev reflection comparing with the normal reflection are discussed below:

- *Charge is conserved in normal reflection but not in Andreev reflection.* The reflected

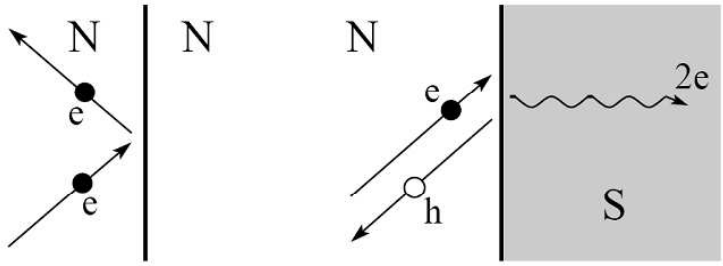

Figure 4.1: Normal reflection in the left panel: an electron is reflected as an electron. The right panel indicate Andreev reflection: an electron is reflected as a hole whose momentum is exactly opposite of that of the electron. A charge $2e$ is absorbed in the superconductor as a Cooper pair.

particle (the hole) has the opposite charge as the incident particle (the electron). The missing charge of 2e is absorbed into the superconductor as a Cooper pair.

- *Momentum is conserved in Andreev reflection but not in normal reflection.* The hole travels along the same line as incident electron but in opposite direction, that means all components of the velocity vector are reversed. The conservation of momentum is an approximation, valid if the superconducting excitation gap Δ is much smaller than the Fermi energy of the normal metal.

- *Energy is conserved in both normal and Andreev reflection.* The electron is at an energy ϵ above the Fermi level and the hole is at an energy ϵ below it. Andreev reflection is an elastic scattering process.

- *Spin is conserved in both normal and Andreev reflection.* To form a Cooper pair which has zero total spin, the reflected hole should have the opposite spin as the electron. For this reason, Andreev reflection is suppressed if the metal is a ferromagnet.

Besides the main properties of Andreev reflection, which are shown above, we find the other properties such as: the Andreev reflection is suppressed when we increase barrier strength between the materials; time reversal symmetry requires that there exists also an Andreev reflection in which a hole is reflected into an electron. The phase difference between the electron and hole in the Andreev reflection is $-\pi/2$ plus the phase of the superconducting order parameter. Notice that Andreev reflection has an analogue in optics, known as a phase–conjugating mirror [77].

As we have discussed above that the Andreev reflection happens at the interfaces of NS junctions or superconductor-superconductor junctions. In the SNS junction for instance, within the normal metal is surrounded by the superconductors, and a number of Andreev reflections appear at the NS interfaces. This effect is called Multiple Andreev Reflection (the related paper can be found in Ref. [78]).

4.2 Transition from metallic to tunneling regimes in superconducting microconstrictions

In Ref. [79], the authors have discussed the transmission and reflection of particles at the normal metal-superconductor interface.

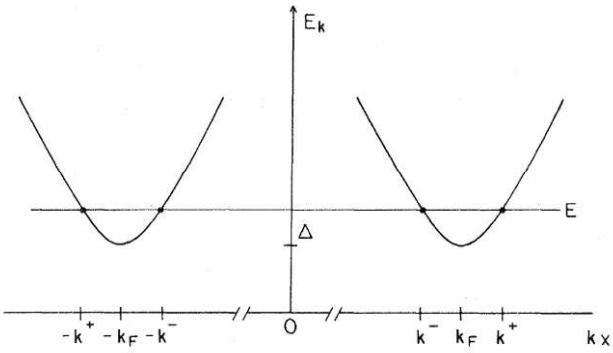

Figure 4.2: The excitation energies E_k vs k in the superconducting state being expanded near $\pm k_F$[79].

4.2.1 The Bogolubov-de Gennes equation

First, we consider the Bogolubov-de Gennes theory applied for the generalized semiconductor model [80, 81].

We are now considering the general electron system, with an applied arbitrary external potential $V(x)$. The effective Hamiltonian of this system is simply written as

$$\begin{aligned} H_{eff} &= \int dx \left\{ \sum_{\sigma} \Psi_{\sigma}^{\dagger}(x) \left(\frac{-\nabla^2}{2m} - \mu_S + V(x) \right) \Psi_{\sigma}(x) \right. \\ &\quad \left. + \Delta(x) \Psi_{\uparrow}^{\dagger}(x) \Psi_{\downarrow}^{\dagger}(x) + \Delta^*(x) \Psi_{\downarrow}(x) \Psi_{\uparrow}(x) \right\} , \end{aligned} \tag{4.1}$$

where the operators Ψ, $\Psi^{\dagger}$ satisfying the anti-commutation rules. They can be decomposed in terms of their Fourier components as

$$\begin{aligned} \Psi_{\sigma}(x) &= \sum_{k} e^{ikx} c_{k\sigma} , \\ \Psi_{\sigma}^{\dagger}(x) &= \sum_{k} e^{-ikx} c_{k\sigma}^{\dagger} , \end{aligned} \tag{4.2}$$

with $c_{k\sigma}^{\dagger}$ ($c_{k\sigma}$) is the creation (annihilation) operator for an electron, which has momentum k and spin σ in the BCS theory [81]. The first term in (4.1) destroys and creates one electron and therefore conserves the number of particles. But the two last terms increase or decrease two particles. The mean of the product $\Psi^{\dagger}\Psi^{\dagger}$, $\Psi\Psi$ are non-vanishing and these terms will play an important role. $\Delta(x)$ is called the pair potential. The effective Hamiltonian (4.1) is diagonalized by the Bogolubov transformation

$$\begin{aligned} \Psi_{\uparrow}(x) &= \sum_{k} \left[u_k(x) \gamma_{k\uparrow} - v_k^*(x) \gamma_{k\downarrow}^{\dagger} \right] , \\ \Psi_{\downarrow}(x) &= \sum_{k} \left[u_k(x) \gamma_{k\downarrow} + v_k^*(x) \gamma_{k\uparrow}^{\dagger} \right] , \end{aligned} \tag{4.3}$$

where γ, $\gamma^{\dagger}$ are new operators still satisfying the fermion commutation relations. They are called fermion quasi-particle operators. The state $u_k(x)$ ($v_k(x)$) corresponds to the wave function of a electron-like (hole-like) quasi-particle at position x. The corresponding

Hamiltonian has a diagonal form

$$H_{eff} = E_g + \sum_{k\sigma} E_k \gamma^\dagger_{k\sigma}\gamma_{k\sigma} \ , \tag{4.4}$$

where E_g is the ground state energy of H_{eff} and E_k is the energy of the excitation n. This Hamiltonian provides that the electron and hole wave functions satisfy the Bogolubov equations

$$\begin{aligned} Eu(x) &= [-\frac{\nabla^2}{2m} - \mu_S + V(x)]u(x) + \Delta(x)v(x) \ , \\ Ev(x) &= -[\frac{-\nabla^2}{2m} - \mu_S + V(x)]v(x) + \Delta^*(x)u(x) \ . \end{aligned} \tag{4.5}$$

In principle, these equations need to be solved self-consistently. The $\binom{u_k}{v_k}$ are eigenfunctions of a linear system with corresponding eigenvalues E_k:

$$E\begin{pmatrix} u \\ v \end{pmatrix} = \hat{\Omega}\begin{pmatrix} u \\ v \end{pmatrix} \ . \tag{4.6}$$

The operator $\hat{\Omega}$ is Hermitian so that the different eigenfunctions $\binom{u}{v}$ are orthogonal.

If $\binom{u}{v}$ is the solution for the eigenvalue E then $\binom{-v^\star}{u^\star}$ is the solution for the eigenvalue $-E$.

In what follows we will assume $V(x) = 0$. We find the eigenfunctions in the general form $\begin{pmatrix} u(x) \\ v(x) \end{pmatrix} = \begin{pmatrix} u_0 \\ v_0 \end{pmatrix} e^{ikx}$. If we only consider energies $E > \Delta$ [1], there will be a pair of magnitudes of k associated with each energy

$$k^\pm = \sqrt{2m}\left[\mu_S \pm (E_k^2 - \Delta^2)^{1/2}\right]^{1/2} \ , \tag{4.7}$$

with $E_k = (\Delta^2 + \epsilon_k^2)^{1/2}$, $\epsilon_k = \frac{k^2}{2m} - \mu_S$. Moreover, because of the BCS pairing of k and $-k$, we must consider both signs of k, so that there is a fourfold degeneracy of relevant states for each E (see Figure 4.2) with the notice that the twofold spin degeneracy only affects normalization since there is no spin-flip processes. Considering the relations of operators in Bogolubov transformation, we find that the excitations at $\pm k^+$ and $\pm k^-$ are predominantly electron-like and hole-like, correspondingly.

In general, we can introduce the electron/hole excitation operators with the energy required to make an excitation with charge e is $E_{ek} = \mu + E_k$, while that to make an excitation with charge $-e$ differs by 2μ and is $E_{hk} = -\mu + E_k = -(\mu - E_k)$. From the conservation of charge and the conservation of energy, we find there are four possible processes involving transfer of a single electronic charge in subsystems 1 and 2: electron transfers from 1 to 2 (or reverse); hole transfers from 1 to 2 (or reverse); create electron in 1 and hole in 2 (or destroy both); create hole in 1 and electron in 2 (or destroy both). We find that these energetically allowed transitions occurs if both $\pm E_{k,i}$ are symmetric with each μ_i (see Figure 4.3).

4.2.2 Transmission and reflections of particles at the NS interface

We first consider the schematic diagram of energy vs momentum at NS interface which is shown in Figure 4.4. One electron incident on the interface from the normal state

[1] We notice that hereafter Δ denotes the superconducting gap in BCS theory, which is in fact the amplitude of pair potential $\Delta(x)$ when it varies spatially.

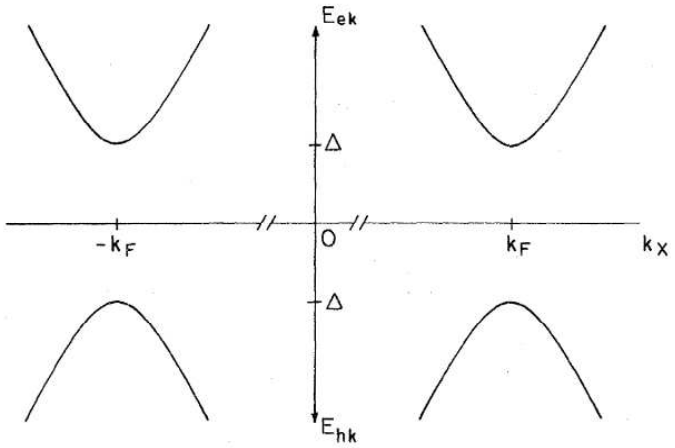

Figure 4.3: Semiconductor version of Figure 4.2. The quasi-particle branches in the lower half plane allows all the tr

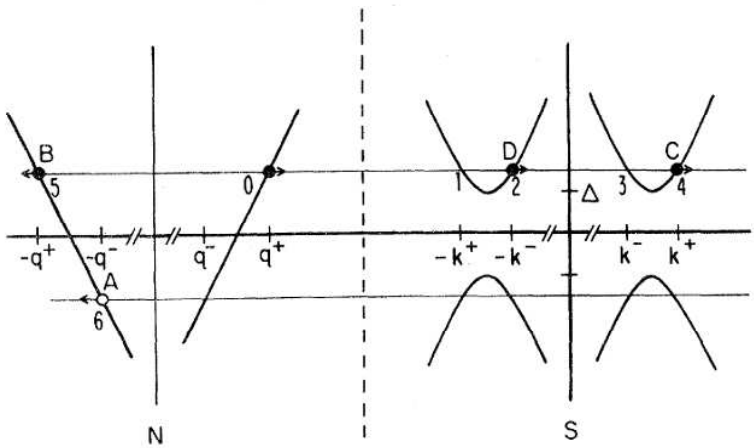

Figure 4.4: Schematic diagram of energy vs momentum at N-S interface, describing an electron (at 0) transmitted (2, 4) or reflected (5, 6). The open circles denote holes, the closed circuits denote electrons, and the arrows point in the directions of the group velocity [79].

with energy $E > \Delta$, as indicated by the arrow at the state labeled 0 in Figure 4.4 can transfer through the interface with the wave vector on the same side of the Fermi surface ($q^+ \rightarrow k^+$, corresponding to the point 4) (with the probability $C(E)$) or with the wave vector crossing through the Fermi surface ($q^+ \rightarrow -k^-$, corresponding to the point 2)(with the probability $D(E)$). This electron can be reflected as an electron with the probability $B(E)$ (corresponding to the point 5), or as a hole on the other side of the Fermi surface by Andreev reflection, with probability $A(E)$ (corresponding to the point 6). The latter process involves a transfer of a pair carrying charge $2e$, while the other processes transfer only a single electronic charge. The conservation of probability requires that

$$A(E) + B(E) + C(E) + D(E) = 1 \ . \tag{4.8}$$

When a voltage is applied to the NS junction, assuming ballistic acceleration of the quasi-particles without scattering for the case of a small orifice connecting massive electrodes, the distribution functions of all incoming particles are given by the equilibrium

Fermi functions, apart from the energy shift due to the acceleration potential. All incoming electrons from the S side have the distribution function $f_0(E)$, while those coming from the N side are described by $f_0(E - eV)$. The current is given as

$$I = 2N(0)ev_F\mathcal{A}\int_{-\infty}^{\infty} dE\,[f_{\rightarrow}(E) - f_{\leftarrow}(E)] \ , \tag{4.9}$$

where $\mathcal{A}$ is an effective-neck cross-section area, in the orifice model of a point contact, $\mathcal{A} = \pi a^2/4$, with a is the radius of the orifice. $N(0)$ refers to the one-spin density of states at ϵ_F. The last formula of the current can be expressed as

$$I_{NS} = 2N(0)ev_F\mathcal{A}\int_{-\infty}^{\infty} dE\,[f_0(E - eV) - f_0(E)]\,[1 + A(E) - B(E)] \ , \tag{4.10}$$

within the quantity $[1 + A(E) - B(E)]$ can be referred to as the "transmission coefficient for electrical current". This formula which describes both Andreev reflection processes and quasiparticle transfer, shows that while ordinary reflection reduces the current, Andreev reflection increases it by giving up to two transferred electrons (a Cooper pair) for one incident one.

4.2.3 The conductance of a normal metal-superconductor junction

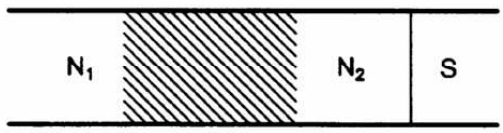

Figure 4.5: Model of a disordered normal region (the dashed region) adjacent to a superconductor (S). N_1 and N_2 are ideal normal leads [82].

In Ref. [82], a quantum transport theory for conduction through an NS interface has been developed. The model considered is illustrated in Figure 4.5. It consists of a disordered normal region inserted between two ideal normal leads N_1 and N_2, and adjacent to a superconductor. The only scattering in the superconductor consists of Andreev reflection at the NS interface is assumed.

An electron incident in the lead N_1 is reflected either as an electron or as a hole. It is similar for the hole, which can be reflected as a hole or an electron. The calculation for the linear-response conductance G_{NS} of the NS junction is applied at zero temperature (the used scattering matrix is at the Fermi level) and no magnetic field (the scattering matrix of the normal region is symmetric). The general formula of conductance, which is developed from [79, 83, 84], has been obtained as [82]

$$G_{NS} = \frac{2e^2}{\pi}\sum_{\alpha=1}^{N}\frac{T_\alpha^2}{(2 - T_\alpha)^2} \ , \tag{4.11}$$

where T_α ($\alpha = 1, 2, ..., N$) are the eigenvalues of the Hermitian matrix $t_{12}t_{12}^\dagger$. The transmission matrix t has dimension N, with N is the number of propagating modes in leads N_1 and N_2. Eq. (4.11) holds for an arbitrary transmission matrix, i.e., for arbitrary disorder potential. It is the multichannel generalization of a formula for the single-channel case[79, 85, 86]. The formula (4.11) is applied to a quantum point contact (yielding conductance quantization at multiples $2e^2/\pi$), to a quantum dot (yielding a non-Lorentzian conductance resonance), and to quantum interference effects in a disordered NS junction (enhanced weak-localization and reflectionless tunneling through a potential barrier)[82].

Chapter 5

Photo-assisted Andreev reflection as a probe of quantum noise

5.1 Introduction

As we have presented in the last section of chapter 3, in experiment, low frequency noise in the kHz–MHz range is more accessible than high frequency (GHz–THz) noise: it can, in principle, be measured using state of the art time acquisition techniques. For higher frequency measurements, it is becoming necessary to build a noise detector on chip for a specific range of high frequencies. In this chapter, we consider a detector circuit which is capacitively coupled to the mesoscopic device. This circuit is composed of a NS junction. Transport in this circuit occurs when the electrons tunneling between the normal metal and the superconductor either tunnel elastically, or are able to gain or to lose energy via photo-assisted Andreev reflections. The "photon" is provided or absorbed from the mesoscopic circuit which is capacitively coupled to the NS detector. The measurement of a dc current in the detector can thus provide information on the absorption and on the emission component of the current noise correlator.

Several theoretical efforts have been made to describe the high frequency noise measurement process. The theoretical idea in Ref. [20] has so far eluded experimental verification, possibly because in the double dot system, additional (unwanted) sources of inelastic scattering render a precise noise measurement quite difficult. It is therefore necessary to look for detection circuits which are less vulnerable to dissipation, as is the case for superconducting circuits, because of the presence of the superconducting gap. More recently, the noise of a carbon nanotube/quantum dot was also measured [23] using capacitive coupling to an SIS detector, with the detection of super-Poissonian noise resulting from inelastic cotunneling processes. The latter proposals, together with their successful experimental implementations, indicate that superconducting detector circuits have advantages over normal detection circuits.

The purpose of the present work is thus to analyze a similar situation, except that the SIS junction is replaced by a NS circuit, which transfers two electrons using Andreev reflection between a normal lead and a superconductor. The present scheme is similar in spirit to the initial proposal of Ref. [20], in the sense that it exploits dynamical Coulomb blockade physics [64]. However, here, two electrons need to be transferred from or to the superconductor, and such transitions involve high lying virtual states which are less prone to dissipation because of the superconducting gap, similarly to the SIS detector of Refs. [21, 22, 23]. Andreev reflection [79] typically assumes a good contact between a normal

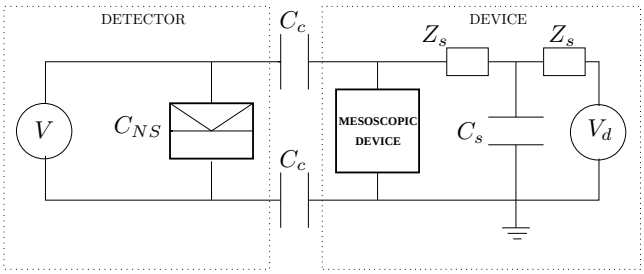

Figure 5.1: Schematic description of the setup: The mesoscopic device to be measured is coupled capacitively to the detector circuit. The latter consists of a NS junction with a dc bias.

metal and a superconductor, but in general it can be applied to tunneling contacts. It then involves tunneling transitions via virtual states. Consequently, depending on the applied dc bias, two successive "inelastic" electron jumps are required for a current to pass through the measurement circuit. The amplitude of the dc current as a function of bias voltage in the measurement circuit provides an effective readout of the noise power to be measured.

5.1.1 Detector consisting of a single NS junction

The detector circuit is depicted in Figure 5.1. Two capacitors are placed, respectively, between each side of the mesoscopic device and each side of the NS tunnel junction. This means that a current fluctuation in the mesoscopic device generates, via the capacitors, a voltage fluctuation across the NS junction. In turn, the voltage fluctuations translate into fluctuations of the phase around the junction. The presence of the neighboring mesoscopic circuit acts as a specific electromagnetic environment for this tunnel junction, which is described in the context of a dynamical Coulomb blockade [64] for this reason.

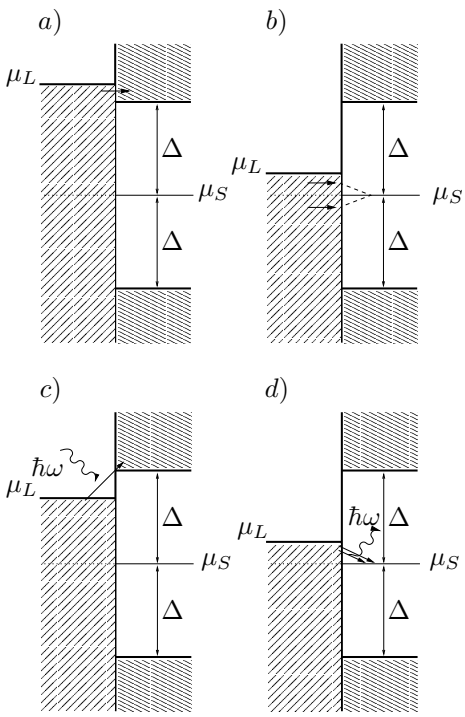

Figure 5.2: Electronic tunneling in a NS junction: a) Quasiparticle electron tunneling. b) Andreev reflection. c) Photo-assisted electron tunneling as a quasiparticle in the superconductor. d) Photo-assisted Andreev reflection.

Figure 5.2 depicts several scenarios for transport through a NS interface. An elastic transfer of single electrons can occur if the voltage applied to the junction is larger than the gap (Figure 5.2a). Below the gap, an elastic transport can only occur via Andreev reflection [79], effectively transferring two electrons with opposite energies with respect to the superconductor chemical potential (Figure 5.2b). Single electron can be transferred with an initial energy below the gap, provided that a photon is provided from the environment in order to create a quasiparticle in the superconductor (Figure 5.2c). Similarly, Andreev reflection can be rendered inelastic by the environment: for instance, two electrons on the normal side, with a total energy above the superconductor chemical potential, can give away a photon to the environment, so that they can be absorbed as a Cooper pair in the superconductor (Figure 5.2d). As we shall see, such inelastic Andreev processes are particularly useful for noise detection.

5.1.2 Detector consisting of a NS junction separated by a quantum dot

After studying the noise detection of the single NS junction, we will turn later to a double junction consisting of a normal metal lead, a quantum dot operating in the Coulomb blockade regime, and a superconductor connected to the latter (Figure 5.3). The charging energy of the dot is assumed to be large enough that double occupancy is prohibited. This setup has the advantage on the previous proposal that additional energy filtering is provided by the quantum dot. Below, we refer to this system as the normal metal–dot–superconductor (NDS) detector circuit. In Figure 5.4, the quantum dot level is located

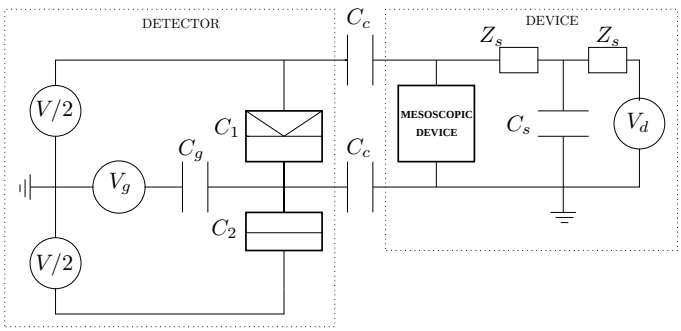

Figure 5.3: Schematic description of the NDS setup: The mesoscopic device to be measured is coupled capacitively to the detector circuit. The latter consists of a normal metal lead–quantum dot–superconductor junction with a dc bias.

above the superconductor chemical potential, and placed well within the gap in order to avoid quasiparticle processes. Because double occupancy is prohibited by the Coulomb blockade, Andreev transport occurs via sequential tunneling of the two electrons. Yet, because of energy conservation, the same energy requirements as in Figure 5.2b have to be satisfied for the final states (electrons with opposite energies, see Figure 5.4a). In the T-matrix terminology, for this transition to occur, virtual states corresponding to the energy of the dot are required, which suppress the Andreev tunneling current because of large energy denominators in the transition rate. Figures 5.4 b, c, d, describe the cases where an environment is coupled to the same NDS circuit. Provided that this environment can yield or give some of its energy to the NDS detector, electronic transitions via the dot

can become much more likely because electron energies on the normal side can be close to that of the dot level. Such transitions can thus occur even if the chemical potential of the normal lead exceeds that of the superconductor. As we shall see later on, the bias voltage can act as a valve for photo-assisted electron transitions. It is precisely these latter situations which will be exploited in order to measure the noise of the measuring circuit (the "environment").

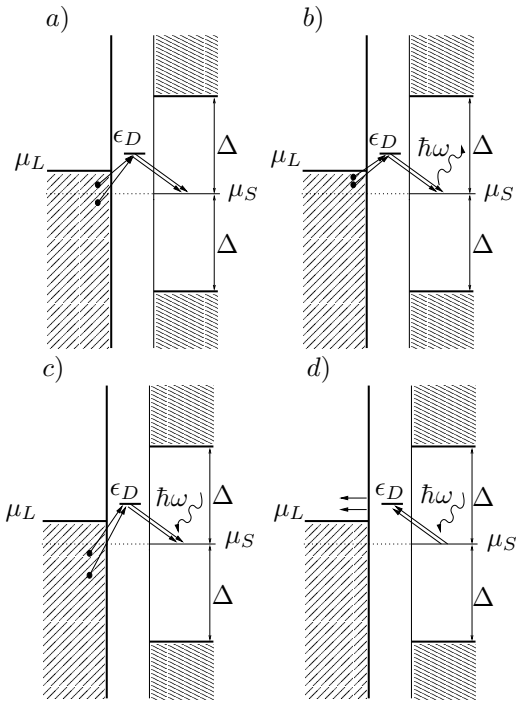

Figure 5.4: Andreev reflection in the NDS junction: a) Andreev reflection in the elastic regime. b) and c) Photo-assisted Andreev reflection, where a photon is provided to or provided by the environment. d) Absorption of a Cooper pair with (reverse) photo-assisted Andreev reflection, where a photon is provided by the environment. For cases b), c), d), which require passing through the dot, the tunneling of electrons is sequential.

5.2 Tunneling current through the NS junction

5.2.1 Model Hamiltonian

The Hamiltonian which describes the decoupled normal metal lead–superconductor–environment (mesoscopic circuit) system reads

$$H_0 = H_{0_L} + H_{0_S} + H_{env} \ , \tag{5.1}$$

where

$$H_{0_L} \quad = \quad \sum_{k,\sigma} \epsilon_k c^\dagger_{k,\sigma} c_{k,\sigma} \ , \tag{5.2}$$

describes the energy states in the lead, with $c^\dagger_{k,\sigma}$ an electron creation operator. The superconductor Hamiltonian has the diagonal form

$$H_{0_S} - \mu_S N_S = \sum_{q,\sigma} E_q \gamma^\dagger_{q,\sigma} \gamma_{q,\sigma} \ , \tag{5.3}$$

where $\gamma_{q,\sigma}, \gamma^\dagger_{q,\sigma}$ are quasiparticle operators, which relate to the Fermi operators $c_{q,\sigma}, c^\dagger_{q,\sigma}$ by the Bogoliubov transformation

$$\begin{aligned} c_{-q,\downarrow} &= u_q \gamma_{-q,\downarrow} - v_q \gamma^\dagger_{q,\uparrow} \ , \\ c^\dagger_{q,\uparrow} &= u_q \gamma^\dagger_{q,\uparrow} + v_q \gamma_{-q,\downarrow} \ , \end{aligned} \tag{5.4}$$

and $E_q = \sqrt{\Delta^2 + \zeta_q^2}$ is the quasiparticle energy, $\zeta_q = \epsilon_q - \mu_S$ is the normal state single-electron energy counted from the Fermi level μ_S and Δ is the superconducting gap which will be assumed to be the largest energy scale in these calculations. Hereafter, we also define $eV = \mu_L - \mu_S$ and assume $\mu_S = 0$.

Here, we do not specify the Hamiltonian of the environment because the environment represents an open system: the mesoscopic circuit which represents the environment will only manifest itself via the phase fluctuations $\langle \phi(t)\phi(0)\rangle$, which are induced at the NS junction (or later on for the NDS circuit, at the dot–superconductor junction) because of the location of the capacitor plates. In what follows, we shall assume that the unsymmetrized noise spectral density $S^+(\omega)$ as defined in Eq. (2.12) in chapter 2 corresponding to photon emission (for positive frequency), or, alternatively, $S_I(\omega)$, the spectral density of noise corresponding to photon absorption, is specified by the transport properties of the mesoscopic circuit [18, 19, 87]. Here $\langle\langle \cdots \rangle\rangle$ stands for an irreducible noise correlator, where the product of average currents has been subtracted out.

The tunneling Hamiltonian describing the electron transferring between the superconductor and the normal metal lead in the NS junction is

$$H_T = \sum_{k,q,\sigma} T_{k,q} c^\dagger_{k,\sigma} c_{q,\sigma} e^{-i\phi} \ , \tag{5.5}$$

where the indices k and q refer to the normal metal lead and superconductor. We consider for simplicity that $T_{k,q} = T_0$. Note that the tunneling Hamiltonian contains a fluctuating phase factor, which represents the coupling to the mesoscopic circuit. Indeed, because of the capacitive coupling between the sides of the NS junction and the mesoscopic circuit, a current fluctuation translates into a voltage fluctuation across the NS junction. Both are related via the trans-impedance of the circuit [20] $V(\omega) = Z(\omega)I(\omega)$. Next, the voltage fluctuations translate into phase fluctuations across the junction, as the phase is the canonical conjugate of the charge at the junctions [64]: the phase is thus considered as a quantum mechanical operator. Given a specific circuit (capacitors, resistances, etc.) the phase correlator is therefore expressed in terms of the trans-impedance of the circuit and the spectral density of noise [20], which is shown in Eq. (3.25).

The present system bears similarities with the study of inelastic Andreev reflection in the case where the superconductor contains phase fluctuations [88, 89]. Such phase fluctuations destroy the symmetry between electrons and holes, and affect the current voltage characteristics of the NS junction.

5.2.2 Tunneling current

The tunneling current associated with two electrons is given by the Fermi golden rule $I = 2e\Gamma_{i\to f}$, with the tunneling rate

$$\Gamma_{i\to f} = 2\pi \sum_f |\langle f|T|i\rangle|^2 \delta(\epsilon_i - \epsilon_f) \ , \tag{5.6}$$

where ϵ_i and ϵ_f are the tunneling energies of the initial and final states, including the environment, and T is the transition operator, which is expressed as

$$T = H_T + H_T \sum_{n=1}^{\infty} \left(\frac{1}{i\eta - H_0 + \epsilon_i} H_T \right)^n , \tag{5.7}$$

where η is positive infinitesimal.

Throughout this chapter, one considers the photo-assisted tunneling (PAT) current due to the high frequency current fluctuations of the mesoscopic device, as the difference [64]:

$$I_{PAT} = I(\text{environment}) - I(\text{no environment}) , \tag{5.8}$$

where, in general, the total current for tunneling of electrons through the junction is $I = I_{\rightarrow} - I_{\leftarrow}$.

However, experimentally, it is difficult to couple capacitively and then to remove the mesoscopic device circuit from the detector circuit [22]. What is, in fact, often measured is the excess noise, i.e., the difference between current fluctuations at a given bias and zero bias in the mesoscopic circuit. Later on, we will calculate the excess noise $S^+_{excess}(\omega)$ of $S^+(\omega)$. In this work, we thus measure the difference between the currents through the detector when a bias voltage and a zero bias are applied to the device circuit, as a function of detector bias voltage, which is defined as

$$\Delta I_{PAT}(eV) = I(eV_d \neq 0, eV) - I(eV_d = 0, eV) . \tag{5.9}$$

This also corresponds to the difference between the PAT currents through the detector when a bias voltage and a zero bias are applied to the device circuit, $\Delta I_{PAT}(eV) = I_{PAT}(eV_d \neq 0, eV) - I_{PAT}(eV_d = 0, eV)$ because the contributions with no environment cancel out. The difference between PAT currents thus provides crucial information on the spectral density of excess noise of the mesoscopic device. Notice that our calculation applies to the zero temperature case for convenience, but it can be generalized to finite temperatures.

5.2.3 Single electron tunneling

Although our focus of interest concerns photo-assisted Andreev reflection, we need to compute all possible contributions. The current associated with one electron tunneling is given by the Fermi golden rule,

$$I = 2\pi e \sum_f |\langle f|H_T|i\rangle|^2 \delta(\epsilon_i - \epsilon_f) . \tag{5.10}$$

The calculation of the current proceeds in the same way as that of a normal metal junction [64], except that one has to take into account the superconducting density of states on the right side of the junction, which is done by exploiting the Bogoliubov transformation. For the case of electrons tunneling from the normal metal lead to the superconductor

$(eV > \Delta)$, the current from left to right reads

$$
\begin{aligned}
I_{\rightarrow} &= e\int_{-\infty}^{\infty} dt e^{-i(\mu_S-\mu_L)t}\langle H_T(t)H_T^\dagger(0)\rangle \\
&= eT_0^2\int_{-\infty}^{\infty} dt e^{-i(\mu_S-\mu_L)t}\sum_{k,k',q,q',\sigma_1,\sigma_2}\langle c^\dagger_{k,\sigma_1}(t)c_{k',\sigma_2}(0)\rangle\langle c_{q,\sigma_1}(t)c^\dagger_{q',\sigma_2}(0)\rangle\langle e^{-i\phi(t)}e^{i\phi(0)}\rangle \\
&= 2eT_0^2\int_{-\infty}^{\infty} dt\sum_{k,q}|u_q|^2 e^{-iE_q t}e^{i\epsilon_k t}e^{J(t)} \\
&= 4\pi e T_0^2\mathcal{N}_N\mathcal{N}_S\int_{-\infty}^{eV} d\epsilon\int_{\Delta}^{\infty} dE\frac{E}{\sqrt{E^2-\Delta^2}}\left[1-\frac{2\pi}{R_K}\int_{-\infty}^{\infty} d\omega\frac{|Z(\omega)|^2}{\omega^2}S_I(\omega)\right]\delta(E-\epsilon) \\
&\quad +\frac{8\pi^2 e T_0^2\mathcal{N}_N\mathcal{N}_S}{R_K}\int_{-\infty}^{eV} d\epsilon\int_{\Delta}^{\infty} dE\frac{E}{\sqrt{E^2-\Delta^2}}\frac{|Z(\epsilon-E)|^2}{(\epsilon-E)^2}S_I(\epsilon-E)\ . \qquad (5.11)
\end{aligned}
$$

with $\mathcal{N}_N$ and $\mathcal{N}_S$ the density of states of the two leads (in the normal state). We notice that this calculation is similar to the calculation of the tunneling rate of electrons in the presence of an environment which is shown in sections 3.1.3 and 3.1.4 (following the same steps). This current includes both an elastic and an inelastic contribution, the former being renormalized by the presence of the environment [20]. Here, ϵ is the energy of an electron in the normal metal lead and E is the energy of a quasiparticle in the superconductor lead. Changing variables in the inelastic term to $\Omega = \epsilon - E$, $\delta = \epsilon + E$, an using $\int dx(x+a)/\sqrt{(x+a)^2-b^2} = \sqrt{(x+a)^2-b^2}/2$, after computing the current from right to left in a similar way, we obtain

$$
\begin{aligned}
\Delta I_{PAT} &= -C_{1e}\left[\int_{-\infty}^{\infty} d\omega\frac{|Z(\omega)|^2}{\omega^2}S^+_{excess}(-\omega)\right]K^{el}_{1e}(eV) \\
&\quad +C_{1e}\int_{-\infty}^{eV-\Delta} d\Omega\frac{|Z(\Omega)|^2}{\Omega^2}S^+_{excess}(-\Omega)K^{inel}_{1e}(\Omega,eV)\ , \qquad (5.12)
\end{aligned}
$$

where the transmission coefficient of the NS junction in the normal state is defined as $\mathcal{T} = 4\pi^2\mathcal{N}_N\mathcal{N}_S T_0^2$, $C_{1e} = e\mathcal{T}/R_K$. The weight functions are defined as

$$
K^{el}_{1e}(eV) = \sqrt{(eV)^2-\Delta^2}\ , \qquad (5.13)
$$

$$
K^{inel}_{1e}(\Omega,eV) = \sqrt{(\Omega-eV)^2-\Delta^2}\ . \qquad (5.14)
$$

Similarly, we obtain the formula of ΔI_{PAT} for the case $eV \leq -\Delta$,

$$
\begin{aligned}
\Delta I_{PAT} &= -C_{1e}\left[\int_{-\infty}^{\infty} d\omega\frac{|Z(\omega)|^2}{\omega^2}S^+_{excess}(-\omega)\right]K^{el}_{1e}(eV) \\
&\quad +C_{1e}\int_{eV+\Delta}^{\infty} d\Omega\frac{|Z(-\Omega)|^2}{\Omega^2}S^+_{excess}(\Omega)K^{inel}_{1e}(\Omega,eV)\ . \qquad (5.15)
\end{aligned}
$$

For the case $-\Delta \leq eV \leq \Delta$, there are no elastic transitions because electrons cannot enter the superconducting gap. Nevertheless, due to the presence of the environment, electrons can absorb or emit energy from or to the environment so that an inelastic quasiparticle current flows,

$$
\begin{aligned}
\Delta I_{PAT} &= C_{1e}\int_{-\infty}^{eV-\Delta} d\Omega\frac{|Z(\Omega)|^2}{\Omega^2}S^+_{excess}(-\Omega)K^{inel}_{1e}(\Omega,eV) \\
&\quad -C_{1e}\int_{eV+\Delta}^{\infty} d\Omega\frac{|Z(-\Omega)|^2}{\Omega^2}S^+_{excess}(\Omega)K^{inel}_{1e}(\Omega,eV)\ . \qquad (5.16)
\end{aligned}
$$

5.2.4 Two electrons tunneling as two quasiparticles

The single electron (quasiparticle) tunneling current is of first order in the tunneling amplitude. We now turn to processes which invoke the tunneling of two electrons through the NS interface. Indeed, because our aim is to show that Andreev reflection can be used to measure noise, we need to examine all two electron processes, we start with the transfer of two electrons as quasiparticles above the gap. Calculations of the matrix element in Eq. (5.6) are then carried out to second order in the tunneling Hamiltonian using the T matrix,

$$I = 4\pi e \sum_f |\langle f|H_T \frac{1}{i\eta - H_0 + \epsilon_i} H_T|i\rangle|^2 \delta(\epsilon_i - \epsilon_f) \ . \tag{5.17}$$

The initial state is a product,

$$|i\rangle = |G_L\rangle \otimes |G_S\rangle \otimes |R\rangle \ , \tag{5.18}$$

where $|G_L\rangle$ denotes a ground state, which corresponds to a filled Fermi sea for the normal electrode. $|G_S\rangle$ is the BCS ground state in the superconductor lead. $|R\rangle$ denotes the initial state of the environment. On the other hand, our guess for the final state should read

$$|f\rangle = c^\dagger_{k,\sigma} c^\dagger_{k',\sigma'} \gamma^\dagger_{q,\sigma} \gamma^\dagger_{q',\sigma'} |G_L\rangle \otimes |G_S\rangle \otimes |R'\rangle \ , \tag{5.19}$$

when two electrons are emitted from the superconductor. The "guess" of Eq. (5.19) is an informed one: an electron pair is broken in the superconductor, and one electron tunnels to the normal metal lead, while the other becomes a quasiparticle in the superconductor; the same process is true for the second electron which tunnels to the normal metal lead. When the superconductor lead absorbs two electrons,

$$|f\rangle = c_{k,\sigma} c_{k',\sigma'} \gamma^\dagger_{q,\sigma} \gamma^\dagger_{q',\sigma'} |G_L\rangle \otimes |G_S\rangle \otimes |R'\rangle \ . \tag{5.20}$$

The "guess" of Eq. (5.20) is that two electrons can tunnel from the normal metal lead and become quasiparticles in the superconductor. Here, $|R'\rangle$ is the final state of the environment.

We are first considering the case of two electrons tunneling from the superconductor lead to the normal metal lead. Introducing the closure relation for the eigenstates of the nonconnected system $\{|\upsilon_i\rangle\}$, and using the fact that $\langle \upsilon|(\epsilon_i - H_0 \pm i\eta)^{-1}|\upsilon\rangle = \mp i \int_0^\infty dt e^{i(\epsilon_i - \epsilon_\upsilon \pm i\eta)t}$, one can exponentiate all the energy denominators. We have

$$\begin{aligned} I_\leftarrow &= 2e \sum_{f,\upsilon_1,\upsilon_2} \int_{-\infty}^{\infty} dt \int_0^\infty dt' \int_0^\infty dt'' e^{-\eta(t'+t'')} e^{i\epsilon_i(t-t''+t')} \langle i|H_T^\dagger|\upsilon_1\rangle \\ &\quad \times e^{i\epsilon_{\upsilon_1} t'} \langle \upsilon_1|H_T^\dagger|f\rangle e^{-i\epsilon_f t} \langle f|H_T|\upsilon_2\rangle e^{-i\epsilon_{\upsilon_2} t'} \langle \upsilon_2|H_T|i\rangle \ . \end{aligned} \tag{5.21}$$

Then, by transforming the time dependent phases into a time dependence of the tunneling Hamiltonian, we can integrate out all final and virtual states. This allows us to rewrite the tunneling current in terms of tunneling operators in the interaction representation to lowest order $O(T_0^4)$. The current reads

$$\begin{aligned} I_\leftarrow &= 2e \int_{-\infty}^{\infty} dt \int_0^\infty dt' \int_0^\infty dt'' e^{-\eta(t'+t'')} e^{i(\mu_S - \mu_L)(2t - t' - t'')} \\ &\quad \times \langle H_T^\dagger(t-t'') H_T^\dagger(t) H_T(t') H_T(0)\rangle \ , \end{aligned} \tag{5.22}$$

where the time dependence of the operators is governed by

$$H_T(t) = e^{i(K_L+K_S+H_{env})t} H_T e^{-i(K_L+K_S+H_{env})t} \ ,$$

with $K_L = H_{0_L} - \mu_L N_L$ and $K_S = H_{0_S} - \mu_S N_S$. The interaction presentation in Eq. (5.22) has the advantage that we only have to calculate statistical averages of (time-dependent) correlation functions. We express the tunneling Hamiltonian in the creation/annihilation operators in the normal- and super-conducting leads. Because there is not any interaction between particles in two leads, we obtain

$$\begin{aligned} I_{\leftarrow} \ = \ & 2eT_0^2 \int_{-\infty}^{\infty} dt \int_0^{\infty} dt' \int_0^{\infty} dt'' e^{-\eta(t'+t'')} e^{i(\mu_S-\mu_L)(2t-t'-t'')} \\ & \times \sum_{k_1..k_4, q_1..q_4, \sigma_1..\sigma_4} \langle c_{k_1\sigma_1}(t-t'') c_{k_2\sigma_2}(t) c^\dagger_{k_3\sigma_3}(t') c^\dagger_{k_4\sigma_4}(0) \rangle \\ & \times \langle c^\dagger_{q_1\sigma_1}(t-t'') c^\dagger_{q_2\sigma_2}(t) c_{q_3\sigma_3}(t') c_{q_4\sigma_4}(0) \rangle \langle e^{i\phi(t-t'')} e^{i\phi(t)} e^{-i\phi(t')} e^{-i\phi(0)} \rangle \ . \end{aligned} \tag{5.23}$$

Eq. (5.23) is true for two electrons tunneling as quasiparticles and as Andreev reflection. For the correlation of operators in the normal metal lead, using the Wick's theorem, we obtain

$$\begin{aligned} \langle c_{k_1\sigma_1}(t-t'') c_{k_2\sigma_2}(t) c^\dagger_{k_3\sigma_3}(t') c^\dagger_{k_4\sigma_4}(0) \rangle \ = & -e^{-i(\epsilon_{k_1}-\mu_L)(t-t''-t')} \delta_{k_1,k_3} e^{-i(\epsilon_{k_2}-\mu_L)t} \delta_{k_2,k_4} \\ & + e^{-i(\epsilon_{k_1}-\mu_L)(t-t'')} \delta_{k_1,k_4} e^{-i(\epsilon_{k_2}-\mu_L)(t-t')} \delta_{k_2,k_4} \ . \end{aligned} \tag{5.24}$$

Here, we consider quasiparticle tunneling, so

$$\begin{aligned} \langle c^\dagger_{q_1\sigma_1}(t-t'') c^\dagger_{q_2\sigma_2}(t) c_{q_3\sigma_3}(t') c_{q_4\sigma_4}(0) \rangle \ = & -|v_{q_1}|^2 |v_{q_2}|^2 e^{-iE_{q_1}(t-t''-t')} \delta_{q_1,q_3} e^{-iE_{q_2}t} \delta_{q_2,q_4} \\ & + |v_{q_1}|^2 |v_{q_2}|^2 e^{-iE_{q_1}(t-t'')} \delta_{q_1,q_4} e^{-iE_{q'}(t-t')} \delta_{q_2,q_3} \ . \end{aligned} \tag{5.25}$$

The exponentials of phase operators are calculated as in the Appendix A (see Eq. 5.58), and the phase-phase correlation function is defined in Eq. (3.15), so that [92, 93]

$$\langle e^{i\phi(t-t'')} e^{i\phi(t)} e^{-i\phi(t')} e^{-i\phi(0)} \rangle \ = \ e^{J(t-t''-t')+J(t-t'')+J(t-t')+J(t)-J(-t'')-J(t')} \ . \tag{5.26}$$

Following Eq. (3.25), we further assume that $J(t) \ll 1$, which means a low trans-impedance approximation, together with the fact that $J(t)$ is well behaved at large times. This allows us to expand the exponential of phase correlators $e^{J(t)} \approx 1 + J(t)$. The result for the current contains both an elastic and an inelastic contribution $I_{\leftarrow} = I^{el}_{\leftarrow} + I^{inel}_{\leftarrow}$, where

$$I^{el}_{\leftarrow} \simeq \frac{e\mathcal{T}^2}{16\pi^3 R_K} \left[\Psi_{0\leftarrow} - \frac{2\pi}{R_K} \int_{-\infty}^{\infty} d\omega \frac{|Z(\omega)|^2}{\omega^2} S_I(\omega) K^{el}_{2e\leftarrow}(\omega, eV, \eta) \right] \ , \tag{5.27}$$

with $\Psi_{0\leftarrow}$ and $K^{el}_{2e\leftarrow}(\omega, eV, \eta)$ defined as in Eqs. (5.59) and (5.60) in Appendix B, and

$$I^{inel}_{\leftarrow} \simeq \frac{e\mathcal{T}^2}{16\pi^2 R_K} \int_{2\Delta+2eV}^{\infty} d\Omega \frac{|Z(-\Omega)|^2}{\Omega^2} S_I(-\Omega) K^{inel}_{2e\leftarrow}(\Omega, eV, \eta) \ , \tag{5.28}$$

where $K^{inel}_{2e\leftarrow}(\Omega, eV, \eta)$ is defined in Eq. (5.61) in Appendix B. The elastic contribution exists only if $eV < -\Delta$. For $-\Delta < eV$ only the inelastic part contributes to $I_{\leftarrow}$.

Similarly we calculate for $I_{\rightarrow}$. There is a symmetry between the magnitude between the right and left moving current upon bias reversal: the expression for $I_{\leftarrow}$ is the same as $I_{\rightarrow}$, if we replace $-eV$ by eV.

So, in the interval $|eV| \leq \Delta$, we obtain

$$\begin{aligned}\Delta I_{PAT}(eV) = & C_{2e}\int_{2\Delta-2eV}^{\infty} d\Omega \frac{|Z(-\Omega)|^2}{\Omega^2} S^{+}_{excess}(\Omega) K^{inel}_{2e\rightarrow}(\Omega, eV, \eta) \\ & -C_{2e}\int_{2\Delta+2eV}^{\infty} d\Omega \frac{|Z(-\Omega)|^2}{\Omega^2} S^{+}_{excess}(\Omega) K^{inel}_{2e\leftarrow}(\Omega, eV, \eta) \ , \end{aligned} \tag{5.29}$$

with $K^{inel}_{2e\rightarrow}(eV) = K^{inel}_{2e\leftarrow}(-eV)$ and $C_{2e} = e\mathcal{T}^2/16\pi^2 R_K$.

5.2.5 Two electron tunneling as a Cooper pair: Andreev reflection

In this case, we also need to carry out calculations of the matrix element in Eq. (5.6) to second order in the tunneling Hamiltonian. Typically, the initial state will be as shown in Eq. (5.18). On the other hand, our guess for the final state reads

$$|f\rangle = 2^{-1/2}(c^{\dagger}_{k,\sigma}c^{\dagger}_{k',-\sigma} - c^{\dagger}_{k',\sigma}c^{\dagger}_{k,-\sigma})|G_L\rangle \otimes |G_S\rangle \otimes |R'\rangle \ , \tag{5.30}$$

when a Cooper pair is emitted from the superconductor, or

$$|f\rangle = 2^{-1/2}[c_{k,\sigma}c_{k',-\sigma} - c_{k',\sigma}c_{k,-\sigma}]|G_L\rangle \otimes |G_S\rangle \otimes |R'\rangle \ , \tag{5.31}$$

when the superconductor lead absorbs a Cooper pair. Here, $|R'\rangle$ is the final state of the environment. The "guess" of Eqs. (5.30) and (5.31) is again an informed one: indeed, the s-wave symmetry of the superconductor imposes that only singlet pairs of electrons can be emitted or absorbed. This phenomenon has been described in the early work on entanglement in mesoscopic physics [90, 91], and the resulting final state can, in principle, be detected through a violation of Bell inequalities [134].

Because we are also considering the tunneling process of two electrons from the superconductor to the normal metal lead, the current is expressed as in Eq. (5.22). In this case, the physical interpretation of Eq. (5.22) is a hopping process of two electrons with opposite spins from the superconductor, thereby removing a Cooper pair in the superconductor, and back again. The delay times between the two tunneling processes of the electrons within a pair is given by t' and t'' respectively, whereas the time between destroying and creating a Cooper pair is given by t. Following Eq. (5.23) and considering only the Andreev process, we can now write the tunneling current as a function of the normal (and anomalous) Green's functions of the normal metal lead, $G_{L\sigma}$, the quantum dot, $G_{D\sigma}$, and the superconductor, F_σ (see Appendix C), which is the same as in Ref. [92]

$$\begin{aligned} I_{\leftarrow} = & 2eT_0^4 \int_{-\infty}^{\infty} dt \int_0^{\infty} dt' \int_0^{\infty} dt'' e^{-\eta(t'+t'')} e^{i(\mu_S-\mu_L)(2t-t'-t'')} \\ & \times \sum_{k,k',q,q',\sigma} \{ -G^{>}_{L\sigma}(k, t-t''-t') G^{>}_{L-\sigma}(k', t) F^{*}_{\sigma}(q', -t'') F_{-\sigma}(q, t') \\ & + G^{>}_{L\sigma}(k, t-t'') G^{>}_{L-\sigma}(k', t-t') F^{*}_{\sigma}(q', -t'') F_{\sigma}(q, t') \} \\ & \times e^{J(t-t''-t')+J(t-t'')+J(t-t')+J(t)-J(-t'')-J(t')} \ . \end{aligned} \tag{5.32}$$

The result for the current contains both an elastic and an inelastic contribution:

$$I_{\leftarrow} = I^{el}_{\leftarrow} + I^{inel}_{\leftarrow} \ , \tag{5.33}$$

where the elastic contribution reads

$$I_{\leftarrow}^{el} \simeq \frac{e\mathcal{T}^2}{2\pi^3}\int_{eV}^{-eV} d\epsilon \int_{\Delta}^{\infty} dE \int_{\Delta}^{\infty} dE' \frac{\Delta^2}{\sqrt{E^2-\Delta^2}\sqrt{E'^2-\Delta^2}}$$
$$\times \left\{ \left[1 - \frac{4\pi}{R_K}\int_{-\infty}^{+\infty} d\omega \frac{|Z(\omega)|^2}{\omega^2} S_I(\omega) \right] \frac{1}{D_{\leftarrow}^0} - \frac{2\pi}{R_K}\int_{-\infty}^{+\infty} d\omega \frac{|Z(\omega)|^2}{\omega^2}\frac{S_I(\omega)}{D_{\leftarrow}^{el}} \right\} . \tag{5.34}$$

The inelastic contribution to $I_{\leftarrow}$ is

$$I_{\leftarrow}^{inel} \simeq \frac{e\mathcal{T}^2}{\pi^2 R_K}\int_{eV}^{\infty} d\epsilon \int_{eV}^{\infty} d\epsilon' \int_{\Delta}^{\infty} dE \int_{\Delta}^{\infty} dE'$$
$$\times \frac{\Delta^2}{\sqrt{E^2-\Delta^2}\sqrt{E'^2-\Delta^2}} \frac{|Z(-(\epsilon+\epsilon'))|^2}{(\epsilon+\epsilon')^2}\frac{S_I(-(\epsilon+\epsilon'))}{D_{\leftarrow}^{inel}} . \tag{5.35}$$

where the denominators are specified in Appendix D. $I_{\rightarrow}$ is derived in a similar manner, but its expression is omitted here. Nevertheless, its effects will be displayed in the measurement of the noise of a point contact.

The above expressions constitute the central result of this work: we understand now how the current fluctuations in the neighboring mesoscopic circuit give rise to inelastic and elastic contributions in the current between a normal metal and a superconductor. We find that both current contributions have the same form, and the current fluctuations of the mesoscopic device affect the current in the detector at the energy corresponding to the total energy of two electrons in the normal lead. Andreev reflection therefore acts as an energy filter.

Next, we can change variables as in the previous sections. With an arbitrary bias eV, we obtain

$$\begin{aligned}\Delta I_{PAT}(eV) \;=\; & -C_{NS}\int_{-\infty}^{+\infty} d\omega \frac{|Z(\omega)|^2}{\omega^2} S_{excess}^{+}(-\omega) K_{NS}^{el}(\omega, eV, \eta) \\ & -\frac{C_{NS}}{2}\int_{-\infty}^{2eV} d\Omega \frac{|Z(\Omega)|^2}{\Omega^2} S_{excess}^{+}(-\Omega) K_{NS}^{inel}(\Omega, eV, \eta) \\ & -\frac{C_{NS}}{2}\int_{2eV}^{\infty} d\Omega \frac{|Z(-\Omega)|^2}{\Omega^2} S_{excess}^{+}(\Omega) K_{NS}^{inel}(\Omega, eV, \eta) \;,\end{aligned} \tag{5.36}$$

with $C_{NS} = e\mathcal{T}^2\Delta^2/\pi^2 R_K$. The kernel functions K_{NS}^{el} and K_{NS}^{inel} are shown in Appendix D.

5.2.6 Quantum point contact as a source of noise

In this section, we illustrate the present results with a simple example. We consider for this purpose a quantum point contact, which is a device whose noise spectral density is well characterized by using the scattering theory[58, 57]. Here, however, we consider unsymmetrized noise correlators, which have been shown in Eq. (2.36).

As pointed out above, we are computing the difference of the PAT currents in the presence and in the absence of the dc bias. This means that we insert the spectral density of excess noise of the mesoscopic device, which for a point contact bears most of its weight

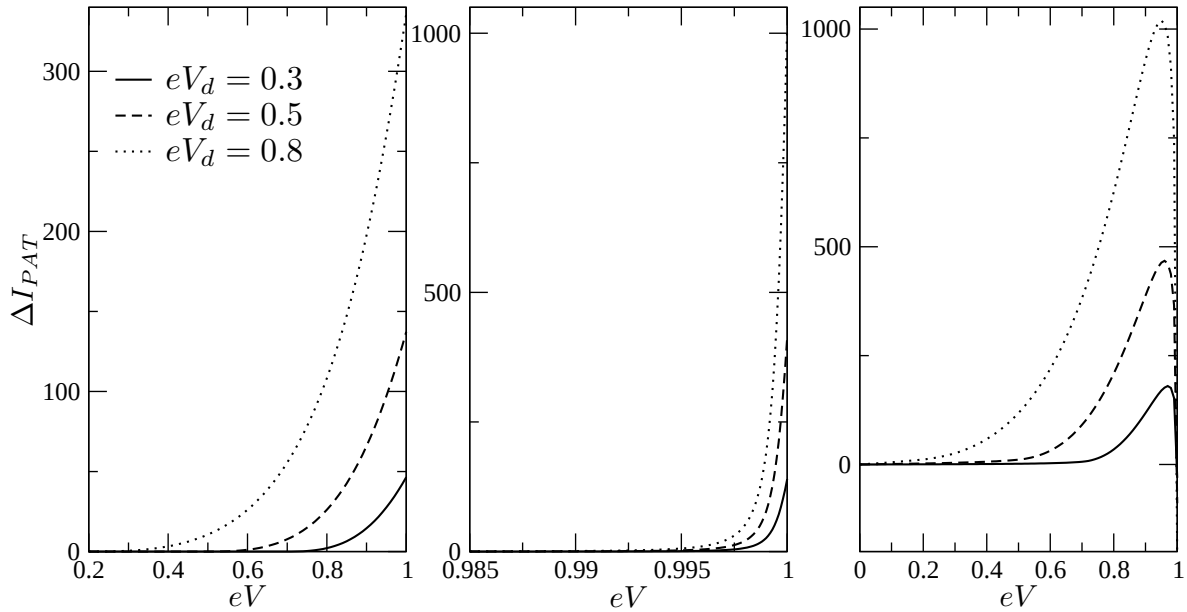

Figure 5.5: ΔI_{PAT} plotted as a function of the dc bias voltage, for a mesoscopic device voltage bias eV_d: 0.3 (continuous line), 0.5 (dashed line) and 0.8 (dotted line). The left, center, and right panels depict single quasiparticle tunneling, two quasiparticle tunneling, and Andreev reflection. ΔI_{PAT} is in units of C_{2e}, with $\mathcal{T} = 0.6$ (see text).

near zero frequencies. Excess noise decreases linearly to zero over a range $[0, \pm eV_d]$ for positive and negative frequencies (here we rewrite Eq. (2.39) with the notice hereafter, we use the notation V_d instead of V to show the voltage of mesoscopic device)

$$S^{+}_{excess}(\omega) = \frac{2e^2}{\pi} T(1-T)(eV_d - |\omega|)\Theta(eV_d - |\omega|)\,. \tag{5.37}$$

We choose a generic form for the transimpedance, similar in spirit to that chosen in Ref. [20]. Considering the circuit in Figures 5.1 and 5.3, at $\omega = 0$, the device and detector are not coupled and the transimpedence should therefore vanish. On the other hand, the transimpedance is predicted to have a constant behavior at large frequencies. We therefore choose the following generic form for the transimpedance

$$|Z(\omega)|^2 = \frac{(R\omega)^2}{\omega_0^2 + \omega^2}\,, \tag{5.38}$$

where R is the typical high frequency impedance and the crossover frequency ω_0 is estimated from the experimental data of Ref. [22]; choosing a finite cutoff frequency ω_0 means that at frequencies $\omega \ll \omega_0$, the mesoscopic circuit has no influence on the detector circuit because low frequencies do not propagate through a capacitor.

We calculate numerically the PAT currents in the above three cases: single and two quasiparticle tunneling and Andreev reflection. All energies are measured with respect to the superconducting gap Δ. In these units, we chose $\omega_0 = 0.3$ and $\eta = 0.001$. Currents are typically plotted as a function of the dc bias voltage eV of the detector for several values of the mesoscopic bias voltage eV_d (the environment). Our motivation is to consider the PAT currents with the condition $|eV| < 1$ ($|eV| < \Delta$), where the effect of the environment on the PAT current is most pronounced, and we shall predict that two electrons tunneling as a Cooper pair (Andreev processes) contributes the most to the PAT current, except close to $eV = \Delta$. Because of the symmetry between negative eV and positive eV, we

display the results for $eV > 0$. The PAT currents for the above three processes are plotted next to one another in Figure 5.5 for comparison.

We find in Figure 5.5 that if the chemical potential of the normal metal lead is close to the potential of the superconductor lead ($eV \ll \Delta$), the PAT currents in the three cases are suppressed. For the two cases of quasiparticle tunneling, the PAT currents are equal to zero below a certain threshold. The single quasiparticle current differs from zero at a threshold, which is identified as $\Delta - eV_d$; that is, quasiparticles are able to tunnel above that superconductor gap only if they can borrow the necessary energy from the mesoscopic device. This explains why the curves associated with different values of the mesoscopic device bias voltage are shifted to the right as eV_d decreases. For two quasiparticle tunneling, we observe that the PAT current has a similar threshold, which, compared to Figure 5.5a, is pushed toward the right in Figure 5.5b, because more energy is needed to transfer two electrons above the gap, compared to a single electron. Not surprisingly the corresponding curves are once again shifted to the right with decreasing eV_d. These curves all have a sharp maximum at $eV = \Delta$.

We turn now to the Andreev PAT difference current, which dominates the above two processes at small and moderate biases. Note that the total Andreev current contains an elastic contribution as well as an inelastic contribution below the gap, contrary to quasiparticle tunneling which has contributions below the gap only because these processes are photo-assisted. Because we are computing the difference between PAT currents with and without the mesoscopic bias voltage, we expect that the elastic contribution cancels out. However, the first term of Eq. (5.36) tells us that the presence of the environment also gives rise to an effective elastic contribution to the PAT Andreev difference current. Unfortunately, this elastic correction is not small compared to the true Andreev current.

Looking at Figure 5.5, we note that the PAT curve for Andreev processes is shifted to the left when the bias of the mesoscopic device is increased. The environment provides energy to or absorbs energy from pairs of electrons whose energies are not symmetrical with respect to the superconducting chemical potential. At very weak eV, the elastic correction is small compared to the true Andreev current. We expect the PAT current contributions to originate from pairs of electrons in the normal metal below the superconducting chemical potential, which can extract a photon from the environment. At the same time, Cooper pairs can be ejected in the normal metal as a reverse Andreev process provided they borrow a photon to the environment. There is a balance between the right and left currents at a very weak bias.

As the bias is increased, electron pairs whose energies are above this chemical potential will now be able to yield a photon to the environment, giving rise to an increase of the inelastic PAT current. Also, the reverse Andreev process mentioned above becomes more restricted because the available empty states for electrons in the leads lie higher at a positive bias. The elastic PAT current (not shown in the figures) increases when we increase the detector bias but it is always smaller than the inelastic contribution. The total PAT current increases gradually (Figure 5.5, right panel).

A zoom of this Andreev contribution is made in the region of small biases. There is, in fact, no threshold for the PAT Andreev current: for a small bias, it has a linear behavior (Figure 5.6). According to Eq. (5.36), when $eV \geq eV_d/2$, the inelastic difference current of a Cooper pair tunneling from superconductor to metal lead by absorbing energy from a mesoscopic device vanishes. The PAT current now describes two electrons tunneling from metal to superconductor elastically or inelastically. In this intermediate bias regime, the elastic and inelastic contributions now have a tendency to cancel each other. The

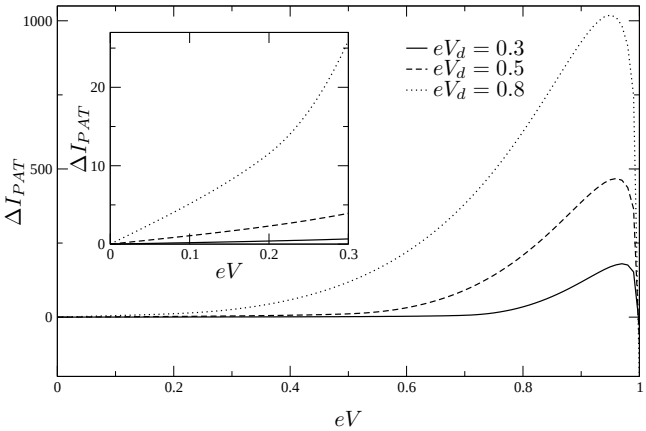

Figure 5.6: Andreev reflection contribution to ΔI_{PAT} plotted as a function of the dc bias voltage for a mesoscopic device voltage bias eV_d: 0.3 (continuous line), 0.5 (dashed line), and 0.8 (dotted line). Same units as in Figure 5.5. The inside panel is a zoom of the same contribution at small eV, displaying a linear behavior.

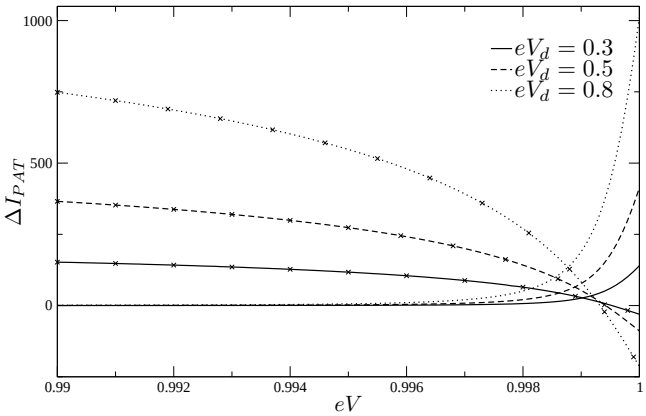

Figure 5.7: Crossover between Andreev reflection (crossed line) and two quasiparticle tunneling current (uncrossed line) close to the gap for a mesoscopic device voltage bias eV_d: 0.3 (continuous line), 0.5 (dashed line), and 0.8 (dotted line). Same units as in Figure 5.5.

current reaches a maximum close to the gap, and then it decreases dramatically at the gap. This is consistent with the fact that for a positive bias, the initial state for two quasiparticle tunneling processes and for Andreev reflection is precisely the same: close to the gap, two quasiparticle tunneling takes over the Andreev process. It becomes more efficient for electrons to be activated above the gap than to be converted into a Cooper pair because the energy loss needed for the latter is quite large. Unlike a conventional NS junction with elastic scattering only, where the relative importance of quasiparticle tunneling and Andreev reflection are interchanged precisely at the gap, here the dominance of quasiparticle tunneling manifests itself before the voltage bias reaches the gap. Note also in Figure 5.5 that the magnitude of the Andreev current before the two quasiparticle threshold is precisely the same as the magnitude of the two quasiparticles at $eV = \Delta$, which confirms this conversion scenario. A comparison of the two processes is displayed in Figure 5.7.

In practice, the different contributions to the PAT current cannot be separated: we measure the sum of the three contributions which are plotted in Figure 5.5. However, we claim that for a broad voltage range (from $eV = 0$ to the two quasiparticle threshold), the main contribution to the current comes from photo-assisted Andreev processes. The

confrontation of Eq. (5.36) with an experimental measurement of the PAT current below the gap could thus serve as an effective noise measurement, as the weight functions $K^{el}_{NS}(\omega, eV, \eta)$ and $K^{inel}_{NS}(\Omega, eV, \eta)$ are known.

Notice that in all our numerical results, the PAT currents are plotted in units of $e^3R^2\mathcal{T}^2T(1-T)\Delta/8\pi^3\hbar^2R_K$. We put some tentative numbers in these quantities. Here, $\mathcal{T} = 0.6$ is the effective transmission coefficient of the NS interface, $\Delta = 240\,\mu eV$, $T = 0.5$ is the transmission of the quantum point contact to be measured, and $R = 0.03R_K$ (R_K is the resistance quantum) is the resistance which enters the transimpedance. This implies, e.g., for the PAT current in Figure 5.6 at the top of the peak that $\Delta I_{PAT} \simeq 10^{-10}A$ with the device bias $V_d = 0.8\Delta/e = 48\,\mu V$, which seems an acceptable value compatible with current measurement techniques.

5.3 Tunneling current through a NDS junction

We now turn to a different setup for noise detection where electrons in a normal metal lead transit through a quantum dot in the Coulomb blockade regime before going into the superconductor. The essential ingredients are the same as in the previous section, except that additional energy filtering occurs because of the dot. In this section, we choose the parameters of the device so that only Andreev processes are relevant.

5.3.1 Model Hamiltonian

The Hamiltonian which describes the decoupled normal metal lead–dot–superconductor–environment (mesoscopic circuit) system reads

$$H_0 = H_{0_L} + H_{0_D} + H_{0_S} + H_{env} \ , \tag{5.39}$$

where the Hamiltonian of the normal metal lead and the superconductor lead are described as above.

The Hamiltonian for the quantum dot reads

$$H_{0_D} \ = \ \sum_{\sigma} \epsilon_D c^{\dagger}_{D,\sigma} c_{D,\sigma} + U n_{\uparrow} n_{\downarrow} \ , \tag{5.40}$$

where U will be assumed to be infinite, assuming a small capacitance of the dot. We consider that the dot possesses only a single energy level for simplicity.

The tunneling Hamiltonian includes the electron tunneling between the superconductor and the dot, as well as the tunneling between the dot and the normal metal lead,

$$\begin{aligned} H_T &= (H_{T1} + H_{T2}) + \text{H.c} \ , \\ H_{T1} &= \sum_{q,\sigma} T_{D,q} c^{\dagger}_{D,\sigma} c_{q,\sigma} e^{-i\phi} \ , \\ H_{T2} &= \sum_{k,\sigma} T_{k,D} c^{\dagger}_{k,\sigma} c_{D,\sigma} \ , \end{aligned} \tag{5.41}$$

where the indices k, D, and q refer to the normal metal lead, quantum dot, and superconductor. We consider the simple case $T_{D,q} = T_1$, and $T_{k,D} = T_2$.

For photo-assisted Andreev processes, we need to carry out calculations of the matrix element in Eq. (5.6) to fourth order in the tunneling Hamiltonian. In what follows, we

assume that the dot is initially empty, owing to the asymmetry between the two tunnel barriers. The barrier between the normal metal lead and the dot is supposed to be opaque compared to that between the dot and the superconductor. As a result, the rate of escape of electrons from the dot to the superconductor is substantially larger than the tunneling rate of electrons from the normal lead to the dot (see below for actual numbers).

There are two possibilities for charge transfer processes: a Cooper pair in the superconductor is transmitted to the normal lead or vice versa. The first process involves the electron from a Cooper pair tunneling onto the dot; next, this electron escapes in the lead; the other electron from the same Cooper pair then undergoes the same two tunneling processes. Similar transitions, in the opposite direction, are necessary for two electrons from the normal lead to end up as a Cooper pair in the superconductor. Note that this description of events assumes implicity that the superconductor lead remains in the ground state in the initial and final states (Andreev process). On the other hand, if the normal metal lead is initially in the ground state (filled Fermi sea), it is left in an excited state with two electrons having energies above Fermi energy E_F in the final state. The extra energy has been provided by the environment. Typically,

$$|i\rangle = |G_L\rangle \otimes |G_S\rangle \otimes |0_{QD}\rangle \otimes |R\rangle \ , \tag{5.42}$$

where $|G_{L,S}\rangle$ denotes a ground state, which corresponds to a filled Fermi sea for the normal electrode. $|0_{QD}\rangle$ is the vacuum of the quantum dot and $|R\rangle$ denotes the initial state of the environment. On the other hand our guess for the final state should read

$$|f\rangle = 2^{-1/2}[c^\dagger_{k,\sigma}c^\dagger_{k',-\sigma} - c^\dagger_{k',\sigma}c^\dagger_{k,-\sigma}]|G_L\rangle \otimes |G_S\rangle \otimes |0_{QD}\rangle \otimes |R'\rangle \ , \tag{5.43}$$

when a Cooper pair is emitted from superconductor, or

$$|f\rangle = 2^{-1/2}[c_{k,\sigma}c_{k',-\sigma} - c_{k',\sigma}c_{k,-\sigma}]|G_L\rangle \otimes |G_S\rangle \otimes |0_{QD}\rangle \otimes |R'\rangle \ , \tag{5.44}$$

when the superconductor lead absorbs a Cooper pair. Here, $|R'\rangle$ is the final state of the environment. The justification for the choice of Eqs. (5.43) and (5.44) is the same as in section 5.2.5.

5.3.2 General formula for the photo-assisted Andreev current

The technique we use to calculate the current through the NDS junction is the same as the way we obtain the Eq. (5.22). Although we also consider the tunneling process of two electrons but the electrons must have virtual states on quantum dot, then the calculation

of the matrix element in Eq. (5.6) to fourth order in the tunneling Hamiltonian gives

$$
\begin{aligned}
I_{\leftarrow} &= 2e\sum_{f,\upsilon_i}\int_{-\infty}^{\infty}dt e^{i(\epsilon_i-\epsilon_f)t}\langle i|H_T^\dagger|\upsilon_1\rangle\int_0^\infty dt_1' e^{-i(\epsilon_i-\epsilon_{\upsilon_1}-i\eta)t_1'}\langle\upsilon_1|H_T^\dagger|\upsilon_2\rangle\int_0^\infty dt_2' e^{-i(\epsilon_i-\epsilon_{\upsilon_2}-i\eta)t_2'}\\
&\times\langle\upsilon_2|H_T^\dagger|\upsilon_3\rangle\int_0^\infty dt_3' e^{-i(\epsilon_i-\epsilon_{\upsilon_3}-i\eta)t_3'}\langle\upsilon_3|H_T^\dagger|f\rangle\langle f|H_T|\upsilon_4\rangle\int_0^\infty dt_3 e^{i(\epsilon_i-\epsilon_{\upsilon_4}+i\eta)t_3}\\
&\times\langle\upsilon_4|H_T|\upsilon_5\rangle\int_0^\infty dt_2 e^{i(\epsilon_i-\epsilon_{\upsilon_5}+i\eta)t_2}\langle\upsilon_5|H_T|\upsilon_6\rangle\int_0^\infty dt_1 e^{i(\epsilon_i-\epsilon_{\upsilon_6}+i\eta)t_1}\langle\upsilon_6|H_T|i\rangle\\
&= 2e\sum_{f,\upsilon_i}\int_{-\infty}^{\infty}dt\int_0^\infty dt_1\int_0^\infty dt_2\int_0^\infty dt_3\int_0^\infty dt_1'\int_0^\infty dt_2'\int_0^\infty dt_3' e^{-\eta(t_1+t_2+t_3+t_1'+t_2'+t_3')}\\
&\times\langle i|H_T^\dagger|\upsilon_1\rangle e^{i\epsilon_i(t-t_1'-t_2'-t_3')}e^{i\epsilon_{\upsilon_1}t_1'}\langle\upsilon_1|H_T^\dagger|\upsilon_2\rangle e^{i\epsilon_{\upsilon_2}t_2'}\langle\upsilon_2|H_T^\dagger|\upsilon_3\rangle e^{i\epsilon_{\upsilon_3}t_3'}\langle\upsilon_3|H_T^\dagger|f\rangle\\
&\times e^{-i\epsilon_f t}\langle f|H_T|\upsilon_4\rangle e^{i\epsilon_i(t_1+t_2+t_3)}e^{-i\epsilon_{\upsilon_4}t_3}\langle\upsilon_4|H_T|\upsilon_5\rangle e^{-i\epsilon_{\upsilon_5}t_2}\langle\upsilon_5|H_T|\upsilon_6\rangle e^{-i\epsilon_{\upsilon_6}t_1}\langle\upsilon_6|H_T|i\rangle\ .
\end{aligned}
\tag{5.45}
$$

Eq. (5.45) describes evidently the tunneling of two electrons from the superconductor to the normal metal lead via a quantum dot, and back again, with the delay times between two hopping steps are given by t_1, t_2, t_3, t_3', t_2', t_1', respectively, and the time between the destroying and creating a Cooper pair is given by t. This tunneling process makes the corresponding current being as

$$
\begin{aligned}
I_{\leftarrow} &= 2e\int_{-\infty}^{\infty}dt\int_0^\infty dt_1\int_0^\infty dt_2\int_0^\infty dt_3\int_0^\infty dt_1'\int_0^\infty dt_2'\int_0^\infty dt_3' e^{-\eta(t_1+t_2+t_3+t_1'+t_2'+t_3')}\\
&\times e^{i\mu_S(2t-t_1'-t_2'-2t_3'-t_1-t_2)}e^{-i\mu_L(2t-t_2'-t_3'-2t_1-t_2-t_3)}\\
&\times\langle H_{T1}^\dagger(t-t_1'-t_2'-t_3')H_{T2}^\dagger(t-t_2'-t_3')H_{T1}^\dagger(t-t_3')H_{T2}^\dagger(t)\\
&\times H_{T2}(t_1+t_2+t_3)H_{T1}(t_1+t_2)H_{T2}(t_1)H_{T1}(0)\rangle\ .
\end{aligned}
\tag{5.46}
$$

The problem is thus reduced to the calculation of correlators of the tunneling Hamiltonian in the ground state. Using Wick's theorem, these can be expressed in terms of a single particle Green's function because the Hamiltonian of the isolated components is quadratic (except maybe for the environment, which is dealt separately). The detail of this calculation is shown in Appendix E. We can now write the tunneling current as a function of the normal (and anomalous) Green's functions of the normal metal lead, $G_{L\sigma}$, the quantum dot, $G_{D\sigma}$, and the superconductor, F_σ (which are shown in Appendix C),

$$
\begin{aligned}
I_{\leftarrow} &= 2eT_1^4T_2^4\int_{-\infty}^{\infty}dt\int_0^\infty dt_1\int_0^\infty dt_2\int_0^\infty dt_3\int_0^\infty dt_1'\int_0^\infty dt_2'\int_0^\infty dt_3' e^{-\eta(t_1+t_2+t_3+t_1'+t_2'+t_3')}\\
&\times e^{i\mu_S(2t-t_1'-t_2'-2t_3'-t_1-t_2)}e^{-i\mu_L(2t-t_2'-t_3'-2t_1-t_2-t_3)}\\
&\times\sum_{k,k',q,q',\sigma}\Big[-F_\sigma^*(q',-t_1'-t_2')F_{-\sigma}(q,t_1+t_2)G_{L\sigma}^>(k,t-t_2'-t_3'-t_1-t_2-t_3)G_{L-\sigma}^>(k',t-t_1)\\
&\times G_{D\sigma}^{\tilde{t}}(-t_1')G_{D-\sigma}^{\tilde{t}}(-t_3')G_{D\sigma}^t(t_3)G_{D-\sigma}^t(t_1)+F_\sigma^*(q',-t_1'-t_2')F_\sigma(q,t_1+t_2)\\
&\times G_{L\sigma}^>(k,t-t_2'-t_3'-t_1)G_{L-\sigma}^>(k',t-t_1-t_2-t_3)G_{D\sigma}^{\tilde{t}}(-t_1')G_{D-\sigma}^{\tilde{t}}(-t_3')G_{D-\sigma}^t(t_3)G_{D\sigma}^t(t_1)\Big]\\
&\times e^{J(t-t_1'-t_2'-t_3')+J(t-t_3')+J(t-t_1'-t_2'-t_3'-t_1-t_2)+J(t-t_3'-t_1-t_2)-J(-t_1'-t_2')-J(t_1+t_2)}\ .
\end{aligned}
\tag{5.47}
$$

The result for the current contains both an elastic and an inelastic contribution. The elastic contribution reads

$$I_{\leftarrow}^{el} \simeq \frac{e\gamma_1^2\gamma_2^2}{2\pi^3}\int_{eV}^{-eV} d\epsilon \int_{\Delta}^{\infty} dE \int_{\Delta}^{\infty} dE' \frac{\Delta^2}{\sqrt{E^2-\Delta^2}\sqrt{E'^2-\Delta^2}}$$
$$\times \left\{ \left[1 - \frac{4\pi}{R_K}\int_{-\infty}^{+\infty} d\omega \frac{|Z(\omega)|^2}{\omega^2} S_I(\omega) \right] \frac{1}{D_{\leftarrow}^0} - \frac{2\pi}{R_K}\int_{-\infty}^{+\infty} d\omega \frac{|Z(\omega)|^2}{\omega^2}\frac{S_I(\omega)}{D_{\leftarrow}^{el}} \right\} , \quad (5.48)$$

where $D_{\leftarrow}^0$ is the original denominator which is not affected by the environment, which is defined by Eq. (5.75), and $D_{\leftarrow}^{el}$ is the denominator product affected by the environment (see Eq. (5.76) of Appendix F). The inelastic contribution reads

$$I_{\leftarrow}^{inel} \simeq \frac{e\gamma_1^2\gamma_2^2}{\pi^2 R_K}\int_{eV}^{\infty} d\epsilon \int_{eV}^{\infty} d\epsilon' \int_{\Delta}^{\infty} dE \int_{\Delta}^{\infty} dE'$$
$$\times \frac{\Delta^2}{\sqrt{E^2-\Delta^2}\sqrt{E'^2-\Delta^2}} \frac{|Z(-(\epsilon+\epsilon'))|^2}{(\epsilon+\epsilon')^2} \frac{S_I(-(\epsilon+\epsilon'))}{D_{\leftarrow}^{inel}}, \quad (5.49)$$

where $D_{\leftarrow}^{inel}$ is the denominator product attributed to the inelastic current, which is defined in Eq. (5.77) of Appendix F.

Here, $\gamma_1 = 2\pi\mathcal{N}_S T_1^2$ and $\gamma_2 = 2\pi\mathcal{N}_N T_2^2$ define the tunneling rates between the superconductor and the dot and between the dot and the normal metal lead, respectively, with $\mathcal{N}_S$ and $\mathcal{N}_N$ as the density of states per spin of the two metals in the normal state at the chemical potentials μ_S and μ_L, respectively. All contributions to the current contain denominators where the infinitesimal η (adiabatic switching parameter) is included in order to avoid divergences. In fact, it has been shown in Refs. [90] and [95] that a proper resummation of the perturbation series, including all round trips from the dot to the normal leads, leads to a broadening of the dot level. We take into account this broadening by replacing η by $\gamma/2$, with $\gamma = \gamma_1 + \gamma_2$ into our calculations (including only a broadening due to the superconductor). As mentioned above, we have assumed that $\gamma_1 \gg \gamma_2$. In order to avoid the excitation of quasiparticles above the gap, these rates also need to fulfill the condition $\epsilon_D + \gamma < \Delta$. In what follows, we keep the notation η in our expressions, bearing in mind that it represents the linewidth associated with the leads. For numerical purposes, it will be sufficient to assume that η is kept very small compared to the superconducting gap, as well as all the relevant level energies (dot level position, bias voltages, etc.).

The above expressions constitute the second main result of this work: we understand now how the current fluctuations in the neighboring mesoscopic circuit give rise to inelastic and elastic contributions in the current in the NDS device.

We find that both right and left current contributions have the same form. The current-current fluctuations of the mesoscopic device affect the detector current at the energy corresponding to the total energy of two electrons exiting in (or entering from) the normal lead. Therefore, we proceed to the same change of variables a for the single NS junction.

For $eV > 0$, elastic current contributions in $I_{\rightarrow}$ are present but the same contributions in $I_{\leftarrow}$ vanish (the opposite is true for the case of $eV < 0$). Changing variables in the inelastic contributions and defining the kernel functions $K_{NDS}^{el}(\omega, eV, \epsilon_D, \eta)$ and

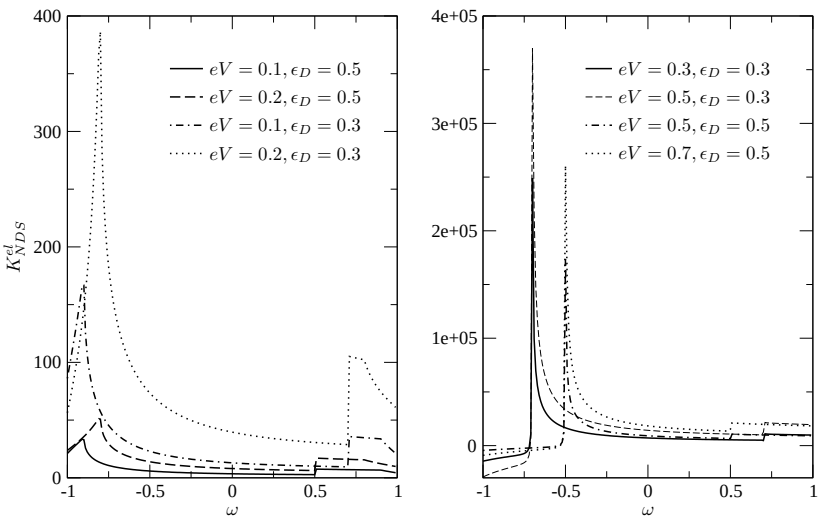

Figure 5.8: The weight function K^{el}_{NDS} as a function of frequency ω. Right panel, $|eV| \geq \epsilon_D$; left panel $|eV| < \epsilon_D$.

$K^{inel}_{NDS}(\Omega, eV, \epsilon_D, \eta)$ as in Appendix F, for $eV > 0$ and $eV < 0$, we obtain

$$\begin{aligned}\Delta I_{PAT}(eV) &= -C_{NDS}\int_{-\infty}^{+\infty} d\omega \frac{|Z(\omega)|^2}{\omega^2} S^+_{excess}(-\omega) K^{el}_{NDS}(\omega, eV, \epsilon_D, \eta) \\ &\quad -\frac{C_{NDS}}{2}\int_{-\infty}^{2eV} d\Omega \frac{|Z(\Omega)|^2}{\Omega^2} S^+_{excess}(-\Omega) K^{inel}_{NDS}(\Omega, eV, \epsilon_D, \eta) \\ &\quad -\frac{C_{NDS}}{2}\int_{2eV}^{\infty} d\Omega \frac{|Z(-\Omega)|^2}{\Omega^2} S^+_{excess}(\Omega) K^{inel}_{NDS}(\Omega, eV, \epsilon_D, \eta) \ , \qquad (5.50)\end{aligned}$$

with $C_{NDS} = e\gamma_1^2\gamma_2^2\Delta^2/\pi^2 R_K$.

The first term in Eq. (5.50) describes the elastic contribution in the PAT current. Although we are less interested in this contribution, we cannot ignore it in practice because it contributes to the total ΔI_{PAT}. The environment affects this current contribution, but at the end of the tunneling processes, there is no energy exchange between the device and the detector circuit. The second term in Eq. (5.50) describes the tunneling of a Cooper pair from the normal lead to the superconductor via the quantum dot, with energy exchange. The electrons can absorb energy (in case their total energy is smaller than the superconductor chemical potential μ_S) or emit energy (if their total energy is bigger than μ_S). The last term in Eq. (5.50) describes the inverse tunneling process: a Cooper pair absorbs energy from the neighboring device; its constituent electrons then tunnel to the normal lead. In this event, the total energy of the outgoing electrons is positive. If, on the contrary, this total energy is negative, then the Cooper pair has emitted energy to the device.

In order to understand how the detector circuit affects the behavior of the current (in the presence of the environment), we investigate the weight functions $K^{el}_{NDS}(\omega, eV, \epsilon_D, \eta)$ and $K^{inel}_{NDS}(\Omega, eV, \epsilon_D, \eta)$ separately. The weight function $K^{el}_{NDS}(\omega, eV, \epsilon_D, \eta)$ is plotted in Figure 5.8 as a function of frequency ω for two values of the bias voltage and two values of the dot level position. This elastic kernel is symmetric under a bias voltage reversal $[K^{el}_{NDS}(-eV) = -K^{el}_{NDS}(eV)]$. From the right panel of this figure, where we consider $|eV| \geq \epsilon_D$, we find that there is a small step at $\omega = \Delta - \epsilon_D$ and a sharp peak at $\omega = -\Delta + \epsilon_D$. The peak is asymmetric, and its height is much larger than that of the

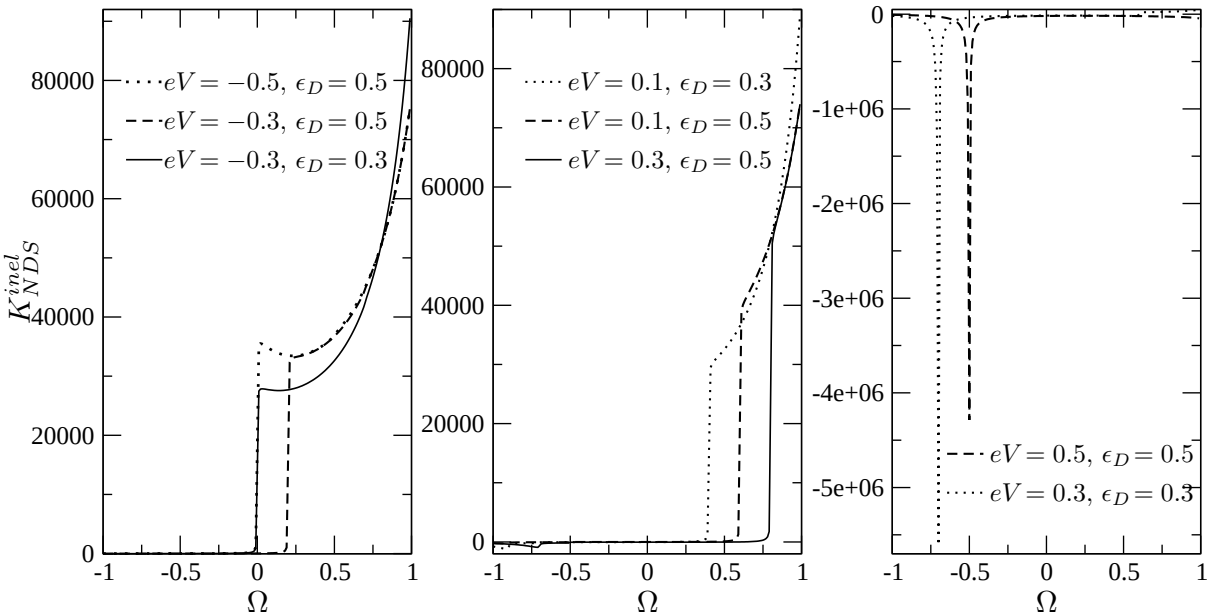

Figure 5.9: the weight function K^{inel}_{NDS} as a function of frequency Ω. Left panel, $eV < 0$; center panel $0 < eV < \epsilon_D$; right panel $eV \geq \epsilon_D$ (the same is true for $eV \geq \epsilon_D$.

step. When $\omega < -\Delta + \epsilon_D$, K^{el}_{NDS} changes sign and becomes negative. The voltage bias eV mainly affects the amplitude of the peak and of the step in K^{el}_{NDS}. The left panel of Figure 5.8 describes K^{el}_{NDS} when $|eV| < \epsilon_D$. The peak height decreases quite fast as a function of eV, and its location is shifted at $\omega = -\Delta + eV$. The peak is symmetric for a large bias.

We turn now to the truly photo-assisted processes, which involve either absorption or emission of energy. The kernel $K^{inel}_{NDS}(\Omega, eV, \epsilon_D, \eta)$ is plotted in Figure 5.9 as a function of frequency Ω, which corresponds to the total energy of two electrons, for $\epsilon_D > 0$. In the left panel, eV is negative, and in the center panel, eV is positive but $eV < \epsilon_D$, and finally the right panel of Figure 5.9 describes $eV \geq \epsilon_D$. We find that when $eV < \epsilon_D$, there is a step at $\Omega = \epsilon_D + eV$. When we increase eV close to ϵ_D, the step still dominates K^{inel}_{NDS} but there is a small peak at $\Omega = -\Delta + eV$. When $eV \geq \epsilon_D$ this, (inverted) peak is very sharp. This is explicit in the right panel. The inverted peak, which has a large amplitude, makes it now difficult to observe the step. The (inverted) peak is located at $\Omega = -\Delta + \epsilon_D$. Again, eV mostly affects the amplitude of K^{inel}_{NDS}. For $\epsilon_D < 0$ (not shown), the result is similar to that of $\epsilon_D > 0$ with opposite eV, but the amplitude of the peak is doubled compared to that of $\epsilon_D > 0$ when $|eV| \geq |\epsilon_D|$.

Note that understanding the behavior of the two weight functions as a function of the different parameters (eV and ϵ_D) of the detector is crucial. It allows us to control the effect of the device voltage bias eV_d on the dc current of the detector, and it is therefore the key for extracting the noise from the measurement of this dc current.

5.3.3 Application to a quantum point contact

We now calculate ΔI_{PAT} from Eq. (5.50) with the spectral density of excess noise of a quantum point contact, given by Eq. (5.37). We consider the PAT current as a function of the detector voltage eV for several values of the device voltage eV_d, which are shown in Figure 5.10. We find that there are two values of eV at which ΔI_{PAT} changes drastically. First, there is a step located at $eV = \epsilon_D$ and second, a Fano-like peak appears at $eV =$

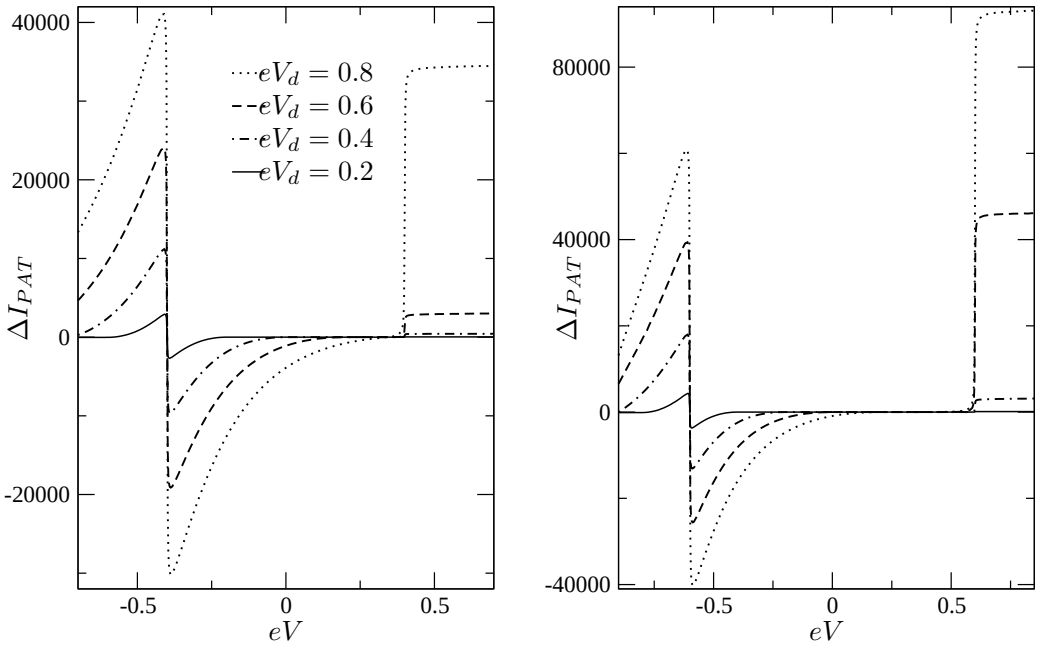

Figure 5.10: ΔI_{PAT} plotted as a function of the detector bias voltage for dot energy level: $\epsilon_D = 0.4$ (left panel) and 0.6 (right panel) and for several values of device bias eV_d.

$-\epsilon_D$. The (negative) derivative at $eV = -\epsilon_D$ seems to diverge. The height of both the peak and the step increases in a monotonous manner as a function of the ratio of the device voltage eV_d divided by the dot level ϵ_D. When eV_d is small, the peak is much higher than the step. Increasing eV_d, the peak further increases, but the step height increases faster, starting from the threshold device voltage $eV_d = \Delta - \epsilon_D$. In Figure 5.10, we find that for $\epsilon_D = 0.4$ and $eV_d = 0.8$, the peak height is still higher than the step, but with $\epsilon_D = 0.6$ and $eV_d = 0.6$, the step becomes higher than the peak. Here, for specificity, we only consider the case where $\epsilon_D > 0$, but results for $\epsilon_D < 0$ can be obtained in a similar manner, exploiting electron hole symmetry.

In order to further understand the behavior of ΔI_{PAT}, we consider the different contributions of this photo-assisted current, which are shown in Figure 5.11. Specifically, we plot the elastic current renormalized by the environment, as well as the right and left inelastic currents. We find that the elastic part is symmetric between eV positive and negative. It is almost equal to zero when $|eV| < \epsilon_D$. It shows a step at $|eV| = \epsilon_D$. This can be understood from the fact that at the threshold $eV = \epsilon_D$, electrons tunnel from the normal metal lead to the superconductor predominantly by making resonant transitions through the dot. Electrons easily tunnel to the quantum dot, in a sequential manner becoming a Cooper pair in the superconductor. For $eV = -\epsilon_D$, the same reasoning can be made for incoming holes or, equivalently, for electrons exiting the superconductor: a Cooper pair in the superconductor is split into two electrons, which tunnel to the quantum dot and then to the normal metal lead. Because of the energy conservation condition, it is then necessary to have $eV < -\epsilon_D$.

Turning now to the inelastic current, we consider the contribution of two electrons being transferred inelastically from the normal metal lead to the superconductor, which is called the I_R^{inel} in Figure 5.11. When $eV < \epsilon_D$, electrons tunnel through the quantum dot to the superconductor by absorbing or emitting energy to the environment. However, as in the elastic case, the transfer from the normal metal to the dot is more favorable when $eV > \epsilon_D$, which explains the presence of the step in I_R^{inel} at this bias voltage.

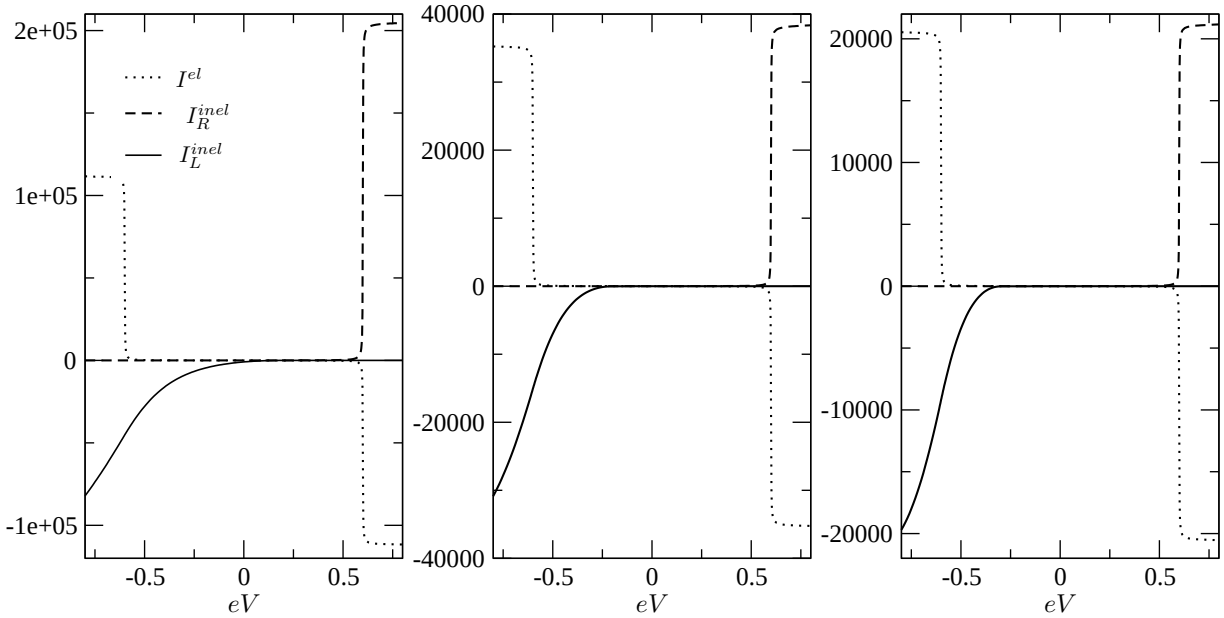

Figure 5.11: Elastic and inelastic contributions to ΔI_{PAT}, as a function of detector bias voltage. The dot energy level is fixed at $\epsilon_D = 0.6$. The mesoscopic device bias eV_d is 0.8 (left panel), 0.4 (center panel), and 0.3 (right panel).

Next, we consider the contribution of two electrons tunneling from the superconductor to the normal metal lead, which is called I_L^{inel} in Figure 5.11. When eV is positive, I_L^{inel} is nonzero only when $eV_d > 2eV$, this case corresponds to the process of the Cooper pair absorbing energy from the environment to tunnel to the normal metal lead. If $2\epsilon_D < eV_d$, a small step occurs (not shown) at $eV = \epsilon_D$ corresponding to the activation of the two Cooper pair electrons on the dot: this small feature can only be seen by zooming in the picture. When eV is negative, the absorption of energy from the environment becomes much more favorable. Because of this, the analog of the step corresponding to $eV = -\epsilon_D$ in the elastic current is smoothed out, and it saturates around $eV = -\epsilon_D$. Nevertheless, I_L^{inel} also contains contributions where electrons emit energy to the environment. Starting from $eV < 0$, the process of the Cooper pair tunneling to the normal metal lead and emitting energy to the environment has, first, a small contribution to I_L^{inel}, but it really becomes noticeable below $eV = -\epsilon_D$ and eventually saturates for a lower bias voltage (not shown). As the voltage of the mesoscopic device is lowered (left to right panels of Figure 5.11), two things occur: first, the amplitude of all current contributions decreases; second, the smoothing of the I_L^{inel} is reduced because the range of energies available to absorption and emission is reduced.

In brief, the sum of the contributions for emission and absorption in I_L^{inel} has a tendency to compensate the elastic current at voltages where saturation is reached. From the above considerations, we can therefore interpret the curve of ΔI_{PAT}, and we understand when the detector circuit absorbs or emits energy from or to the mesoscopic device: when eV is negative, the PAT current is mainly due to absorption for $|eV| < \epsilon_D$ and emission for $|eV| > \epsilon_D$.

Note that in all our numerical results, the PAT current is in units of $2e^3R^2\gamma_1^2\gamma_2^2T(1-T)/\pi^3\hbar^2\Delta^3R_K$. To check the observability of these predictions we estimate $\gamma_1 = 0.2\Delta$, $\gamma_2 = 0.02\Delta$, $\Delta = 240\,\mu eV$, $R = 0.03R_K$, and $T = 0.5$ (see also Refs. [20, 21, 22, 92]). This implies, e.g., for the PAT current in Figure 5.10 when the detector bias is close to $\pm\epsilon_D$ that $I_{PAT} \simeq 5 - 10\,pA$ with the device bias $V_d = 0.8\Delta/e = 48\,\mu V$. This value is

acceptable if we compare it with the value of current which has been estimated in Ref. [20]. It is also acceptable with present day detection techniques.

5.4 Conclusion

In conclusion, we have presented a capacitive coupling scheme to study the high frequency spectral density of noise of a mesoscopic device. As in the initial proposal of Ref. [20], the effect of the noise originating from a mesoscopic device triggers an inelastic dc current in the detector circuit. This inelastic contribution can be thought as a dynamical Coulomb blockade effect where the phase fluctuations at a specific junction in the detector circuit junction are related to voltage fluctuations in the same junction. In turn, such voltage fluctuations originate from the current fluctuations in the nearby mesoscopic device, and both are related by a trans-impedance. The novelty is that here, because the junction contains a superconducting element, in the subgap regime, two electrons need to be transferred as the elementary charge tunneling process. In a conventional elastic tunneling situation, the two electrons injected from (ejected in) the normal metal lead need to have exactly opposite energies in order to combine as a Cooper pair in the superconductor. Here, this energy conservation can be violated in a controlled manner because a photon originating from the mesoscopic circuit can be provided to or from the constituent electrons of the Cooper pair in the tunneling process.

We have computed the dc current in the detector circuit for two different situations. In a first step, we considered a single NS junction, and we computed all lowest order inelastic charge transfer processes which can be involved in the measurement of noise: the photo-assisted transfer of single (and pairs of) electrons (with energies within the gap) into quasiparticle(s) above the gap and the photo-assisted Andreev transfer of electrons as a Cooper pair in the subgap regime. It was shown that the latter process dominates when the source drain bias is kept well within the gap. Close but below the gap, the absorption of quasiparticle dominates, and we observe a crossover in the current between the Andreev and quasiparticle contributions. For the above processes, we demonstrated the dependence of the dc current on the voltage bias of the mesoscopic device, chosen here to be a quantum point contact. When this bias eV_d is increased, the overall amplitude of the spectral density and its width scale as V_d, so that the phase space (the energy range) of electrons, which can contribute to the Andreev processes is magnified. We have therefore gained an understanding about how the measurement of the dc current can provide useful information on the noise of the mesoscopic device. Nevertheless, we should point out that with this NS setup, it is difficult to isolate the contribution of the photo-assisted current which involves, respectively, the absorption and the emission of photons from the mesoscopic device. For biases close to the chemical potential of the superconductor, both will typically contribute to the photo-assisted current.

Next, we considered a more complex detector circuit where the normal metal and the superconductor are separated by a quantum dot which can only accommodate a single electron at a given time. There, the dot acts as an additional energy filtering device, with the aim of achieving a selection between photon emission and absorption processes. We decided to restrict ourselves to the photo-assisted Andreev (subgap) regime, assuming that the dot level is well within the gap. By computing the total excess photo-assisted current as well as its different contributions for absorption and emission, and right and left currents, we found that for dc bias voltages comparable to $eV = -\epsilon_D$ it is possible to make such a distinction. The NDS detection setup could therefore provide more information

on the spectral density of noise than the NS setup, but its diagnosis would involve the measurement of smaller currents than the NS setup, because of the presence of two tunnel barriers instead of one.

Note that the normal metal lead–quantum dot–superconductor setups have already been investigated theoretically [96] and experimentally recently [97]. In such works, the emphasis was to study how the physics of Andreev reflection affected the Kondo anomaly in the current voltage characteristics. In Ref. [97], the quantum dot consisted of a carbon nanotube making the junction between a normal metal lead and a superconductor. Here, we did not consider the quantum dot in the Kondo regime, and we included interactions on the dot in the Coulomb blockade regime.

A central point of this study is the fact that all contributions to the photo-assisted current, for both the NS and NDS setups, can be cast in the same form,

$$\Delta I_{PAT}(eV) \propto \int d\Omega \frac{|Z(\Omega)|^2}{\Omega^2} S^+_{excess}(\pm\Omega) K_{process}(\Omega, eV, \cdots) \ . \tag{5.51}$$

Where $K_{process}$ is a kernel which depends on the nature (elastic or inelastic) as well as the mechanism (single quasi-particle or pair tunneling) of the charge transfer process. When dealing with an elastic process, we understand that the environment renormalizes the dc current even when no photon is exchanged between the two circuits. In the case of inelastic tunneling only, the frequency Ω corresponds to the total energy of the two electrons which enter (exit) the superconductor from (to) the normal metal lead. Finally, the sign of the frequency (and thus the bound of the integral in Eq. (5.51), which are left "blank" here) decides whether a given contribution corresponds to the absorption or to the emission of a photon from the mesoscopic circuit.

The present proposal has been tested using a quantum point contact as a noise source because the spectral density of excess noise is well characterized and because it has a simple form. It would be useful to test the present model to situations where the noise spectrum exhibits cusps or singularities. Cusps are known to occur in the high frequency (close to the gap) noise of normal superconducting junctions. Singularities in the noise are known to occur in chiral Luttinger liquid, tested in the context of the fractional quantum Hall effect[98]. Such singularities or cusps should be easy to recognize in our proposed measurement of the photo-assisted current.

On general grounds, we have proposed a mechanism which couples a normal metal–superconductor circuit to a mesoscopic device with the goal of understanding the noise of the latter. The present setup suggests that it is plausible to extract information about high frequency noise. High frequency noise detection now constitutes an important subfield of nanoscopic or mesoscopic physics. Measurement setup schemes which can be placed "onchip" next to the circuit to be measured are useful for a further understanding of high frequency current moments.

5.5 Appendix

5.5.1 Appendix A

In this appendix, we consider the average of exponents of the phase at different time.

Following the theorem in quantum mechanic for operators, if $C \equiv [A, B]$ satisfies $[A, C] = [B, C] = 0$, then

$$e^A e^B = e^{A+B} e^{C/2} \ , \tag{5.52}$$

and if A is linear in Bose creation and annihilation operators, we have

$$\langle e^A \rangle = e^{\langle A^2 \rangle/2} \ . \tag{5.53}$$

From these two properties, if C is a $\mathbb{C}$-number then $C = \langle C \rangle = \langle AB \rangle - \langle BA \rangle$, we easily obtain

$$\langle e^A e^B \rangle = \exp\left[\left\langle AB + \frac{A^2+B^2}{2} \right\rangle\right] \ . \tag{5.54}$$

Similar, for a four-point correlation function,

$$\langle e^{A_1} e^{A_2} e^{A_3} e^{A_4} \rangle = \langle e^{A_1+A_2} e^{A_3+A_4} \rangle e^{[A_1,A_2]/2} e^{[A_3,A_4]/2} \ . \tag{5.55}$$

Since $A_i + A_j$, $(i,j = 1,2,3,4)$ is also linear in Bose creation and annihilation operators, we can perform the average of the exponents as

$$\begin{aligned} \langle e^{A_1+A_2} e^{A_3+A_4} \rangle &= \exp\left[\left\langle (A_1+A_2)(A_3+A_4) + \frac{(A_1+A_2)^2 + (A_3+A_4)^2}{2} \right\rangle\right] \\ &= \exp\left[\left\langle \sum_{i<j} A_i A_j + \frac{1}{2}\sum_i A_i^2 \right\rangle\right] \ . \end{aligned} \tag{5.56}$$

We apply these results to our calculations with the phase $\phi(t) = e\int_{-\infty}^{t} dt' V(t')$, $V(t)$ voltage of the mesoscopic device where we would like to measure noise. If noise is Gaussian, $\phi(t)$ is linear in bosons. We also find that $[\phi(t), \phi(t')] = 0$. These properties of $\phi(t)$ satisfy the conditions to apply Eqs. (5.54) and (5.56). Indeed, $\langle \phi^2(t) \rangle = \langle \phi^2(0) \rangle$, we have

$$\langle e^{i\phi(t)} e^{-i\phi(0)} \rangle = e^{J(t)} \ , \tag{5.57}$$

and

$$\langle e^{i\phi(t3)} e^{i\phi(t2)} e^{-i\phi(t1)} e^{-i\phi(0)} \rangle = \exp[J(t_3) + J(t_2) + J(t_3 - t_1) + J(t_2 - t_1) - J(t_3 - t_2) - J(t_1)] \ , \tag{5.58}$$

where we recall here $J(t) = \langle [\phi(t) - \phi(0)]\phi(0) \rangle$.

5.5.2 Appendix B

In this appendix, we define $\Psi_{0\leftarrow}$, $K^{el}_{2e\leftarrow}(\omega, eV, \eta)$, and $K^{inel}_{2e\leftarrow}(\Omega, eV, \eta)$ in Eqs. (5.27) and (5.28) as

$$\Psi_{0\leftarrow} = \int_{\Delta+eV}^{-\Delta-eV} d\delta \sqrt{(\delta - eV)^2 - \Delta^2}\sqrt{(\delta + eV)^2 - \Delta^2} \frac{1}{\delta + i\eta}\left(\frac{1}{\delta + i\eta} - \frac{1}{\delta - i\eta}\right) \ , \tag{5.59}$$

$$\begin{aligned} K^{el}_{2e\leftarrow}(\omega, eV, \eta) &= \int_{\Delta+eV}^{-\Delta-eV} d\delta \sqrt{(\delta - eV)^2 - \Delta^2}\sqrt{(\delta + eV)^2 - \Delta^2} \\ &\times \left[\left(2\frac{1}{\delta + i\eta} + \frac{1}{\delta + \omega + i\eta}\right)\left(\frac{1}{\delta + i\eta} - \frac{1}{\delta - i\eta}\right) + \frac{1}{\delta + i\eta}\left(\frac{1}{\delta - \omega + i\eta} - \frac{1}{\delta + \omega - i\eta}\right)\right] \ , \end{aligned} \tag{5.60}$$

$$\begin{aligned} K^{inel}_{2e\leftarrow}(\Omega, eV, \eta) &= \int_{2\Delta+2eV-\Omega}^{\Omega-2\Delta-2eV} d\delta \sqrt{(\Omega + \delta - 2eV)^2 - 4\Delta^2}\sqrt{(\Omega - \delta - 2eV)^2 - 4\Delta^2} \\ &\times \left(\frac{1}{\frac{\Omega+\delta}{2} + i\eta} - \frac{1}{\frac{\Omega-\delta}{2} - i\eta}\right)\left(\frac{1}{\frac{\Omega-\delta}{2} - i\eta} + \frac{1}{\frac{\Omega+\delta}{2} - i\eta} - \frac{1}{\frac{\Omega+\delta}{2} + i\eta} - \frac{1}{\frac{\Omega-\delta}{2} + i\eta}\right) \ . \end{aligned} \tag{5.61}$$

5.5.3 Appendix C

In this appendix, we recall the definition of Keldysh Green's functions[99].

First, we define the anomalous Green's function, describing the pairing of electrons with opposite spins in the superconductor,

$$F_\sigma(q, t-t') \equiv -\langle T_K c_{-q,-\sigma}(t) c_{q,\sigma}(t')\rangle \ ,$$

$$F^*_\sigma(q, t-t') \equiv \langle T_K c^\dagger_{q,\sigma}(t) c^\dagger_{-q,-\sigma}(t')\rangle \ .$$

If both t and t' are in the upper branch, and $t > t'$ or both t and t' are in the lower branch, and $t' > t$ then $F_\sigma(q, t_+ - t'_+) = F^*_\sigma(q, t_- - t'_-) = \mathrm{sgn}(\sigma) u_q v_q e^{-iE_q(t-t')}$. These Green's functions enter the description of the Andreev process. If we consider the single quasiparticle tunneling in the superconductor, we use the conventional definition of the Green's function as for normal metals.

Secondly, we define the Green's function of the one level QD

$$G_{D\sigma}(t-t') \equiv \langle T_K c_{D\sigma}(t) c^\dagger_{D\sigma}(t')\rangle \ . \tag{5.62}$$

Simplifications occur because the quantum dot has a singly occupied level with energy ϵ_D. The first electron is transferred to the lead before the second hops on the quantum dot so that in our work, we only consider the QD Green's function where both time quantities t and t' are in the upper or lower branch, and the Green's function values only when $t > t'$ if t, t' in the upper branch $G^t_{D\sigma}(t-t') = e^{-i\epsilon_D(t-t')}$ and $t' > t$ if t, t' in the lower branch, then $G^{\tilde{t}}_{D\sigma}(t-t') = e^{-i\epsilon_D(t-t')}$.

The Green's function in the normal metal lead reads

$$G_{L\sigma}(k, t-t') \equiv \langle T_K c_{k\sigma}(t) c^\dagger_{k\sigma}(t')\rangle \ . \tag{5.63}$$

In our work, we consider the cases where two electrons tunneling from or to the normal metal lead, so that we only consider normal metal Green's functions where t and t' are in the different branches. For the case of electrons tunneling from the superconductor to the normal metal, we use the greater Green's function $G^>_{L\sigma}(k, t-t') = e^{-i(\epsilon_k-\mu_L)(t-t')}$, with $\epsilon_k > \mu_L$. For the case of electrons tunneling from the normal metal to the superconductor, we use the lesser Green's function $G^<_{L\sigma}(k, t-t') = -\langle c^\dagger_{k\sigma}(t') c_{k\sigma}(t)\rangle = -e^{-i(\epsilon_k-\mu_L)(t-t')}$, with $\epsilon_k \leq \mu_L$.

5.5.4 Appendix D

In this part, we present the denominator products which appear in the tunneling current through the NS junction as a Cooper pair. Such denominators come from the energy denominators of the transition operator T:

$$(D^0_\leftarrow)^{-1} = \frac{1}{E' + \epsilon + i\eta}\left(\frac{1}{E - \epsilon - i\eta} + \frac{1}{E + \epsilon - i\eta}\right) \ , \tag{5.64}$$

$$\begin{aligned}(D^{el}_\leftarrow)^{-1} &= \frac{1}{E' + \epsilon + \omega + i\eta}\left(\frac{1}{E - \epsilon - i\eta} + \frac{1}{E + \epsilon - i\eta}\right) \\ &+ \frac{1}{E' + \epsilon + i\eta}\left(\frac{1}{E - \epsilon + \omega - i\eta} + \frac{1}{E + \epsilon + \omega - i\eta}\right) \ ,\end{aligned} \tag{5.65}$$

$$
\begin{aligned}
(D_{\leftarrow}^{inel})^{-1} &= \left(\frac{1}{E'-\epsilon'+i\eta}+\frac{1}{E'+\epsilon+i\eta}\right) \\
&\quad \times\left(\frac{1}{E+\epsilon'-i\eta}+\frac{1}{E+\epsilon-i\eta}+\frac{1}{E-\epsilon-i\eta}+\frac{1}{E-\epsilon'-i\eta}\right) . \quad (5.66)
\end{aligned}
$$

We change variables in $I_{\rightarrow}^{inel}$, $I_{\leftarrow}^{inel}$ as

$$
\begin{cases} \Omega = \epsilon + \epsilon' , \\ \delta = \epsilon - \epsilon' . \end{cases}
$$

We define

$$
\chi(x,\eta) \equiv \int_{\Delta}^{\infty} dE \frac{1}{\sqrt{E^2-\Delta^2}} \frac{1}{E-x-i\eta} = \frac{\pi + 2\arcsin(\frac{x+i\eta}{\Delta})}{2\sqrt{\Delta^2-(x+i\eta)^2}} , \quad (5.67)
$$

then, we define the weight functions as

$$
\begin{aligned}
K^{el}(\omega, eV, \eta) &= \int_{-eV}^{eV} d\epsilon \left\{ [2\chi(-\epsilon,-\eta)+\chi(-\epsilon-\omega,-\eta)]\,[\chi(\epsilon,\eta)+\chi(-\epsilon,\eta)] \right. \\
&\quad \left. + \chi(-\epsilon,-\eta)\,[\chi(\epsilon-\omega,\eta)+\chi(-\epsilon-\omega,\eta)] \right\} , \quad (5.68)
\end{aligned}
$$

$$
\begin{aligned}
K^{inel}(\Omega, eV, \eta) &= \int_{2eV-\Omega}^{\Omega-2eV} d\delta \left[\chi(\frac{\Omega-\delta}{2},-\eta)+\chi(-\frac{\Omega+\delta}{2},-\eta)\right] \\
&\quad \times \left[\chi(-\frac{\Omega-\delta}{2},\eta)+\chi(-\frac{\Omega+\delta}{2},\eta)+\chi(\frac{\Omega+\delta}{2},\eta)+\chi(\frac{\Omega-\delta}{2},\eta)\right] . \quad (5.69)
\end{aligned}
$$

5.5.5 Appendix E

In this appendix, we compute the product of tunneling Hamiltonian operators in the (initial) ground state, which is shown in Eq. (5.46).

$$
\begin{aligned}
& \langle H_{T1}^{\dagger}(t-t_1'-t_2'-t_3')H_{T2}^{\dagger}(t-t_2'-t_3')H_{T1}^{\dagger}(t-t_3')H_{T2}^{\dagger}(t) \\
& \times H_{T2}(t_1+t_2+t_3)H_{T1}(t_1+t_2)H_{T2}(t_1)H_{T1}(0)\rangle \\
= \; & T_1^4 T_2^4 \sum_{k_1..k_4,q_1..q_4,\sigma_1..\sigma_8} \langle c_{q_1\sigma_1}^{\dagger}(t-t_1'-t_2'-t_3')c_{q_2\sigma_3}^{\dagger}(t-t_3')c_{q_3\sigma_6}(t_1+t_2)c_{q_4\sigma_8}(0)\rangle \\
& \times \langle c_{k_1\sigma_2}(t-t_2'-t_3')c_{k_2\sigma_4}(t)c_{k_3\sigma_5}^{\dagger}(t_1+t_2+t_3)c_{k_4\sigma_7}^{\dagger}(t_1)\rangle \\
& \times \langle c_{D\sigma_1}(t-t_1'-t_2'-t_3')c_{D\sigma_2}^{\dagger}(t-t_2'-t_3')c_{D\sigma_3}(t-t_3')c_{D\sigma_4}^{\dagger}(t) \\
& \times c_{D\sigma_5}(t_1+t_2+t_3)c_{D\sigma_6}^{\dagger}(t_1+t_2)c_{D\sigma_7}(t_1)c_{D\sigma_8}^{\dagger}(0)\rangle \\
& \times \langle e^{i\phi(t-t_1'-t_2'-t_3')}e^{i\phi(t-t_3')}e^{-i\phi(t_1+t_2)}e^{-i\phi(0)}\rangle . \quad (5.70)
\end{aligned}
$$

Simplifications occur because the quantum dot has a singly occupied level with energy ϵ_D. As in Ref. [90], the first electron is transferred to the lead before the second hops on the quantum dot. Therefore,

$$
\begin{aligned}
& \langle c_{D\sigma_1}(t-t_1'-t_2'-t_3')c_{D\sigma_2}^{\dagger}(t-t_2'-t_3')c_{D\sigma_3}(t-t_3')c_{D\sigma_4}^{\dagger}(t) \\
& \times c_{D\sigma_5}(t_1+t_2+t_3)c_{D\sigma_6}^{\dagger}(t_1+t_2)c_{D\sigma_7}(t_1)c_{D\sigma_8}^{\dagger}(0)\rangle \\
= \; & \langle c_{D\sigma_1}(t-t_1'-t_2'-t_3')c_{D\sigma_2}^{\dagger}(t-t_2'-t_3')\rangle\langle c_{D\sigma_3}(t-t_3'))c_{D\sigma_4}^{\dagger}(t)\rangle \\
& \times \langle c_{D\sigma_5}(t_1+t_2+t_3)c_{D\sigma_6}^{\dagger}(t_1+t_2)\rangle\langle c_{D\sigma_7}(t_1)c_{D\sigma_8}^{\dagger}(0)\rangle \\
= \; & G_{D\sigma_1}^{\tilde{t}}(-t_1')\delta_{\sigma_1\sigma_2}G_{D\sigma_3}^{\tilde{t}}(-t_3')\delta_{\sigma_3\sigma_4}G_{D\sigma_5}^{t}(t_3)\delta_{\sigma_5\sigma_6}G_{D\sigma_7}^{t}(t_1)\delta_{\sigma_7\sigma_8} , \quad (5.71)
\end{aligned}
$$

Describing the Andreev process, we assume

$$\begin{aligned}
&\sum_{q_1..q_4}\langle c^\dagger_{q_1\sigma_1}(t-t'_1-t'_2-t'_3)c^\dagger_{q_2\sigma_3}(t-t'_3)c_{q_3\sigma_6}(t_1+t_2)c_{q_4\sigma_8}(0)\rangle \\
=&\sum_{q_1..q_4}\langle c^\dagger_{q_1\sigma_1}(t-t'_1-t'_2-t'_3)c^\dagger_{q_2\sigma_3}(t-t'_3)\rangle\langle c_{q_3\sigma_6}(t_1+t_2)c_{q_4\sigma_8}(0)\rangle \\
=&\sum_{q_1,q_4}F^*_{\sigma_1}(q_1,-t'_1-t'_2)\delta_{\sigma_3,-\sigma_1}F_{\sigma_8}(q_4,t_1+t_2)\delta_{\sigma_6,-\sigma_8}\ ,
\end{aligned} \tag{5.72}$$

For the correlation of operators in normal metal lead, using the Wick's theorem, we obtain

$$\begin{aligned}
&\sum_{k_1..k_4}\langle c_{k_1\sigma_2}(t-t'_2-t'_3)c_{k_2\sigma_4}(t)c^\dagger_{k_3\sigma_5}(t_1+t_2+t_3)c^\dagger_{k_4\sigma_7}(t_1)\rangle \\
=&\sum_{k_1..k_4}[-\langle c_{k_1\sigma_2}(t-t'_2-t'_3)c^\dagger_{k_3\sigma_5}(t_1+t_2+t_3)\rangle\langle c_{k_2\sigma_4}(t)c^\dagger_{k_4\sigma_7}(t_1)\rangle \\
&+\langle c_{k_1\sigma_2}(t-t'_2-t'_3)c^\dagger_{k_4\sigma_7}(t_1)\rangle\langle c_{k_2\sigma_4}(t)c^\dagger_{k_3\sigma_5}(t_1+t_2+t_3)\rangle] \\
=&-G^>_{L\sigma_2}(t-t'_2-t'_3-t_1-t_2-t_3)\delta_{\sigma_2,\sigma_5}G^>_{L\sigma_4}(t-t_1)\delta_{\sigma_4,\sigma_7} \\
&+G^>_{L\sigma_2}(t-t'_2-t'_3-t_1)\delta_{\sigma_2,\sigma_7}G^>_{L\sigma_4}(t-t_1-t_2-t_3)\delta_{\sigma_4,\sigma_5}\ ,
\end{aligned} \tag{5.73}$$

Concerning the phase fluctuations, the four-point correlator, which is implicit in the expression of the tunneling current is written as a time ordered product. Once ordered, the product of the exponential gives the exponential of the sum of all pairings between phase operators as shown in Appendix A. As a result, with the definition of Eq. (3.15), from Eq. (5.58), we get

$$\begin{aligned}
&\langle e^{i\phi(t-t'_1-t'_2-t'_3)}e^{i\phi(t-t'_3)}e^{-i\phi(t_1+t_2)}e^{-i\phi(0)}\rangle \\
=&\frac{e^{J(t-t'_1-t'_2-t'_3)+J(t-t'_3)+J(t-t'_1-t'_2-t'_3-t_1-t_2)+J(t-t'_3-t_1-t_2)}}{e^{J(-t'_1-t'_2)+J(t_1+t_2)}}\ .
\end{aligned} \tag{5.74}$$

5.5.6 Appendix F

In this appendix, we present the denominator products which appear in the tunneling current through the NDS junction.

D^0 is the original denominator which is not affected by the environment

$$\begin{aligned}
(D^0_\leftarrow)^{-1} =& \frac{1}{(E'+\epsilon+i\eta)(E'+\epsilon_D+i\eta)(\epsilon+\epsilon_D+i\eta)(E+\epsilon_D-i\eta)} \\
&\times\left[\frac{1}{(-\epsilon+\epsilon_D-i\eta)(E-\epsilon-i\eta)}+\frac{1}{(\epsilon+\epsilon_D-i\eta)(E+\epsilon-i\eta)}\right]\ ,
\end{aligned} \tag{5.75}$$

and $D^{el}_\leftarrow$ is the denominator product affected by the environment,

$$\begin{aligned}
(D^{el}_\leftarrow)^{-1} =& \frac{1}{(E'+\epsilon+\omega+i\eta)(E'+\epsilon_D+\omega+i\eta)(\epsilon+\epsilon_D+i\eta)(E+\epsilon_D-i\eta)} \\
&\times\left[\frac{1}{(-\epsilon+\epsilon_D-i\eta)(E-\epsilon-i\eta)}+\frac{1}{(\epsilon+\epsilon_D-i\eta)(E+\epsilon-i\eta)}\right] \\
&+\frac{1}{(E'+\epsilon+i\eta)(E'+\epsilon_D+i\eta)(\epsilon+\epsilon_D+i\eta)(E+\epsilon_D+\omega-i\eta)} \\
&\times\left[\frac{1}{(-\epsilon+\epsilon_D-i\eta)(E-\epsilon+\omega-i\eta)}+\frac{1}{(\epsilon+\epsilon_D-i\eta)(E+\epsilon+\omega-i\eta)}\right]\ ,
\end{aligned} \tag{5.76}$$

where D^{inel} is the denominator product attributed to the inelastic current (affected by environment) and is defined as

$$
\begin{aligned}
(D^{inel}_{\leftarrow})^{-1} &= \left[\frac{1}{(E'+\epsilon_D-\epsilon-\epsilon'+i\eta)(E'-\epsilon'+i\eta)}+\frac{1}{(E'+\epsilon_D+i\eta)(E'+\epsilon+i\eta)}\right] \\
&\times\left\{\frac{1}{(\epsilon_D-\epsilon'+i\eta)(\epsilon_D-\epsilon-i\eta)}\left[\frac{1}{(E+\epsilon_D-\epsilon-\epsilon'-i\eta)(E-\epsilon-i\eta)}\right.\right. \\
&\left.+\frac{1}{(E+\epsilon_D-i\eta)(E+\epsilon'-i\eta)}\right]+\frac{1}{(\epsilon_D-\epsilon'+i\eta)(\epsilon_D-\epsilon'-i\eta)} \\
&\left.\times\left[\frac{1}{(E+\epsilon_D-\epsilon-\epsilon'-i\eta)(E-\epsilon'-i\eta)}+\frac{1}{(E+\epsilon_D-i\eta)(E+\epsilon-i\eta)}\right]\right\} \quad .(5.77)
\end{aligned}
$$

We define

$$
\Pi(x_1,x_2,\eta)=\int_\Delta^\infty dE\frac{1}{\sqrt{E^2-\Delta^2}}\frac{1}{(E-x_1-i\eta)(E-x_2-i\eta)} \quad . \tag{5.78}
$$

If $x_1\neq x_2$, then

$$
\Pi(x_1,x_2,\eta)=\frac{1}{2(x_1-x_2)}\left(\frac{\pi+2\arcsin(\frac{x_1+i\eta}{\Delta})}{\sqrt{\Delta^2-(x_1+i\eta)^2}}-\frac{\pi+2\arcsin(\frac{x_2+i\eta}{\Delta})}{\sqrt{\Delta^2-(x_2+i\eta)^2}}\right) \quad ,
$$

or else,

$$
\Pi(x_1,x_2,\eta)=\frac{(x_1+i\eta)(\pi+2\arcsin(\frac{x_1+i\eta}{\Delta}))}{2(\Delta^2-(x_1+i\eta)^2)^{3/2}}+\frac{1}{\Delta^2-(x_1+i\eta)^2} \quad .
$$

Then, we define

$$
\begin{aligned}
&\Psi^0_{\leftarrow}(\epsilon,\epsilon_D,\eta) \\
&=\int_\Delta^\infty dE\int_\Delta^\infty dE'\frac{1}{\sqrt{E^2-\Delta^2}\sqrt{E'^2-\Delta^2}}\frac{1}{D^0_{\leftarrow}} \\
&=\Pi(-\epsilon,-\epsilon_D,-\eta)\left\{\frac{\Pi(\epsilon,-\epsilon_D,\eta)}{(\epsilon+\epsilon_D+i\eta)(-\epsilon+\epsilon_D-i\eta)}+\frac{\Pi(-\epsilon,-\epsilon_D,\eta)}{(\epsilon+\epsilon_D+i\eta)(\epsilon+\epsilon_D-i\eta)}\right\} \quad ,
\end{aligned} \tag{5.79}
$$

$$
\begin{aligned}
&\Psi^{el}_{\leftarrow}(\epsilon,\epsilon_D,\omega,\eta) \\
&=\int_\Delta^\infty dE\int_\Delta^\infty dE'\frac{1}{\sqrt{E^2-\Delta^2}\sqrt{E'^2-\Delta^2}}\frac{1}{D^{el}_{\leftarrow}} \\
&=\frac{\Pi(-\epsilon-\omega,-\epsilon_D-\omega,-\eta)\Pi(\epsilon,-\epsilon_D,\eta)+\Pi(\epsilon-\omega,-\epsilon_D-\omega,\eta)\Pi(-\epsilon,-\epsilon_D,-\eta)}{(\epsilon+\epsilon_D+i\eta)(-\epsilon+\epsilon_D-i\eta)} \\
&+\frac{\Pi(-\epsilon-\omega,-\epsilon_D-\omega,-\eta)\Pi(-\epsilon,-\epsilon_D,\eta)+\Pi(-\epsilon-\omega,-\epsilon_D-\omega,\eta)\Pi(-\epsilon,-\epsilon_D,-\eta)}{(\epsilon+\epsilon_D+i\eta)(\epsilon+\epsilon_D-i\eta)} \quad ,
\end{aligned} \tag{5.80}
$$

$$
\begin{aligned}
&\Psi^{inel}_{\leftarrow}(\epsilon,\epsilon',\epsilon_D,\eta) \\
&=\int_\Delta^\infty dE\int_\Delta^\infty dE'\frac{1}{\sqrt{E^2-\Delta^2}\sqrt{E'^2-\Delta^2}}\frac{1}{D^{inel}_{\leftarrow}} \\
&=(\Pi(\epsilon+\epsilon'-\epsilon_D,\epsilon',-\eta)+\Pi(-\epsilon_D,-\epsilon,-\eta)) \\
&\times\left\{\frac{\Pi(\epsilon+\epsilon'-\epsilon_D,\epsilon,\eta)+\Pi(-\epsilon_D,-\epsilon',\eta)}{(\epsilon_D-\epsilon'+i\eta)(\epsilon_D-\epsilon-i\eta)}+\frac{\Pi(\epsilon+\epsilon'-\epsilon_D,\epsilon',\eta)+\Pi(-\epsilon_D,-\epsilon,\eta)}{(\epsilon_D-\epsilon'+i\eta)(\epsilon_D-\epsilon'-i\eta)}\right\} \quad .
\end{aligned} \tag{5.81}
$$

Since $D^0_{\rightarrow}(\epsilon) = D^0_{\leftarrow}(-\epsilon)$ and $D^{el}_{\rightarrow}(\epsilon) = D^{el}_{\leftarrow}(-\epsilon)$, $\Psi^0_{\rightarrow}(\epsilon) = \Psi^0_{\leftarrow}(-\epsilon)$ and $\Psi^{el}_{\rightarrow}(\epsilon) = \Psi^{el}_{\leftarrow}(-\epsilon)$. However, in fact, if we change the name of variable $\epsilon \rightarrow \epsilon'$ then change variable $\epsilon' = -\epsilon$, we will obtain the same formula for both cases $eV > 0$ and $eV < 0$. Since ϵ and ϵ' are independently equivalent, it is evident that $\Psi^{inel}_{\rightarrow}(\epsilon, \epsilon', \epsilon_D, \eta) = \Psi^{inel}_{\leftarrow}(\epsilon, \epsilon', \epsilon_D, \eta)$. Hereafter, we neglect the $\leftarrow$ or $\rightarrow$ index in these functions.

If $eV > 0$, the elastic current contributions in $I_{\rightarrow}$ exist but the elastic current contributions in $I_{\leftarrow}$ vanish (in contrast to the case of $eV < 0$).

We change variables in inelastic contributions as

$$\begin{cases} \Omega = \epsilon + \epsilon' \ , \\ \delta = \epsilon - \epsilon' \ , \end{cases}$$

and define

$$K^{el}_{NDS}(\omega, eV, \epsilon_D, \eta) = \int_{-eV}^{eV} d\epsilon \Psi^{el.tot}(\epsilon, \epsilon_D, \eta) \ , \tag{5.82}$$

$$K^{inel}_{NDS}(\Omega, eV, \epsilon_D, \eta) = \int_{2eV-\Omega}^{\Omega-2eV} d\delta \Psi^{inel}(\frac{\Omega+\delta}{2}, \frac{\Omega-\delta}{2}, \epsilon_D, \eta) \ , \tag{5.83}$$

with $\Psi^{el.tot}(\epsilon, \epsilon_D, \omega, \eta) = 2\Psi^0(\epsilon, \epsilon_D, \eta) + \Psi^{el}(\epsilon, \epsilon_D, \omega, \eta)$.

Part II

Dephasing of a quantum dot level in the presence of a fluctuating current

Chapter 6

Introduction to the quantum Hall effect

6.1 Hall effect

6.1.1 The classical Hall effect

The Hall effect, discovered by Edwin Hall in 1879, happens when an electric current flows through a conducting plate in a magnetic field perpendicular to the plane. The magnetic field exerts a Lorentz force on the moving charge carriers which tends to push them to one side of the conductor. A buildup of charge at the sides of the conductors will balance this magnetic influence, producing a measurable voltage V_H between two sides of the conductor (see Figure 6.1). The Hall resistivity is proportional to the amplitude of the magnetic field.

6.1.2 Integer quantum Hall effect

In 1980, Klaus von Klitzing *et al.* [100] found that at temperatures of only a few Kelvin and high magnetic field (3 - 10 Tesla), the Hall resistance did not vary linearly with the field. It varied in a stepwise fashion (see Figure 6.2). It was also found that where the Hall resistance was flat, the longitudinal resistance disappeared. The field at which the plateaus appeared, or where the longitudinal resistance vanished, was independent of the material, temperature, or other variables of the experiment, but only depended on a combination of fundamental constants h/e^2. This phenomenon can be understood in terms of the Landau levels formed in a magnetic field.

The Hamiltonian for a particle subjected to a magnetic field perpendicular to its direction of motion can be written down as

$$H = \sum_i^N \frac{\mathbf{p}_i - e\mathbf{A}(\mathbf{r}_i)^2}{2m} \ , \tag{6.1}$$

with the vector potential $\mathbf{A}(\mathbf{r})$ chosen in the following gauge

$$\mathbf{A}(\mathbf{r}_i) = \frac{1}{2}B(y_i, -x_i) \ , B = B\hat{z} \ . \tag{6.2}$$

The energy eigenvalues of the above Hamiltonian are

$$E_{n,k_y} = (n + 1/2)\omega_c \ , \tag{6.3}$$

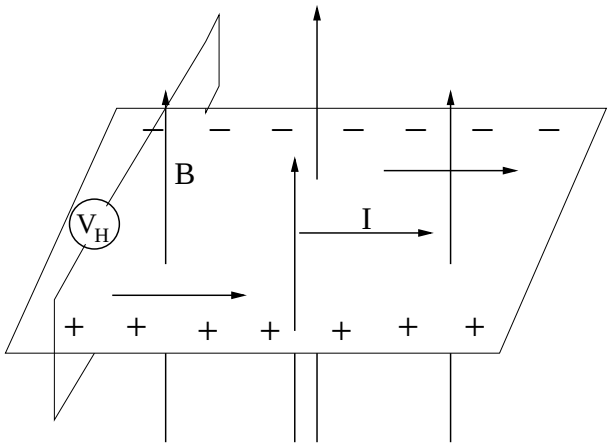

Figure 6.1: The Hall effect occurs when an electrical current is subjected to a transverse magnetic field. Due to the Lorentz force, the Hall voltage is produced between two sides of the conductors.

with $\omega_c = eB/mc$ is the cyclotron frequency, $n = 0, 1, 2, ...$ Each value of n corresponds to a Landau level. Since the Landau levels do not depend on the quantum number k_y, they are highly degenerate. This degeneracy, defined as the number of states per unit area, may be quantified by the relation $\rho_B = eB/hc$. It is useful to describe the integer quantum Hall effect (IQHE) by the filling factor

$$\nu = \rho/\rho_B \ , \tag{6.4}$$

which is the number of electrons per Landau level and acts as a measure of the applied magnetic field.

In Figure 6.2, the plateaus occur at each integer value of the filling factor ν. This can be understood that when each of the degenerate states of a Landau level is filled, the resistivity increases because fewer and fewer states remain unoccupied within that energy level. When the Landau level is completely full, a gap exists requiring a finite jump in energy to reach the next set of degenerate energy states (i.e., the next Landau level).

However, due to impurities in a sample, the density of states will evolve from sharp Landau levels to a broader spectrum of levels (see Figure 6.3). There are two kinds of levels, localized and extended, in the new spectrum, and it is expected that the extended states occupy a core near the original Landau level while the localized states trigger a broadening of the density of states. Only the extended states can carry current at zero temperature. The existence of the localized states can explain the appearance of plateaus. As the density is increased the localized states gradually fill up without any change in occupation of the extended states, thus without any change in the Hall resistance. In these cases, the Hall resistance is on a step and the longitudinal resistance vanishes (at zero temperature).

6.1.3 Fractional quantum Hall effect

In 1982, D. C. Tsui *et al.* [101] repeated Klitzing's earlier experiments with higher mobility semiconductor hetero-structures and higher magnetic field. Their goal was to minimize the role of impurities and to enhance the effects of electron-electron interactions. They have found that the plateaus at integer filling factors are much narrower, and between them more plateaus are seen at fractional filling factor, especially 1/3 and 2/3 (see Figure 6.4).

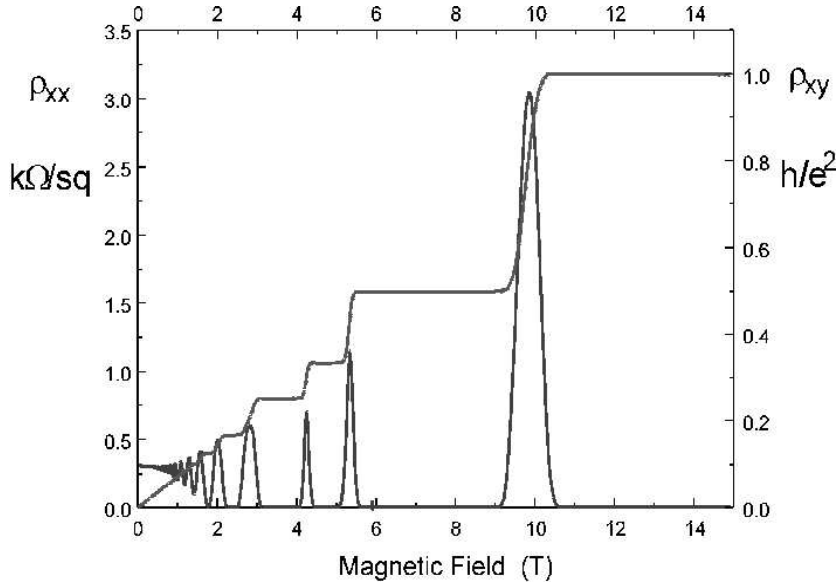

Figure 6.2: The stepwise behavior of the transverse resistivity (ρ_{xy}) and the longitudinal resistivity (ρ_{xx}) as a function of magnetic field. The plateaus of the transverse resistivity coincide with the dissipationless behavior of the longitudinal resistivity at each integer value of ν.

These observations could not be explained by the non-interacting quantum mechanical theory. They are realized to be a result of the many-body effects on interacting electrons. That means now, we need to include the effects of interactions in the Hamiltonian (6.1), then

$$H = \sum_{i}^{N} \frac{\mathbf{p}_i - e\mathbf{A}(\mathbf{r}_i)^2}{2m} + \sum_{i<j}^{N} \frac{e^2}{|\mathbf{r}_i - \mathbf{r}_j|} \ . \tag{6.5}$$

In this Hamiltonian, the potential energy is no longer a small term compared with the kinetic term. It induces the fractional quantum Hall effect (FQHE) being one of the strong correlation problems.

The Laughlin variational wave function

In 1983, Robert Laughlin [102] proposed his ansatz for a variational wave function which contained no free parameters:

$$\psi = \prod_{i<j} (z_i - z_j)^{2p+1} \exp\left(- \sum_i \frac{|z_i|^2}{4l^2} \right) \ , \tag{6.6}$$

where $z_i = x_i + iy_i$ is the complex coordinate of the ith particle and $l^2 = hc/eB$ is the magnetic length. The Laughlin wave function gave an accurate description of all filling fractions $\nu = 1/(2p+1)$ and was shown to almost exactly match numerical ground state wave functions found for small FQHE systems. However, the Laughlin wave function can not be used to explain the remaining filling fractions, such as 2/5, 3/7, ...

The Laughling approach allowed to make predictions about the excitations of a fractional quantum Hall system. These excitations were shown to carry anomalous fractional charge νe, and to have fractional statistics. On general grounds, the Laughlin approach

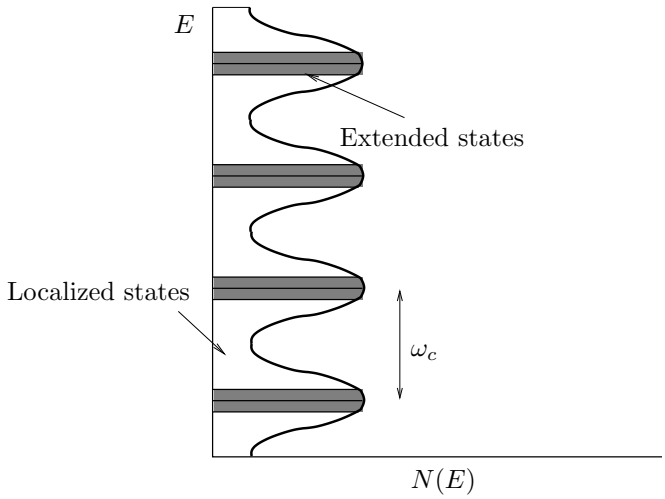

Figure 6.3: Diagram of Landau levels due to impurities in the sample.

can be understood in terms of electrons adjusting to the magnetic field, which is represented by flux tubes threading the two dimensional plane. Electrons adjust their location in order to minimize the ground state energy with these magnetic field constrains.

Composite fermions and Chern-Simons theory

In 1989, Jainendra Jain [103] identified a suitable set of quasi-particles for the FQHE system, calling them "composite fermions": electrons with $2n$ flux quanta attached to each of them. When each of the composite fermion Landau levels is filled there exists an energy gap separating it from the next composite Landau level. The FQHE of Jain states can be understood as an IQHE of composite fermions at an effective integer filling: $p =$ number of composite fermion/number of unattached flux quanta $= \nu/(1-2n\nu)$. Then the relation between the filling factor ν and integers n and p for Jain states is $\nu = p/(2np+1)$. This composite fermion picture is able to explain both the Laughlin fractions ($p = 1$) as well as many of the remaining fractions ($p \neq 1$).

The quasi-particles in the composite fermion system are composed of both particles (the electrons) and field (the flux quanta). It requires a gauge transformation to move particles to quasi-particles, which is known as the Chern-Simons theory [104].

6.2 Edge states

In the thermodynamic limit a noninteracting two-dimensional electron gas has an incompressible ground state whenever an integral number of Landau levels is full, i.e., the chemical potential jumps from $\omega_c(n + 1/2)$ to $\omega_c(n + 3/2)$ after the nth Landau level is filled. It follows that for a finite sample all single-particle states which occurs at energies in these gaps must be localized at the edge of the sample. The quantum Hall edge states are chiral (see Figure 6.5). They constitute the quantized analogue of the classical skipping orbits of charged particles in a magnetic field subject to electrostatic confinement.

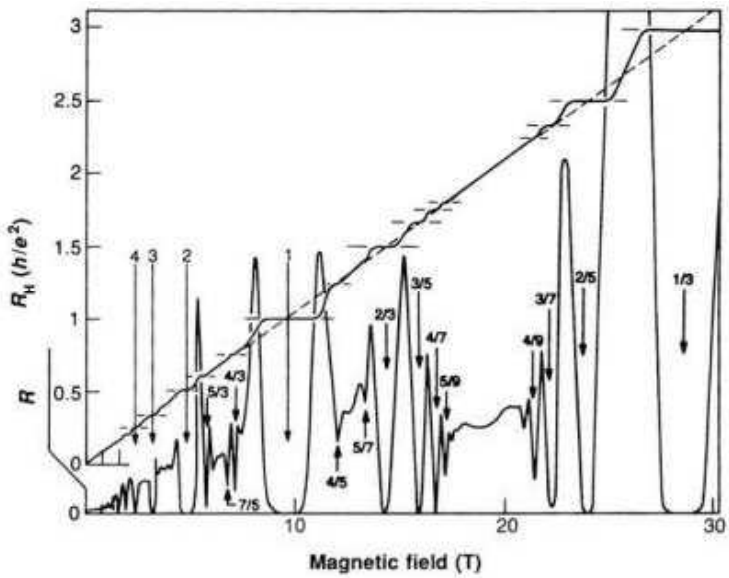

Figure 6.4: The stepwise behavior of the transverse Hall resistance (R_H) and the longitudinal resistance (R) as a function of magnetic field. The plateaus of the transverse resistivity coincide with the dissipationless behavior of the longitudinal resistivity at fractions of ν.

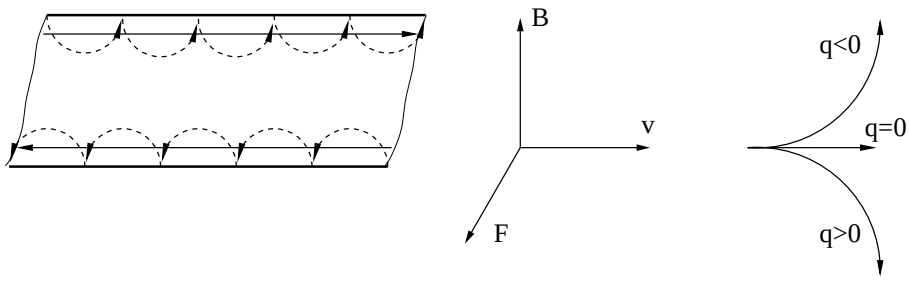

Figure 6.5: The chirality of the quantum Hall edge states is due to the Lorentz force.

6.2.1 The integer quantum Hall edge states

Halperin [105] first introduced a simple picture of the integer quantum Hall edge states of non-interacting electrons in a filled Landau level and found that the edge excitations can be represented by a one dimensional chiral Fermi liquid. In this picture, the bulk of Landau levels with an energy spacing of ω_c are bent upward near the edge of the sample by the confining potential with an electric field $\mathbf{E}$ (see Figure 6.6). For a macroscopically large sample, there are many edge states near the Fermi energy E_F of electrons even when there are no states near E_F in the bulk.

Following Stone [106] we consider the $\nu = 1$ quantum Hall ground state with a single particle wave function for each k_y eigenstate $\psi_k(x, y) = e^{ikx}e^{-eB(y-k/eB)^2/2}$ in the linear gauge $A_x = -By$. If a linear confining potential $V(y) = Ey$ is put in, the degeneracy is lifted, the energy of a state with $k_x = k$ becomes $\epsilon(k) = Ek/B$, and each state carries a Hall current. Further, the physical surface of the two dimensional electron gas is at $y = 0$ then the states to the left are full and those at the right are empty (see Figure 6.6). The physical edge of the droplet in y space can be identified with the "Fermi surface" at

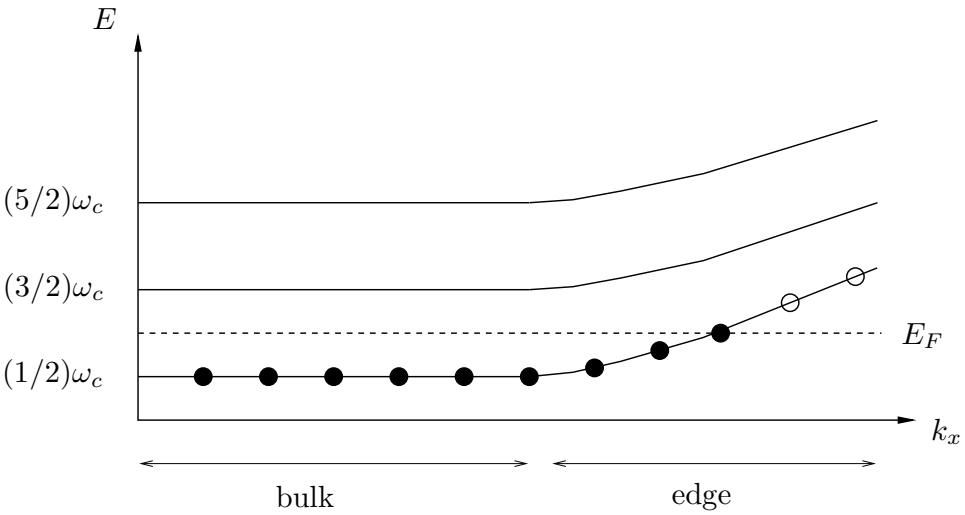

Figure 6.6: Landau levels and the edge states for a non-interacting two dimensional electron gas at $\nu = 1$ in a confining potential with Fermi energy E_F and cyclotron frequency ω_c.

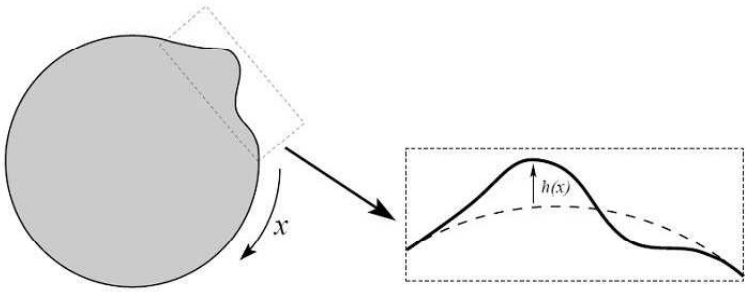

Figure 6.7: The gapless edge excitations are surface waves of edge distortions, i.e., a displacement $h(x)$ at point x along the edge propagating with velocity v.

$k = 0$ with a "Fermi velocity" being the drift velocity E/B. Since all the states move in the same direction, the excitations can be described by a Dirac equation. This edge state description has allowed to explain in a rather intuitive manner the physics of the IQHE [107, 108], as they provide a direct representation of the Landauer-Büttiker formula of a mesoscopic conductor.

6.2.2 The fractional quantum Hall edge states

In the FQHE, the Landau level is filled partially. In the absence of electron-electron interactions there would then be an enormous ground state degeneracy, but this degeneracy is lifted by the interactions. At special filling factors, such as $\nu = 1/3$, the system is expected to condense into a correlated liquid state. This liquid state is incompressible, and has a gap for all excitations. In the presence of edges we anticipate low lying edge excitations, as in the IQHE. There are several ways to describe the fractional quantum Hall edge states. But the first and simplest way to understand the dynamics of fractional quantum Hall edge excitations is to use the hydrodynamic picture introduced by Wen

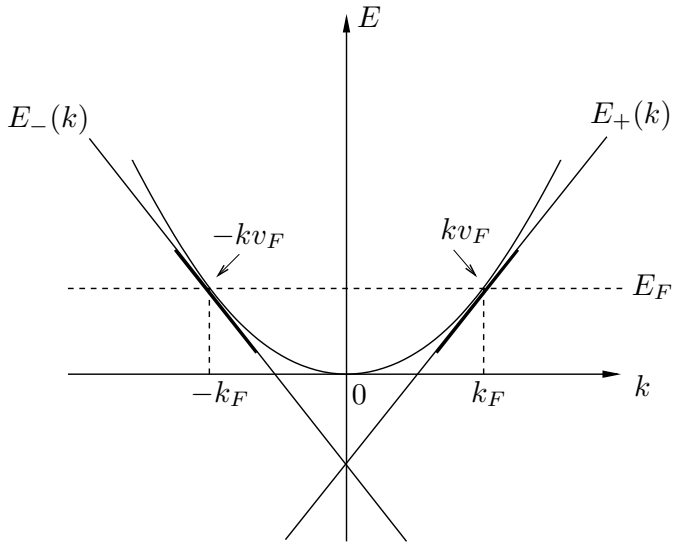

Figure 6.8: Parabolic band structure of metallic wire and linearization.

[109] in which the neutral edge excitation is a deformation of the edge as shown as wavy solid line in the Figure 6.7. The electrostatic potential can be expressed in terms of the local displacement (or height) of the fluid h at a point x along the edge. The author showed that the dynamical properties of the edge excitations are described by the U(1) Kac-Moody algebras. These edge excitations are shown to form a new kind of state which is called the chiral Luttinger liquid (see also Ref. [30]). This theory will be discussed in the next section.

6.3 Luttinger liquid theory

Electrons in one-dimensional (1D) systems form a quantum liquid which can not be described with the Fermi liquid theory since there are no single electron quasi-particles. It is due to the presence of the Coulomb electron-electron interactions. To describe the dynamic of electrons in 1D systems, we must use the Luttinger liquid theory [110, 111] in which the excitations consist of collective electron-hole excitations of the whole Fermi sea.

6.3.1 Non-chiral Luttinger liquid theory

We consider a 1D metallic wire with parabolic dispersion band as shown in Figure 6.8. The kinetic part of the Hamiltonian reads:

$$H_0 = \sum_k E(k) a_k^\dagger a_k \ , \tag{6.7}$$

with $E(k) = k^2/2m$ and $a_k^\dagger$ (a_k) is the creation (annihilation) operator of one electron in state with momentum k. Notice that we do not include spin degree of freedom here. In the Tomonaga model [110] the dispersion relation $E(k)$ is linearized in the vicinity of Fermi energy E_F: $E_+(k) = E_F + v_F(k - k_F)$ for $k \approx k_F$ and $E_-(k) = E_F - v_F(k + k_F)$ for $k \approx -k_F$. In the Luttinger model [111], the linearization is extended to all values

of k. An infinite number of fictive states are added which have no physical signification. However, Luttinger model has an important advantage over the Tomonaga model: it is exactly solvable using the bosonization technique.

We rewrite the electron creation operator after linearization as

$$a_k^\dagger = a_{+,k}^\dagger \Theta(k) + a_{-,k}^\dagger \Theta(-k) \ , \tag{6.8}$$

where $\Theta(k)$ is the Heaviside function and $a_{r,k}^\dagger$ (with $r = \pm$) is the creation operator for right or left moving electrons corresponding to the dispersion relation $E_+(k)$ or $E_-(k)$, which obeys to the anti-commutation relations.

Neglecting the constant terms in energy, the kinetic Hamiltonian can be simply written as

$$H_0 = v_F \sum_{r,k} rk a_{r,k}^\dagger a_{r,k} \ . \tag{6.9}$$

On the other hand, this non-interacting Hamiltonian can be expressed in term of electron density operator as

$$H_0 = \pi v_F \sum_r \int_{-L/2}^{L/2} dx \rho_r^2(x) \ , \tag{6.10}$$

with $\rho_r(x) = \psi_r^\dagger(x)\psi_r(x)$, where $\psi_r^\dagger(x)$ and $\psi_r(x)$ are the Fourier transform of $a_{r,k}^\dagger$ and $a_{r,k}$:

$$\psi_r^\dagger(x) = \frac{1}{\sqrt{L}} \sum_k e^{-ikx} a_{r,k}^\dagger \ , \tag{6.11}$$

$$\psi_r(x) = \frac{1}{\sqrt{L}} \sum_k e^{ikx} a_{r,k} \ , \tag{6.12}$$

and L is the length of wire.

We define the non-chiral bosonic field:

$$\phi_r(x) = \frac{i}{\sqrt{L}} \sum_{k>0} \frac{2\pi}{k} [\rho_r(k) e^{-ikx} - \rho_r(-k) e^{ikx}] e^{-\alpha|k|/2} \ , \tag{6.13}$$

where $\alpha \to 0$ is a distance cutoff which is introduced in Luttinger liquid theory to insure the convergence of the integrals.

The fermionic operator ψ_r is written in the bosonized form as

$$\psi_r(x) = \frac{M_r}{\sqrt{2\pi\alpha}} e^{irk_F x + ir\phi_r(x)} \ . \tag{6.14}$$

The factor $M_r/\sqrt{2\pi\alpha}$ allows to obtain the adequate anticommutation relations, and k_F in the exponent is needed to describe correctly the energy band.

Taking the derivative of Eq. (6.13), we have $\partial_x \phi_r(x) = 2\pi\rho_r(x)$, then we can rewrite the non-interacting Hamiltonian given by Eq. (6.10) as

$$H_0 = \frac{v_F}{4\pi} \sum_r \int_{-L/2}^{L/2} dx (\partial_x \phi_r(x))^2 \ . \tag{6.15}$$

If we define the total field

$$\phi(x) = \phi_+(x) + \phi_-(x) \ , \tag{6.16}$$
$$\varphi(x) = \phi_+(x) - \phi_-(x) \ , \tag{6.17}$$

then

$$H_0 = \frac{v_F}{8\pi} \int_{-L/2}^{L/2} dx[(\partial_x \phi(x))^2 + (\partial_x \varphi(x))^2] \ . \tag{6.18}$$

We include now the Coulomb interactions between the electrons. The total Hamiltonian is $H = H_0 + H_{int}$ with

$$H_{int} = \int_{-L/2}^{L/2} dx \int_{-L/2}^{L/2} dx' \rho(x) U(x - x') \rho(x') \ , \tag{6.19}$$

where the electron density operator $\rho(x)$ contains a slow variation $\rho_+(x) + \rho_-(x)$ and fast $2k_F$ oscillations with a non-linear dependence on $\phi_\pm$. If we neglect these fast oscillations, the interaction Hamiltonian becomes quadratic in the bosonic field. U is the Coulomb interaction potential. If the Coulomb potential is shot range $U(x - x') = U_0 \delta(x - x')$, it leads to

$$H_{int} = \frac{U_0}{4\pi^2} \int_{-L/2}^{L/2} dx (\partial_x \phi(x))^2 \ , \tag{6.20}$$

and the total Hamiltonian reads

$$H = \frac{v_F}{8\pi g} \int_{-L/2}^{L/2} dx \left[\frac{1}{g} (\partial_x \phi(x))^2 + g (\partial_x \varphi(x))^2 \right] \ , \tag{6.21}$$

where $g = 1/\sqrt{(1 + 2U_0/\pi v_F)}$ is the Coulomb interaction parameter. We find that Eq. (6.21) is quadratic, then the total Hamiltonian is exactly solvable and its eigenstates are similar to the eigenstates of hamonic oscillator.

6.3.2 Chiral Luttinger liquid in the fractional quantum Hall effect

The Hamiltonian which describes the edge modes is simply an electrostatic term [33]:

$$H = \frac{1}{2} \int_0^L dx V(x) e \rho(x) \ , \tag{6.22}$$

where x is a curvilinear coordinate along the edge, L is the length of the edge and $V(x)$ is the confining potential related to the applied electric field $\mathbf{E}$ [30, 87]: $V(x) = Eh(x) = v_F B \rho(x)/n_s$ with n_s is the two dimensional electron density. The Hamiltonian can be rewritten as

$$H = \frac{\pi v_F}{\nu} \int_0^L dx \rho^2(x) dx \ , \tag{6.23}$$

and in the Fourier space it is transformed as

$$H = \frac{\pi v_F}{\nu} \sum_k \rho_k \rho_{-k} \ , \tag{6.24}$$

with ρ_k is the Fourier transform of $\rho(x)$: $\rho(x) = 1/\sqrt{L} \sum_k e^{-ikx} \rho_k$. The continuity equation for this chiral density reads $\dot{\rho}_k = i v_F k \rho_k$. By comparing Eq. (6.24) with the classical

Hamiltonian equation of motion, we find that we can identify ρ_k as the canonical "coordinate" q_k and the corresponding canonical "momenta" can be identified as $p_k = -i2\pi\rho_k/\nu k$. Thus, after quantization, we have

$$[\rho_k, \rho_{k'}] = -\frac{\nu k}{2\pi}\delta_{k'-k} \ . \tag{6.25}$$

This is the Kac-Moody commutation relation and it is obtained due to the chirality of edge wave determined by magnetic field. The electron creation operator satisfies

$$[\rho(x'), \psi^\dagger(x)] = \delta(x - x')\psi^\dagger(x) \ , \tag{6.26}$$

which implies that the measurement of the electronic density on a state on which $\psi^\dagger(x)$ is acting tells us that an electron has been added.

We introduce the chiral Luttinger bosonic field

$$\phi(x) = \frac{i}{\sqrt{L}}\frac{\pi}{\sqrt{\nu}}\sum_k \frac{e^{-\alpha|k|/2}}{k}e^{-ikx}\rho_k \ . \tag{6.27}$$

Here the small factor α is a spacial cutoff which is introduced in Luttinger liquid theory to insure the convergence of the integrals. The derivative of ϕ is proportional to the density:

$$\partial_x\phi(x) = \frac{\pi}{\sqrt{\nu}}\rho(x) \ . \tag{6.28}$$

This allows to re-express the Hamiltonian in term of ϕ [30]

$$H = \frac{v_F}{\pi}\int_0^L (\partial_x\phi(x))^2 dx \ . \tag{6.29}$$

The form of the electron operator $\psi(x)$ is found by an analogy with the properties of canonical conjugate variables: $p(x)$ and $q(x)$, which are identified as $\rho(x)$ and $\phi(x)/\sqrt{\nu}$:

$$\psi(x) = \frac{1}{\sqrt{2\pi a}}e^{-ikx}e^{i\phi(x)/\sqrt{\nu}} \ . \tag{6.30}$$

This operator obviously depends on the filling factor. Fermion operators are known to anti-commute, so what is the condition for filling factor in order to insure anti-commutation relations $\{\psi(x), \psi(x')\} = 0$? This anti-commutator can be computed using the Baker-Campbell-Hausdorff formula $e^A e^B = e^{A+B-[A,B]/2}$ if $[A, B]$ is a c-number. The bosonic field needs to satisfy the commutation relation

$$[\phi(x), \phi(x')] = -i\pi\mathrm{sgn}(x - x') \ , \tag{6.31}$$

which induces to

$$\psi(x)\psi(x') = e^{\pm i\pi/\nu}\psi(x')\psi(x) \ . \tag{6.32}$$

From the Eq. (6.32), we find that to insure the anti-commutation relations for electron operators, we need to set $\nu = 1/m$ with m is an odd integer. This conclusion is consistent with the assumption that in the bulk, we deal with a fractional quantum Hall fluid.

In order to obtain information on the dynamics of electrons (or of fractional quasi-particles), we need to specify the bosonic Green's function. The Euclidean action for this bosonic field is [87]

$$S = -\frac{1}{\pi}\int d\tau \int dx[\partial_x\phi(x,\tau)(v_F\partial_x + i\partial_\tau)\phi(x,\tau)] \ . \tag{6.33}$$

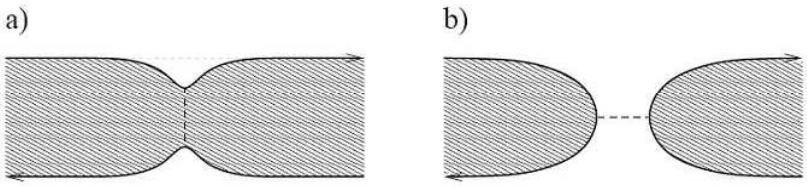

Figure 6.9: Quantum transport in a quantum Hall bar: a) in the case of weak backscattering, the quantum Hall fluid stays as a whole (dashed area) and only quasiparticles tunnel between the two edges. b) in the case of strong backscattering, the quantum Hall fluid is split into two and only electrons tunnel between the two fluids.

The operator which is implicit in this quadratic action allows to define the Green's function $G(x,\tau) = \langle T_\tau \phi(x,\tau)\phi(0,0)\rangle$ – the correlation function of the bosonic field. This Green's function is defined by the differential equation

$$(i\partial_\tau + v_F\partial_x)\partial_x G(x,\tau) = 2\pi\delta(x)\delta(\tau) \ . \tag{6.34}$$

The thermal Green's function is obtained as

$$G(x,\tau) = -\ln\left[\sinh\left(\pi\frac{x/v_F + i\tau}{\beta}\right)\right] \ , \tag{6.35}$$

with $\beta = 1/k_B\theta$.

6.4 Transport between two quantum Hall edges

We consider now a point contact in the fractional quantum Hall regime, which is typically achieved by placing metallic gates on top of the two dimensional electron gas in a high perpendicular magnetic field. We apply a voltage between the two gates, which are placed on two edges of fractional quantum Hall fluid (Figure 6.9). By varying the gate voltage, we can switch from a weak backscattering situation to a strong backscattering situation. In the former case, the Hall liquid remains in one piece, the entities which tunnel are edge quasiparticle excitations. In the latter case, the Hall fluid is split into two pieces and between these two fluids, only electrons can tunnel.

Hereafter we will discuss for the weak backscattering case, where the physics of FQHE quasiparticle is most obvious. The description of the strong backscattering case can be readily obtained using a duality transformation. Because the transport between two edges is out of equilibrium, it is necessary to resume the Keldysh formulation in the next part.

6.4.1 Keldysh digest for tunneling

Let us consider a system represented by the time-independent Hamiltonian $H = H_0 + H_{int}$, where H_0 represents free particles and H_{int} describes an interaction which is "difficult" to address. In many body physics [112, 113], it is convenient to work with a Wick's theorem (or one of its generalizations) in order to compute products of fermion and boson operators where the operators are time-dependent: $A_H(t) = e^{iHt}Ae^{-iHt}$ in the Heisenberg picture. The problem with the Heisenberg representation is that the operators contains the "difficult" part (the interaction part) of the Hamiltonian. It induce the problem of translating these products into interaction representation products where the operators

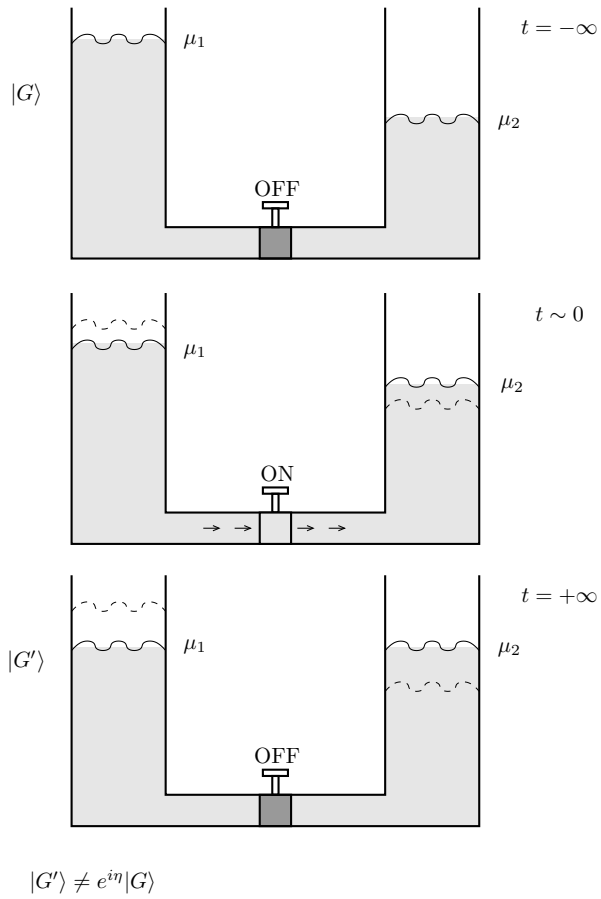

Figure 6.10: The groundstates of the system which is out of equilibrium. The groundstate at $t = +\infty$ is no longer related to the groundstate at $t = -\infty$ by a phase factor.

develop under the influence of the "easy" non-interacting Hamiltonian H_0 only: $A(t) = e^{iH_0 t} A e^{-iH_0 t}$.

Consider the ground state average of a time-ordered product of Heisenberg operators:

$$\langle A_H(t_0) B_H(t_1) C_H(t_2) D_H(t_3) \ldots \rangle \quad \text{with } t_0 > t_1 > t_2 > t_3 > \ldots \tag{6.36}$$

When translating to the interaction representation, the evolution operator reads:

$$S(t, t') = T \exp\left\{ -i \int_{t'}^{t} dt_1 H_{int}(t_1) \right\} \ . \tag{6.37}$$

The product of ordered operators then becomes:

$$\langle S(-\infty, +\infty) T(A_I(t_0) B_I(t_1) C_I(t_2) D_I(t_3) \ldots \quad S(+\infty, -\infty)) \rangle \ , \tag{6.38}$$

where T is the time ordering operator.

The central quantity to compute the product in Eq. (6.38) by using Wick's theorem is the S-matrix $S(+\infty, -\infty)$. When the system is at zero temperature or in equilibrium, the ground state (or thermal) expectation of this S–matrix is just a phase factor, because we assume that the perturbation is turned on adiabatically. This means that $\langle S(+\infty, -\infty) \rangle = e^{i\eta}$. Therefore the T–product is easily computed with the help of Wick's theorem.

However, if the system is out of equilibrium, there is no guarantee that the system return to its initial state for asymptotically large time. For example, in Figure 6.10 we illustrate this phenomenon with a hydrodynamical picture. Two reservoirs, having different levels, are not connected at $t = -\infty$ (the faucet is switched off). We switch (adiabatically) the faucet on between the two reservoirs, and a stationary flow is established. If at later time $t = +\infty$, we switch off the faucet again, we notice that the two reservoirs are now at the same level but different from the levels in the state at $t = -\infty$. We understand in this picture that the water flow through the faucet means the tunneling of particles from one reservoir to the other, which is described in the tunneling Hamiltonian H_{int}. Now, the ground state at $t = +\infty$ is no longer related to the ground state at $t = -\infty$ by the phase factor: $S(+\infty, -\infty)|G\rangle = |G'\rangle \neq e^{i\eta}|G\rangle$. To remedy this problem, Keldysh proposed a new contour, which is shown in Figure 6.11. This contour, corresponding new time ordering operator T_K, goes from $t = -\infty$ to $t = +\infty$ and back to $t = -\infty$ [114]. Because times on the lower contour are "larger" than times on the upper contour, the product of operators can be written as:

$$\langle T_K(A_I(t_0)B_I(t_1)C_I(t_2)D_I(t_3)\ldots S_K(-\infty,-\infty))\rangle \ , \tag{6.39}$$

where the integral over the Keldysh contour K goes from $-\infty$ to $+\infty$ and then back to $-\infty$. In this case, we have

$$\begin{aligned} S_K(-\infty,-\infty) &= T_K \exp\left\{-i\int_K dt_1 H_{int}(t_1)\right\} \\ &= T_K \exp\left\{-i\sum_{\eta=\pm}\eta\int_{-\infty}^{+\infty} dt_1 H_{int}(t_1)\right\} \ . \end{aligned} \tag{6.40}$$

Note that in general, the times appearing in the operator product $A_I(t_0)B_I(t_1)C_I(t_2)D_I(t_3)$ can be located either on the upper or on the lower contour.

The Green's function is an example of a time ordered product. The Green's function associated with the two-branches Keldysh contour is therefore a 2×2 matrix because there are four possible orderings:

$$G(t-t') = \begin{pmatrix} G^{++}(t-t') & G^{+-}(t-t') \\ G^{-+}(t-t') & G^{--}(t-t') \end{pmatrix} = \begin{pmatrix} G_0(|t-t'|) & G_0(t'-t) \\ G_0(t-t') & G_0(-|t-t'|) \end{pmatrix} \ , \tag{6.41}$$

where $G_0(t)$ can be computed from the thermal Green's function using a Wick rotation.

Note that the use of Keldysh Green's function allows us to write directly the operators like the current, by choosing appropriately the times on the contour. For example,

$$\langle \psi_2^\dagger(t)\psi_1(t)\rangle = \langle T_K\left\{\psi_1(t_+)\psi_2^\dagger(t_-)S_K(-\infty,-\infty)\right\}\rangle \ . \tag{6.42}$$

In this equation, the operators in left hand side are in the Heisenberg presentation and ones in the right hand side are in the interaction presentation with the time order follows the Keldysh contour. The average of operators product on the right hand side is a time ordered quantity, which can be calculated by using Wick's theorem.

6.4.2 Backscattering current

In this section, we consider the stationary current flowing between two edge states which is called backscattering current. The edge states is in the fractional quantum Hall regime.

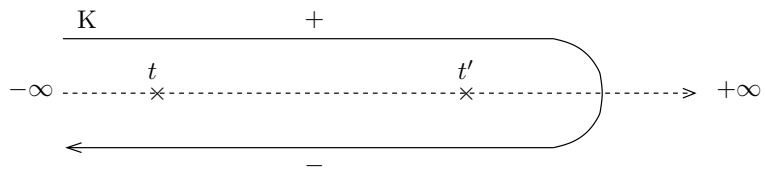

Figure 6.11: The two-branches of the Keldysh contour.

The Hamiltonian which describes the system is $H = H_1 + H_2 + H_B$ with $H_{1/2}$ describes the left/right edge states $H_{1/2} = (v_F/\pi)\int_0^L (\partial_x \phi_{1/2}(x,t))^2 dx$, with $\phi_{1/2}$ are the chiral bosonic fields for excitations with charge νe, and the tunneling Hamiltonian H_B describing the coupling between the two edges 1 and 2:

$$H_B = \Gamma(t)\psi_2^\dagger(t)\psi_1(t) + \Gamma^*(t)\psi_1^\dagger(t)\psi_2(t) \ , \tag{6.43}$$

where

$$\psi_{1/2}(t) = \frac{M_{1/2}}{\sqrt{2\pi\alpha}} e^{i\sqrt{\nu}\phi_{1/2}(t)} \ , \tag{6.44}$$

within $M_{1/2}$ is a Klein factor, which will be omitted hereafter by noticing that $M_{1/2}^2 = 1$. Upon the gauge transformation the tunneling amplitude between the edge states is $\Gamma(t) = \Gamma_0 e^{-ie^*\chi(t)/c}$ where $e^* = \nu e$ is the fractional charge. The gauge function χ depends only on time for a constant dc bias V_0 imposed between two edges: $\chi(t) = cV_0 t$, so that in this case $\Gamma(t) = \Gamma_0 e^{i\omega_0 t}$ with $\omega_0 = e^* V_0$.

The backscattering current operator can be derived from the Heisenberg equation of motion for the density operator, or alternatively by calculating $I_B = -c\partial H_B/\partial\chi$, then

$$I_B(t) = ie^* \left(\Gamma(t)\psi_2^\dagger(t)\psi_1(t) - \Gamma^*(t)\psi_1^\dagger(t)\psi_2(t)\right) \ . \tag{6.45}$$

The average backscattering current is expressed using Keldysh contour which allows to treat nonequilibrium situation:

$$\langle I_B(t)\rangle = \frac{1}{2}\sum_\eta \langle T_K \left\{ I_B(t^\eta) e^{-i\int_K dt_1 H_B(t_1)} \right\}\rangle \ . \tag{6.46}$$

To lowest order in the tunneling amplitude Γ_0, we have

$$\begin{aligned} \langle I_B(t)\rangle &= \frac{e^*\Gamma_0^2}{2} \sum_{\eta\eta_1\epsilon\epsilon_1} \epsilon\eta_1 e^{i\epsilon\omega_0 t + i\epsilon_1\omega_0 t_1} \\ &\times \left\langle T_K \left\{ \left[\psi_2^\dagger(t^\eta)\psi_1(t^\eta)\right]^{(\epsilon)} \left[\psi_2^\dagger(t_1^{\eta_1})\psi_1(t_1^{\eta_1})\right]^{(\epsilon_1)} \right\} \right\rangle \ . \end{aligned} \tag{6.47}$$

The correlator is different from zero only when $\epsilon_1 = -\epsilon$, that means the quasiparticles are conserved in the tunneling process. In the calculation, we are led to introduce the chiral Green's function of the bosonic field at position $x = 0$, which does not depend on the chirality 1/2:

$$G^{\eta\eta'}(t-t') = \left\langle T_K \left\{ \phi_{1/2}(t^\eta)\phi_{1/2}(t'^{\eta'}) \right\} \right\rangle - \frac{1}{2}\left\langle T_K \left\{ \phi_{1/2}^2(t^\eta) \right\} \right\rangle - \frac{1}{2}\left\langle T_K \left\{ \phi_{1/2}^2(t'^{\eta'}) \right\} \right\rangle \ . \tag{6.48}$$

This Green's function is associated with the two-branches Keldysh contour as we have discussed before. The average current can now be expressed as an integral over time of Keldysh Green's function

$$\langle I_B(t)\rangle = -\frac{ie^*\Gamma_0^2}{4\pi^2\alpha^2}\sum_\eta \eta \int_{-\infty}^{+\infty} d\tau \sin(\omega_0\tau) e^{2\nu G^{\eta-\eta}(\tau)} \ , \tag{6.49}$$

where $\tau = t - t_1$. At finite temperatures, the Green's function is given by (see Eq. (6.35)):

$$G^{\eta-\eta}(\tau) = -\ln\left(\frac{\sinh\left(\frac{\pi}{\beta}(\eta\tau + i\tau_0)\right)}{\sinh\left(\frac{i\pi\tau_0}{\beta}\right)}\right) \ , \tag{6.50}$$

where $\tau_0 = \alpha/v_F$. Applying this Green's function, we can obtain the analytical expression for the average current as

$$\langle I_B(t)\rangle = \frac{e^*\Gamma_0^2}{2\pi^2\alpha^2\mathbf{\Gamma}(2\nu)}\left(\frac{\alpha}{v_F}\right)^{2\nu}\left(\frac{2\pi}{\beta}\right)^{2\nu-1}\sinh\left(\frac{\omega_0\beta}{2}\right)\left|\mathbf{\Gamma}\left(\nu + i\frac{\omega_0\beta}{2\pi}\right)\right|^2 \ , \tag{6.51}$$

where $\mathbf{\Gamma}$ is the gamma function. At zero temperature, the average current is

$$\langle I_B(t)\rangle = \frac{e^*\Gamma_0^2}{2\pi\alpha^2\mathbf{\Gamma}(2\nu)}\left(\frac{a}{v_F}\right)^{2\nu} \operatorname{sgn}(\omega_0)|\omega_0|^{2\nu-1} \ . \tag{6.52}$$

6.4.3 Backscattering current noise

In this section we consider the symmetrized noise because latter on noise at $\omega = 0$ is considered, so the issue of symmetrized versus asymmetrized does not matter. Using the symmetric combination of current – current correlators

$$\begin{aligned} S(t,t') &= \langle I_B(t)I_B(t')\rangle + \langle I_B(t')I_B(t)\rangle - 2\langle I_B(t)\rangle\langle I_B(t')\rangle \\ &= \sum_\eta \left\langle T_K\left\{I_B(t^\eta)I_B(t'^{-\eta})e^{-i\int_K dt_1 H_B(t_1)}\right\}\right\rangle - 2\langle I_B\rangle^2 \ , \end{aligned} \tag{6.53}$$

to lowest order in the tunneling amplitude Γ_0, it is not necessary to expand the Keldysh evolution operator because the current itself contain Γ_0.

$$\begin{aligned} S(t,t') &= -(e^*)^2\Gamma_0^2\sum_{\eta\epsilon\epsilon_1}\epsilon\epsilon_1 e^{i\epsilon\omega_0 t + i\epsilon_1\omega_0 t'} \\ &\quad\times\left\langle T_K\left\{\left[\psi_2^\dagger(t^\eta)\psi_1(t^\eta)\right]^{(\epsilon)}\left[\psi_2^\dagger(t'^{-\eta})\psi_1(t'^{-\eta})\right]^{(\epsilon_1)}\right\}\right\rangle \\ &= \frac{(e^*)^2\Gamma_0^2}{2\pi^2\alpha^2}\sum_\eta \cos(\omega_0(t-t'))e^{2\nu G^{\eta-\eta}(t-t')} = S(t-t') \ . \end{aligned} \tag{6.54}$$

From this expression, the spectral density of backscattering current noise is obtained by calculating the Fourier transform. At finite temperature, the noise at zero-frequency is

$$S(\omega=0) = \frac{(e^*)^2\Gamma_0^2}{\pi^2\alpha^2\mathbf{\Gamma}(2\nu)}\left(\frac{\alpha}{v_F}\right)^{2\nu}\left(\frac{2\pi}{\beta}\right)^{2\nu-1}\cosh\left(\frac{\omega_0\beta}{2}\right)\left|\mathbf{\Gamma}\left(\nu + i\frac{\omega_0\beta}{2\pi}\right)\right|^2 \ , \tag{6.55}$$

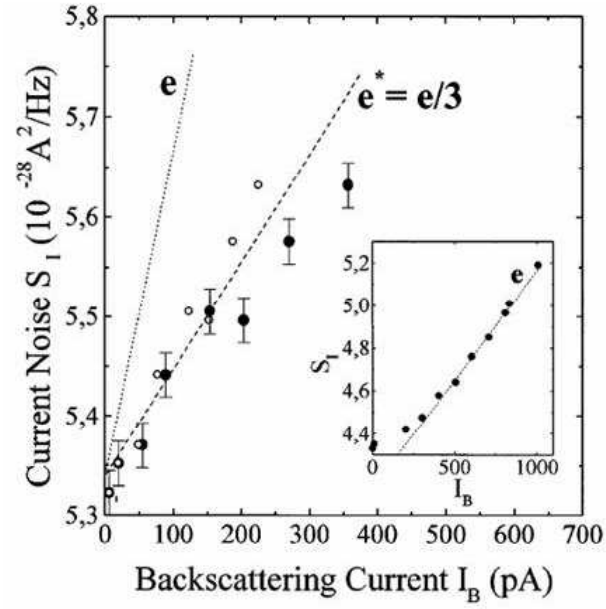

Figure 6.12: Tunneling current noise at $\nu = 1/3$ ($\nu_L = 2/3$) versus backscattering current I_B (filled circles) from Ref. [40]. The slopes for $e/3$ quasiparticles (dashed line) and electrons (dotted line) are shown. The temperature θ=25mK. Inset: data in the same units, electrons tunnel in the IQHE regime ($\nu_L = 4$). The temperature θ=42mK.

and in the limit zero temperature

$$S(\omega = 0) = \frac{(e^*)^2 \Gamma_0^2}{\pi \alpha^2 \mathbf{\Gamma}(2\nu)} \left(\frac{\alpha}{v_F}\right)^{2\nu} |\omega_0|^{2\nu - 1} \ . \tag{6.56}$$

In conclusion, at zero temperature, we recover the Schottky-like relation with the fractional charge $e^* = \nu e$:

$$S(\omega = 0) = 2e^* \langle I_B(t) \rangle \ . \tag{6.57}$$

At finite temperature, the shot/thermal noise crossover is recovered

$$S(\omega = 0) = 2e^* \langle I_B(t) \rangle \coth(\omega_0 \beta / 2) \ . \tag{6.58}$$

These results are consistent with the results shown in Ref. [32] in the general framework for treating nonequilibrium transport phenomena in Luttinger liquids. The Schottky relation in the fractional quantum Hall effect allows the direct observation of a fractional charge which we discuss in the next section.

6.4.4 The direct observation of a fractional charge

Can fractional charge carry the current? The first proposal of fractionally charged excitations above the gap was shown by R. Laughlin [102]. Soon after D. C. Tsui suggested that shot noise could reveal the charge of these unusual excitations [101], and X. G. Wen extended this concept of fractional excitations to the gapless modes carrying the current at the edge of clean samples using a Luttinger liquid model [30]. In this frame, C. Kane and M. Fisher [32] proposed to detect the quasiparticles using the shot noise associated with a weak tunnel current between fractional edges through the FQHE fluid. Thereafter,

in Refs. [33, 115], it was shown that a Poissonian quasiparticle shot noise must be recovered for weak coupling and that its measurement should give a direct determination of the fractional charge.

These theoretical predictions of current–noise characteristics in fractional quantum Hall effect have been verified in remarkable point contact experiments at filling factor $\nu = 1/3$ in Weizmann institute and in Saclay at the same time [40, 41]. Ref. [40] was performed at low temperature in the shot noise dominated regime, while Ref. [41] used a fit to the thermal-shot noise crossover curve to identify the fractional charge. The data of Ref. [40] is displayed in Figure 6.12. This experiment showed that for very low tunnel coupling, tunneling is coherent, and the $1/3$ noise reduction is a direct evidence of fractional charge $e/3$. Subsequently, the group in Weizmann also measured the fractional charge $e/5$ in the $\nu = 2/5$ fractional state [42].

Chapter 7

Dephasing in a quantum dot

7.1 Phase measurement in a quantum dot via a double-slit interference

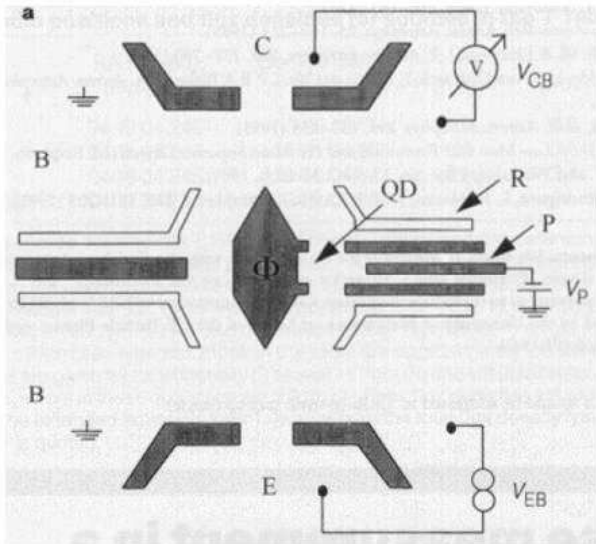

Figure 7.1: Schematic description of the double-path interference experiment with a quantum dot replacing one path. Reflector gates (R) are drawn in white. The excitation voltage V_{EB} is applied between emitter E and base B. The collector voltage V_{CB} is measured between the base B and collector C. A voltage V_P on the plunger gate P changes the occupation of the quantum dot [27].

The transport properties of electronic devices are usually characterized on the basic of conductance measurements. Such measurements are adequate for device in which transport occurs incoherently, but for very small devices, such as quantum dots, the wave nature of electrons plays an important role. Because the phase of an electron's wave function changes as it passes through such a device, phase measurements are required to characterize the transport properties fully.

In an interference experiment with a quantum dot imbedded in one arm of the Aharonov-Bohm ring [25, 26, 27, 116], the conductance was shown to depend not only on the magnitude of the transmission through the quantum dot, but also on the phase acquired by

electrons traversing the quantum dot. For instance, we consider here a four-terminal configuration to measure directly the magnitude and the phase of transmission coefficient through a quantum dot in the Coulomb blockade regime which is experimentally investigated in Ref. [27] (see Figure 7.1). The configuration consists of emitter E and collector C constrictions, and a base region B in between. The base contacts serve as draining reservoirs with a chemical potential $\mu_B = 0$. The voltage difference between E and B is V_{EB}, and between C and B is V_{CB}. The E and C constrictions are separated by a barrier with two openings: one opening consists of the quantum dot whose behavior we want to measure, and the other is a reference opening in a form of another quantum point contact. At low temperatures both the phase coherent length and the elastic mean free path exceed the entire sample size. Using the multiprobe conductance formula [107], we found that the current at the collector is given by

$$I_C = \frac{e^2}{\pi}(\tau_{EC}V_{EB} \pm \tau_C V_{CB}) \ , \tag{7.1}$$

where τ_{EC} and τ_C are the transmission probabilities from emitter to collector and through the collector quantum point contact respectively. When the collector circuit is open ($I_C = 0$), we can measure directly the transmission probability τ_{EC} by measuring the collector voltage $V_{CB} = (V_{EB}/\tau_C)\tau_{EC}$.

In fact the transmission probability τ_{EC} is a coherent sum over all path amplitudes from emitter to collector. In the two-path case $\tau_{EC} = |t_{EC}|^2$, where $t_{EC} = t_{QD} + t_{sl}$, t_{QD} is the transmission amplitude associated with the path transversing the quantum dot, and t_{sl} refers to the transmission through the other path. When a magnetic field was applied, a magnetic flux Φ, threading the area A, enclosed by these two paths results in an Aharonov-Bohm phase difference $\Delta\phi = 2\pi\Phi/\Phi_0$ ($\Phi_0 = h/e$ is the flux quantum) between the two interfering paths. For single-channel transmission:

$$\tau_{EC} = |t_{QD} + e^{i\Delta\phi}t_{sl}|^2 \ . \tag{7.2}$$

Assuming fully coherent transport through the quantum dot, the interference term is proportional to $|t_{sl}||t_{QD}|\cos[\Delta\phi + \theta(t_{sl}) - \theta(t_{QD})]$, where $\theta(t_{sl})$ and $\theta(t_{QD})$ account for the phase accumulated in the two corresponding paths. As the $\theta(t_{sl})$ is a good approximation constant, a change in the phase of t_{QD} leads to a similar change in the phase of the collector signal.

In the experiment of Yacoby *et al.* [25], the Aharonov-Bohm phase could take only two values 0 and π as a consequence of microreversibility in a two-terminal configuration [26, 117]. The results of this four-terminal configuration are shown experimentally in Ref. [27], allowing a determination of the continuous phase shift of the transmission amplitude through the quantum dot. The success of these experiments gave rise to a number of other works. Hereafter, we will consider the problem of decoherence of electron propagation through the quantum dot due to the effect of environment.

7.2 Dephasing in quantum dot due to coupling with a quantum point contact

Transport through a quantum dot is typically affected by the environment which surrounds it: the level of such a dot acquires a finite linewidth if this environment has strong charge fluctuations. The environment of the quantum dot can be a wire containing a quantum

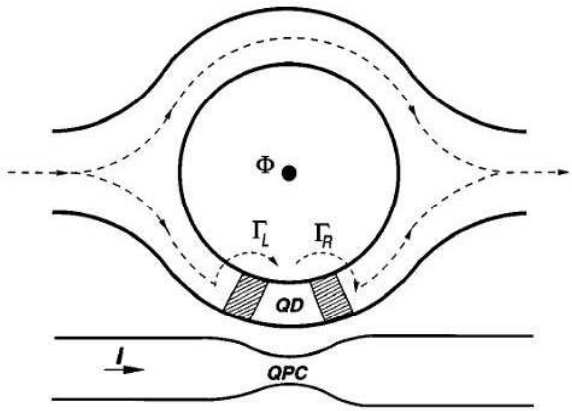

Figure 7.2: Scheme of the "which path" interferometer. A quantum point contact is in the proximity of the quantum dot which is built in the lower arm of an Aharonov-Bohm ring [29].

point contact, which is close or coupled capacitively to the quantum dot [28, 29]. This proposal setup is shown in Figure 7.2. Charge fluctuations in the quantum point contact create a fluctuating potential at the dot, modulate the electron levels in the dot, and destroy the coherence of the transmission through the dot. In this case, the amplitude t_{QD} has to be replaced by its average $\langle t_{QD} \rangle$ with respect to effect of the environment. The destruction of coherence is not necessary related to inelastic scattering and this is why we call it "dephasing".

On the other hand, the electrostatic field of an extra electron on the quantum dot changes the transmission probability T of the nearby quantum point contact, and hence changes the conductance of the wire. The change in the current in the wire "measures" which path the electron took around the ring. To estimate the dephasing rate, we consider the following argument: An electron entering the quantum dot changes the transmission probability of the quantum point contact by ΔT. The rate at which particles probe the quantum point contact at zero temperature is $2eV/h$, where V is the bias voltage in the wire. During the time τ_φ of the electron in the quantum dot, the number of particles probing the quantum point contact is $N = \tau_\varphi 2eV/h$ (see also Figure 3.4). Detection of an electron in the quantum dot requires that the change in this number of particles N exceeds the typical quantum shot noise

$$\tau_\varphi \frac{2eV}{h} \Delta T \geq \sqrt{\tau_\varphi \frac{2eV}{h} T(1-T)} \ . \tag{7.3}$$

The dephasing rate, therefore, depends on both the bias across the quantum point contact and its transmission coefficient:

$$(\tau_\varphi)^{-1} \propto \frac{eV}{h} \frac{(\Delta T)^2}{T(1-T)} \ . \tag{7.4}$$

The formula (7.4) has been obtained by Aleiner *et al.* in Ref. [29]. They showed that the presence of the wire suppresses the Aharonov-Bohm oscillations in two ways. First, real electron-hole-pair creation in the wire measures which path the electron took around the ring, and so causes the paths to decoherence. Second, virtual electron-hole-pair creation in the wire decreases the transmission amplitude through the quantum dot, leading to power-law dependence of the Aharonov-Bohm oscillations on the temperature or the current

through the wire. This result also was obtained in experiment [118] where the sensitivity of the quantum point contact affects the visibility of the oscillatory interference signal.

At the same time, Levinson has calculated independently dephasing rate of a state in quantum dot induced by its capacitive coupling to a quantum point contact and interested mainly in the additional contribution to the dephasing rate which is due to the current in the quantum point contact [28].

The quantum dot is assumed to be isolated from the leads and only one state existing with energy ϵ_0. The Hamiltonian of the quantum dot is $H_{QD} = \epsilon_0 c^\dagger c$, where c is an operator removing one electron from the quantum dot state. The interaction between the quantum dot and the quantum point contact, assumed to be weak, is describes by hamiltonian: $H_{int} = c^\dagger c W$. We can see that W is the change of the quantum dot state energy ϵ_0 due to the interaction of the electron in the quantum dot with the electron density in the point contact.

The coherence of the quantum dot state is described by the average amplitude $\langle c \rangle$, which contains information about the phase of the quantum dot wave function. The quantum dot has a coherent part if $\langle c \rangle \neq 0$. The time evolution of the coherence is given by $\langle c(t) \rangle$, where $c(t) = e^{iHt} c e^{-iHt}$ in Heisenberg representation with the total Hamiltonian $H = H_{QPC} + H_{QD} + H_{int}$ with H_{QPC} and H_{QD} are Hamiltonian of quantum point contact and quantum dot, respectively. The Hamiltonian H_{int} describing the interaction between quantum dot and quantum point contact is assumed to be weak. The motion equation of the operator gives

$$\frac{dc(t)}{dt} = i[H, c(t)] = -i[\epsilon_0 + W(t)]c(t) \ , \tag{7.5}$$

with $W(t) = e^{iHt} W e^{-iHt}$ is demonstrated in this case as the time depending modulation of the energy level ϵ_0. Eq. (7.5) gives the expression of $c(t)$, whose average amplitude can be written as

$$\langle c(t) \rangle = \langle c(0) e^{-i\epsilon_0 t} T_t e^{-i \int_0^t dt W(t)} \rangle \ , \tag{7.6}$$

where T_t means time ordering. By assuming that the level modulation is a Gaussian process described by a quantum correlator $K(t) = [\langle W(t)W(0) \rangle + \langle W(0)W(t) \rangle]/2$, we can decouple the average in Eq. (7.6) as

$$\langle c(t) \rangle = \langle c(0) \rangle e^{-i\epsilon_0 t} e^{-\Phi(t)} \ , \tag{7.7}$$

with

$$\Phi(t) = \int_0^t dt' \int_0^t dt'' K(t' - t'') \ . \tag{7.8}$$

Assuming that the quantum dot does not perturb the quantum point contact, the average in $\langle W(t)W(t') \rangle$ reduces to the average with respect to the state of the point contact. The correlator $K(t)$ decays in time with some time scale τ_C which is the correlation time of the quantum dot state energy modulation. For $t \gg \tau_C$, the second integral over t'' will saturate to a constant, we have

$$\langle c(t) \rangle = \langle c(0) \rangle e^{-i\epsilon_0 t} e^{-t/\tau_\varphi} \ , \tag{7.9}$$

with assuming that, for long times, we can replace the second integral of t'' over the whole time domain:

$$(\tau_\varphi)^{-1} = \frac{1}{2} \int_{-\infty}^{\infty} dt K(t) \ . \tag{7.10}$$

The decay of $\langle c(t) \rangle$ with the time constant τ_φ is dephasing, not energy relaxation or escape from the quantum dot [28]. The author showed that the contribution to the dephasing rate due to the bias depends on temperature θ and bias eV in the same way as shot noise in the point contact at zero-frequency, but do not follow the $T(1-T)$ suppression. The nonequilibrium contribution to dephasing rate is estimated as

$$(\tau_\varphi^{-1})_V \simeq \lambda eV \quad \text{for high bias} \quad eV \gg \theta \ , \tag{7.11}$$

$$(\tau_\varphi^{-1})_V \simeq \lambda (eV)^2/\theta \quad \text{for low bias} \quad eV \ll \theta \ , \tag{7.12}$$

where λ is the coupling constant which describes the interaction between the quantum dot and the quantum point contact.

The problem of dephasing rate of an electron state in a pinched quantum dot also studied with a nearby voltage-biased ballistic nanostructure [119]. In this work, the author presented a generalization of the theory given in Ref. [28] that takes into account the specific effects appearing due to the complicated geometry, and the chirality of the states in the nanostructure.

Chapter 8

Quantum dot dephasing by fractional quantum Hall edge states

8.1 Introduction

As we have introduced in the previous chapter, the decoherence of the electron transport through the quantum dot is due to the charge fluctuations in the quantum point contact [28, 29, 119, 120]. In these results, the dephasing rate typically increases when the voltage bias of the quantum point contact is increased.

The purpose of the present work is to discuss the case of dephasing from a quantum point contact in the fractional quantum Hall effect regime [102]. Quantum point contact transmission can then be described by tunneling between edge states [30], the quantized analog of classical skipping orbits of electrons. In this strongly correlated electron regime, edge states represent collective excitations of the quantum Hall fluid: depending on the pinching of the quantum point contact, it is either fractional quantum Hall quasiparticles or electrons which tunnel. It is particularly interesting because the current–voltage and the noise characteristics deviate strongly from the case of normal conductors [31, 32, 33]: for the weak backscattering case, the current at zero temperature may increase when the voltage bias is lowered, while in the strong backscattering case the $I(V)$ is highly nonlinear. It is thus important to address the issue of dephasing from a Luttinger liquid. Here, we consider the case of simple Laughlin fractions, with filling factor $\nu = 1/m$ (m odd integer). As in Ref. [28], the dephasing of a state in the dot is induced by its capacitive coupling to the biased quantum point contact, assuming that the level modulation in the dot is a Gaussian process and neglecting back-action effects.

In this chapter, we will first compute the dephasing rate in the weak and strong backscattering limit with the assumption that the Coulomb interaction is screened by nearby metallic gate: the Coulomb interaction is then reduced to a delta function potential. Next, we will extend our results to the case of arbitrary backscattering, using the exact solution of the boundary Sine Gorden model developed by Fendley, Ludwig, and Saleur [115]. Finally, we will show that these results can be extended to the case of arbitrary screening.

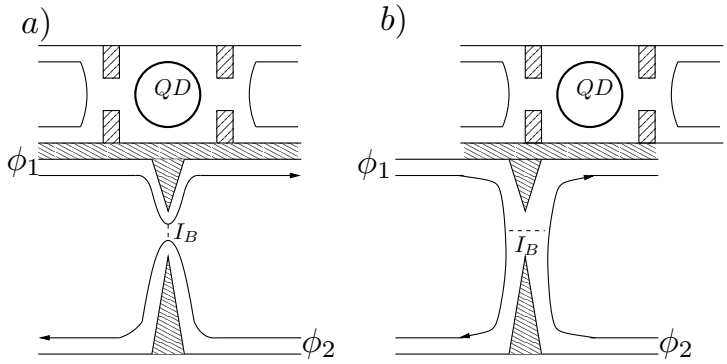

Figure 8.1: Schematic description of the setup: the quantum dot (top) is coupled capacitively to a quantum point contact in the FQHE regime: a) Case of weak backscattering, b) Case of strong backscattering.

8.2 Model setup and Hamiltonian

In Figure 8.1, a gate voltage controls the transmission in the fractional quantum Hall fluid through the quantum point contact. The single level Hamiltonian for the dot reads

$$H_{QD} = \epsilon_0 c^\dagger c \ , \tag{8.1}$$

where $c^\dagger$ creates an electron. This dot is coupled capacitively to the nanostructure–a point contact in the FQHE. The Hamiltonian which describes the edge modes in the absence of tunneling is

$$H_0 = \frac{v_F}{\pi} \int dx[(\partial_x \phi_1)^2 + (\partial_x \phi_2)^2] \ , \tag{8.2}$$

with $\phi_i(x)$ $(i = 1, 2)$ the Luttinger bosonic field, which relates to the electron density operator $\rho_i(x)$ by $\partial_x \phi_i(x) = \frac{\pi}{\sqrt{\nu}} \rho_i(x)$.

By varying the gate potential of quantum point contact, one can switch from a weak backscattering situation, where the Hall liquid remains in one piece (Figure 8.1a), to a strong backscattering situation where the Hall liquid is split in two (Figure 8.1b). In the former case, the entities which tunnel are edge quasiparticle excitations. In the latter case, between the two fluids, only electrons can tunnel. Here, we consider first the weak backscattering case, and then we use a duality transformation[31, 98] to describe the strong backscattering case. The tunneling Hamiltonian between edges 1 and 2 reads:

$$H_t = e^{i\omega_0 t} \Gamma_0 \psi_2^\dagger(0) \psi_1(0) + \text{H.c.} \ , \tag{8.3}$$

where we have used the Peierls substitution to include the voltage: for the weak backscattering, $\omega_0 = e^\star V$, ($e^\star = \nu e$ is the effective charge and ν the filling factor), while $\omega_0 = eV$ for the strong backscattering case. The quasiparticle operator in the case of weak backscattering is $\psi_i(x) = e^{i\sqrt{\nu}\phi_i(x)}/\sqrt{2\pi\alpha}$ (the spatial cutoff is $\alpha = v_F \tau_0$, with τ_0 the temporal cutoff), and in the strong backscattering case the electron operator is obtained with the substitution $\nu \to 1/\nu$.

The Hamiltonian describing the interaction, assumed to be weak, between the dot and quantum point contact reads

$$H_{int} = c^\dagger c W \equiv c^\dagger c \int dx f(x) \rho_1(x) \ , \tag{8.4}$$

with $f(x)$ is a Coulomb interaction kernel, which is assumed to include screening by the nearby gates

$$f(x) \simeq e^2 \frac{e^{-|x|/\lambda_s}}{\sqrt{x^2+d^2}} \ , \tag{8.5}$$

where d is the distance from the dot to the edge and λ_s is the screening length. We can see that W is the change of the quantum dot state energy ϵ_0 due to the interaction of the electron in the quantum dot with the electron density in the quantum point contact.

8.3 Dephasing rate

The dephasing of an electron state in a dot coupled to a fluctuating current is caused by the electron density fluctuations, which generate a fluctuating potential in the dot, resulting in a blurring of the energy level ϵ_0.

The dephasing rate, expressed in terms of irreducible charge fluctuations in the adjacent wire in the fractional quantum Hall effect, is written as [28, 119]

$$\tau_\varphi^{-1} = \frac{1}{4}\int_{-\infty}^{\infty} dt \int dx f(x) \int dx' f(x') \langle\langle \rho_1(x,t)\rho_1(x',0) + \rho_1(x',0)\rho_1(x,t)\rangle\rangle \ . \tag{8.6}$$

In normal and superconducting systems, the dephasing rate can be calculated using the scattering approach. For Luttinger liquids and in particular for the FQHE, because of the electronic interaction, it is convenient to use the Keldysh approach[33, 87]. It induces to generate the symmetrized charge density–density correlator, taking into account backscattering

$$\begin{aligned}\langle\langle \rho_1(x,t)\rho_1(x',t')\rangle\rangle_{sym} = & \sum_{\eta=\pm} \langle T_K \rho_1(x,t^\eta)\rho_1(x',t'^{-\eta}) e^{-i\int_K H_t dt_1}\rangle \\ & -\frac{1}{2}\left[\sum_{\eta=\pm}\langle T_K \rho_1(x,t^\eta) e^{-i\int_K H_t dt_1}\rangle\right]\left[\sum_{\eta=\pm}\langle T_K \rho_1(x',t'^\eta) e^{-i\int_K H_t dt_1}\rangle\right] \ .\end{aligned} \tag{8.7}$$

Here a tunneling event (at $x=0$) creates an excitation which needs to propagate to the location of the dot. The equilibrium (zero point) contribution to the dephasing rate corresponds to the zero order in the tunneling amplitude Γ_0 [it is labeled $(\tau_\varphi^{-1})^{(0)}$]. There is no contribution to first order in the tunneling Hamiltonian since we assume $\langle\phi(x)\rangle = 0$, while the nonequilibrium contribution corresponding to the second order in Γ_0 exists,

$$\tau_\varphi^{-1} = (\tau_\varphi^{-1})^{(0)} + (\tau_\varphi^{-1})^{(2)} + \cdots \ . \tag{8.8}$$

The dephasing rate contributions in the weak backscattering case are calculated as follow:

For the zero-order contribution, we have

$$\begin{aligned}\langle T_K \rho_1(x,t^\eta)\rho_1(x',t'^{-\eta})\rangle &= \frac{\nu}{\pi^2}\langle T_K \partial_x\phi_1(x,t^\eta)\partial_{x'}\phi_1(x',t'^{-\eta})\rangle \\ &= \frac{\nu}{\pi^2}\frac{1}{\gamma\gamma'}\partial^2_{xx'}\langle T_K e^{\gamma\phi_1(x,t^\eta)} e^{\gamma'\phi_1(x',t^{-\eta})}\rangle|_{\gamma,\gamma'=0} \ .\end{aligned} \tag{8.9}$$

In this formula we find $\gamma' = -\gamma$ following the quasiparticle conservation, thus the equilibrium dephasing rate is obtained as[121]:

$$(\tau_\varphi^{-1})^{(0)} = \frac{\nu}{4\pi^2}\int_{-\infty}^{\infty} dt \int dx f(x) \int dx' f(x') \sum_{\eta=\pm} \partial^2_{xx'} G_1^{\eta-\eta}(x-x',t) \ . \tag{8.10}$$

The bosonic Green's function of edge i ($i = 1, 2$) is $G_i^{\eta_1\eta_2}(x-x', t_1-t_2) = \langle \phi_i(x, t_1^{\eta_1})\phi_i(x', t_2^{\eta_2}) - \phi_i^2\rangle$. The coefficients η,$\eta_{1,2} = \pm$ identify the upper and lower branches of the Keldysh contour.

For second order contribution to the dephasing rate, since ψ_1, ψ_2 are independent in the absence of tunneling, we obtain

$$\begin{aligned}
&\sum_{\eta=\pm}\left\langle T_K\rho_1(x,t^\eta)\rho_1(x',t'^{-\eta})\frac{(-i)^2}{2}\int_K dt_1\int_K dt_2 H_t(t_1)H_t(t_2)\right\rangle \\
&= -\frac{\Gamma_0^2}{2}\sum_{\eta=\pm;\epsilon_1,\epsilon_2=\pm}\langle T_K\rho_1(x,t^\eta)\rho_1(x',t'^{-\eta})\int_K dt_1\int_K dt_2 e^{i(\epsilon_1\omega_0 t_1+\epsilon_2\omega_0 t_2)} \\
&\quad [\psi_2^\dagger(t_1)\psi_1(t_1)]^{\epsilon_1}[\psi_2^\dagger(t_2)\psi_1(t_2)]^{\epsilon_2}\rangle \\
&= -\frac{\Gamma_0^2\nu}{2\pi^2(2\pi\alpha)^2}\sum_{\eta,\eta_1,\eta_2,\epsilon_1,\epsilon_2}\int_{-\infty}^{\infty}dt_1\int_{-\infty}^{\infty}dt_2 e^{i(\epsilon_1\omega_0 t_1+\epsilon_2\omega_0 t_2)}\eta_1\eta_2 \\
&\quad \times\left\langle T_K\partial_x\phi_1(x,t^\eta)\partial_{x'}\phi_1(x',t'^{-\eta})e^{i\sqrt{\nu}\epsilon_1\phi_1(0,t_1^{\eta_1})}e^{i\sqrt{\nu}\epsilon_2\phi_1(0,t_2^{\eta_2})}\right\rangle \\
&\quad \times\left\langle T_K e^{-i\sqrt{\nu}\epsilon_1\phi_2(0,t_1^{\eta_1})}e^{-i\sqrt{\nu}\epsilon_2\phi_2(0,t_2^{\eta_2})}\right\rangle \ .
\end{aligned} \tag{8.11}$$

Quasiparticle conservation imposes $\epsilon_1 = -\epsilon_2 \equiv \epsilon$, so

$$\begin{aligned}
(\tau_\varphi^{-1})^{(2)} &= -\frac{\nu}{4\pi^2}\frac{\Gamma_0^2}{2(2\pi\alpha)^2}\int_{-\infty}^{\infty}dt\int dx f(x)\int dx' f(x')\sum_{\eta,\eta_1,\eta_2,\epsilon}\eta_1\eta_2 \\
&\quad \times\int_{-\infty}^{\infty}dt_1\int_{-\infty}^{\infty}dt_2 e^{i\epsilon\omega_0(t_1-t_2)}e^{\nu G_2^{\eta_1\eta_2}(0,t_1-t_2)}e^{\nu G_1^{\eta_1\eta_2}(0,t_1-t_2)}\left\{\partial_{xx'}^2 G_1^{\eta-\eta}(x-x',t)\right. \\
&\quad \left. +\nu[\partial_x G_1^{\eta\eta_1}(x,t-t_1)-\partial_x G_1^{\eta\eta_2}(x,t-t_2)][\partial_{x'}G_1^{-\eta\eta_1}(x',-t_1)-\partial_{x'}G_1^{-\eta\eta_2}(x',-t_2)]\right\} \ .
\end{aligned} \tag{8.12}$$

The dephasing rate depends on the geometry of the setup via the length scales d, λ_s, and α. The equivalent result for strong backscattering is obtained by replacing $\nu \to 1/\nu$ next to the Green's function (duality).

The Green's function at finite temperature is given as

$$G_1^{\eta\eta'}(x,t) = -\ln\left[\frac{\sinh\left(\frac{\pi}{\beta}\left[(x/v_F-t)\left(\frac{\eta+\eta'}{2}\mathrm{sgn}(t)-\frac{\eta-\eta'}{2}\right)+i\tau_0\right]\right)}{\sinh\left(\frac{i\pi\tau_0}{\beta}\right)}\right] \ . \tag{8.13}$$

In the zero temperature limit, we expand the $\sinh(\cdots)$ function into a Taylor series and takes into account only the lowest order contribution, we obtain the Green's function at zero-temperature as in Ref. [33]:

$$G_1^{\eta\eta'}(x,t) = -\ln\left[\tau_0 + i(t-x/v_F)\left(\frac{\eta+\eta'}{2}\mathrm{sgn}(t)-\frac{\eta-\eta'}{2}\right)\right] \ . \tag{8.14}$$

8.3.1 Dephasing rate for the case of weak and strong backscattering and strong screening

The assumption of strong screening $\lambda_s \sim \alpha = v_F\tau_0$ is made, that means the Coulomb interaction $f(x)$ as we have chosen above acts in very short range. Regarding the formula

of $f(x)$ in Eq. (8.5) with $\lambda_s \sim \alpha$, we find that $e^{-|x|/\alpha}$ decreasing fast to zero with the value of x is non-infinitesimal. In this case, it turns out $x \ll d$ and thus $\sqrt{x^2+d^2} \simeq d$. The Coulomb interaction is reduced to the delta function,

$$f(x) \simeq 2e^2 \frac{\alpha}{d} \delta(x) \ . \tag{8.15}$$

However, we find that this assumption is not necessary, and it will be relaxed later on. Inserting the Green's function in Eq. (8.13) in the dephasing rate [Eq. (8.10) and Eq. (8.12)] gives

$$(\tau_\varphi^{-1})^{(0)} = \frac{4e^4\tau_0^2\nu}{\pi\beta d^2} \ , \tag{8.16}$$

and with the change of variables $\tau = t_1 - t_2$, $\tau_1 = t - t_1$, and $\tau_2 = t_2$, we obtain:

$$\begin{aligned}(\tau_\varphi^{-1})^{(2)} = &-\frac{e^4\nu^2\Gamma_0^2}{4\beta^2\pi^2 v_F^2 d^2} \sum_\eta \int_{-\infty}^{\infty} d\tau \cos[\omega_0\tau] \left[\frac{\sinh^{2\nu}\left(\frac{\pi}{\beta} i\tau_0\right)}{\sinh^{2\nu}\left[\frac{\pi}{\beta}(\eta\tau + i\tau_0)\right]} + \frac{\sinh^{2\nu}\left(\frac{\pi}{\beta} i\tau_0\right)}{\sinh^{2\nu}\left[\frac{\pi}{\beta}(-\eta\tau + i\tau_0)\right]} \right] \\ &\times \int_{-\infty}^{\infty} d\tau_1 \left[\mathrm{sgn}(\tau_1) \coth\left(\frac{\pi}{\beta}[-\eta \mathrm{sgn}(\tau_1)\tau_1 + i\tau_0]\right) + \coth\left(\frac{\pi}{\beta}[\eta\tau_1 + i\tau_0]\right) \right] \\ &\times \int_{-\infty}^{\infty} d\tau_2 \left[-\mathrm{sgn}(\tau_2) \coth\left(\frac{\pi}{\beta}[\eta \mathrm{sgn}(\tau_2)\tau_2 + i\tau_0]\right) + \coth\left(\frac{\pi}{\beta}[\eta\tau_2 + i\tau_0]\right) \right] \ . \end{aligned} \tag{8.17}$$

In the integral over τ, we change variables to $t = -\tau \mp i\tau_0 \pm i\beta/2$ for the first (second) term, and the integral now runs in the complex plane form $-\infty \mp i\tau_0 \pm \beta/2$ to $+\infty \mp i\tau_0 \pm \beta/2$. We bring it back to $(-\infty, +\infty)$ by deforming the contour because there are no poles in the integrand. For $\tau_0 \ll \omega_0^{-1}, \beta$, we obtain

$$(\tau_\varphi^{-1})^{(2)} = \frac{e^4\Gamma_0^2}{\pi^2 v_F^2 d^2} \frac{\nu^2\tau_0^{2\nu}}{\mathbf{\Gamma}(2\nu)} \left(\frac{2\pi}{\beta}\right)^{2\nu-1} \cosh\left(\frac{\omega_0\beta}{2}\right) \left| \mathbf{\Gamma}\left(\nu + i\frac{\omega_0\beta}{2\pi}\right) \right|^2 \ . \tag{8.18}$$

In the zero temperature limit, we have $(\tau_\varphi^{-1})^{(0)} = 0$ and

$$(\tau_\varphi^{-1})^{(2)} = \frac{e^4\Gamma_0^2}{\pi v_F^2 d^2} \frac{\nu^2\tau_0^{2\nu}}{\mathbf{\Gamma}(2\nu)} |\omega_0|^{2\nu-1} \ . \tag{8.19}$$

Comparing the formula of nonequilibrium dephasing rate in Eq. (8.18) with the backscattering current noise in Eq. (6.55) [also comparing Eq.(8.19) with Eq. (6.56)], we find

$$(\tau_\varphi^{-1})^{(2)} = \left(\frac{e\tau_0}{d}\right)^2 S(0) \ , \tag{8.20}$$

Eq. (8.20) shows that the nonequilibrium dephasing rate is proportional to the backscattering current noise, which can be understood by noticing the continuity equation with assumption that the edge current without backscattering does not fluctuate in time. This interesting result suggest us to extend our problem to the case of arbitrary backscattering which is considered latter on.

Using duality, we readily obtain results for the strong backscattering case: the equilibrium contribution in the dephasing rate is the same as in the weak backscattering case. The nonequilibrium contribution can be obtained from the weak backscattering case by replacing $\nu \to 1/\nu$ (recall that ω_0 is defined in a different manner in the two limits).

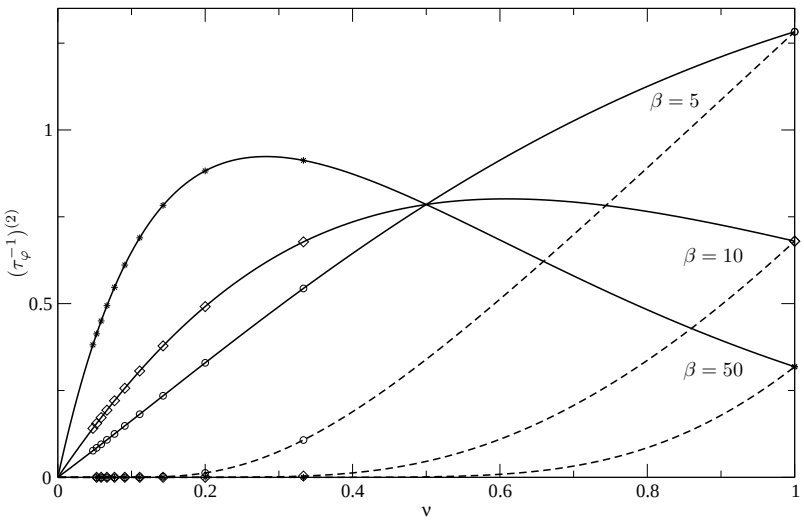

Figure 8.2: Dependance of the nonequilibrium contribution of the dephasing rate on the filling factor for both case weak (full line) and strong (dashed line) backscattering at $\beta = 5, 10, 50$ and quantum point contact bias $eV = 0.1$. The star, diamond and circle points correspond to the Laughlin fractions $\nu = 1/m$, m odd integer.

Numerical results and discussion

The nonequilibrium contribution of the dephasing rate is proportional to the zero-frequency noise in the quantum Hall liquid, which is computed in Refs. [32, 33, 87, 98]. The theoretical predictions of noise in the weak and strong backscattering limits have been verified in point contact experiments at filling factor $\nu = 1/3, 1/5$ [40, 41, 42]. This is understood from the continuity equation, which relates the current operator to the density operator[120]. At zero temperature, the nonequilibrium dephasing rate of Eq. (8.19) for weak backscattering depends on the quantum point contact bias with the exponent $2\nu - 1 < 0$. This is in sharp contrast with Ref. [28], where the quantum point contact bias dependence is linear. We also calculate numerically this contribution at finite temperatures and consider it as a function of the filling factor or the quantum point contact voltage bias. In our numerical calculations, we choose the inverse cutoff τ_0^{-1} as the energy scale and the nonequilibrium contribution for the dephasing rate is plotted in units of $e^4\Gamma_0^2\tau_0/(\pi^2\hbar^4 v_F^2 d^2)$.

In Figure 8.2, we plot the dependence of this contribution on the filling factor ν for both weak and strong backscattering cases for several temperatures ($\beta = 5, 10, 50$) at fixed quantum point contact bias. ν is considered here as a continuous variable, while it has physical meaning only at Laughlin fractions[102]. For the strong backscattering case, the dephasing rate increases when the filling factor increases. At small ν, it is zero; then, it increases rapidly. The higher the temperature, the faster the increase. For the weak backscattering case, the shape of the dephasing rate depends on the ratio of quantum point contact bias and temperature. At low temperature ($1/\beta \ll eV$), the dephasing rate function has a local maximum at $\nu < 1/2$, the position of which depends on temperature: when the temperature increases, it gets closer to $\nu = 1/2$ and its height decreases, the rate at $\nu = 1$ is smaller than that at $\nu = 1/3$. This result demonstrates that for two different filling factors, we can have comparable dephasing rates. Around the crossover in temperature ($\beta eV \simeq 1$), the local maximum in the dephasing rate broadens. At high

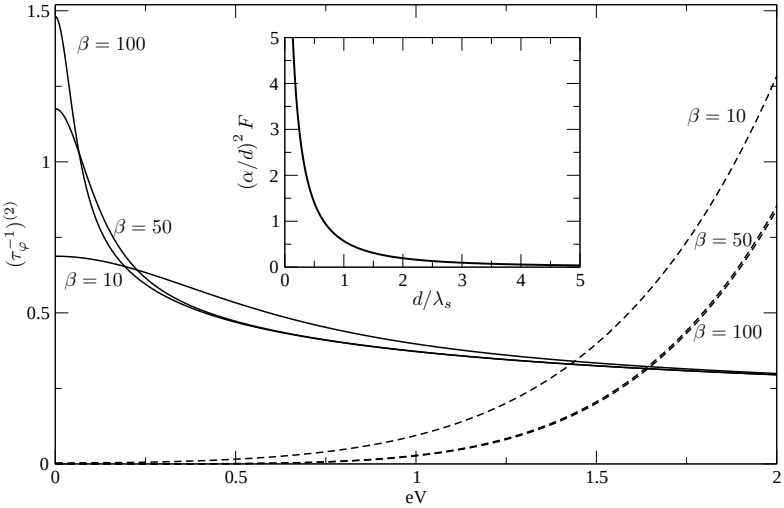

Figure 8.3: Nonequilibrium contribution in the dephasing rate as a function of quantum point contact bias with the filling factor $\nu = 1/3$ at some values of temperature $\beta = 10, 50, 100$ for the weak and strong backscattering cases (correspond to the solid and the dashed lines). The inset is the ratio of nonequilibrium contribution in the dephasing rate between the arbitrary screening and strong screening multiplied by $(\alpha/d)^2$ as a function of d/λ_s.

temperature ($1/\beta > eV$), the dephasing rate increases when the filling factor increases. We find that the dephasing rates evaluated at different temperatures coincide at the (unphysical) value $\nu = 1/2$, because the hyperbolic cosine multiplied by the squared modulus of the Gamma function in Eq. (8.18) does not depend on temperature, while at the same time the exponent $(2\nu - 1)$ is zero: this is known for perturbative calculations of the backscattering current and noise.

In Figure 8.3, the dependence of the nonequilibrium contribution of the dephasing rate on the quantum point contact bias voltage is plotted for several temperatures. In the case of strong backscattering, the dephasing rate increases when the bias eV increases. When the temperature is low enough ($1/\beta \ll eV$), the dephasing rate saturates. In the case of high temperatures ($1/\beta > eV$), the dephasing rate also increases when eV increases, but it increases from a finite value (not shown), which is proportional to the temperature. Things are quite different at weak backscattering. At high temperatures, the dephasing rate decreases when we increase eV: this behavior is symptomatic of current and noise characteristic in a Luttinger liquid. In the low-temperature case $1/\beta \ll eV$, for small eV, the lower the temperature, the larger the dephasing rate and the faster it decreases when we increase eV. At $\theta = 0$, the dephasing rate is "infinite" at $eV = 0$. This Luttinger liquid behavior is in sharp contrast with the result of Ref. [28].

8.3.2 General expression of dephasing rate for arbitrary backscattering

As we have seen before, the dephasing rate is proportional to the zero-frequency tunneling current noise (see Eq. (8.20)). This is because the charge fluctuations are directly related to the current fluctuations along the edges following the continuity equation. The continuity equation relates the current operator to the density operator as it holds in second

quantized form:

$$\rho(x,\omega) = \frac{1}{i\omega}\nabla.\mathbf{J}(x,\omega) \ . \tag{8.21}$$

From Eq. (8.21), we can write a connection formula between the edge current noise correlator and the density-density correlator at finite frequency as

$$\langle\langle\rho(x_1,\omega)\rho(x_2,-\omega)\rangle\rangle = \int_{-\infty}^{+\infty}\frac{dt}{\omega^2}e^{i\omega t}\partial_{x_1}\partial_{x_2}\langle\langle I(0)I(t)\rangle\rangle \ . \tag{8.22}$$

In our case, the density-density correlations is considered with $\omega = 0$. Taking the derivative with respect to the positions, the ω^2 term in the denominator is canceled, for all bias regimes, giving a finite contribution to the density fluctuations. in a perturbative calculation of the tunneling Hamiltonian. Note that at zero temperature, the current along the edge without backscattering does not make a shot noise, then the fluctuations of the currents along the edges are also identical to the fluctuations of the tunneling current. The tunneling current fluctuations were computed non perturbatively using Bethe-ansatz techniques[115, 122, 123].

Here, before showing the relation between the dephasing rate and the current noise for arbitrary backscattering, I will rederive the general expression of the current noise as shown in Ref. [115]. In this work, the authors consider the fractional quantum Hall model in terms of even and odd left-moving bosons $\phi^{e,o}(x+t) = [\phi_1(x,t) \pm \phi_2(-x,t)]/\sqrt{2}$. The even and odd charges are thus related to the charges of the original left- and right-moving edges by $\Delta Q = Q_1 - Q_2 = \sqrt{2}Q^o$ and $Q_1 + Q_2 = \sqrt{2}Q^e$. Q^e is the total charge on both edges and is conserved even in the presence of the interaction. The backscattering current thus depends only on the odd boson theory. The description of our model in terms of quasiparticles allows us to calculate exact transport properties. Integrability ensures the existence of a quasiparticle basis where the scattering is one by one. These results are known in Refs. [124, 125, 126]. For any ν, the spectrum containing a kink and an antikink with the charges $Q^o = 1/\sqrt{2}$ and $-1/\sqrt{2}$ respectively, is characterized by the rapidity θ defined by $E = -pv_F = Me^{\theta}/2$, where M is an arbitrary scale.

When a positive voltage is turned on, the positively charged quasiparticles (the kinks) fill the sea. If they do not interact, the kinks will fill all momentum states with $v_F p < eV/2$ at zero temperature. The position of the Fermi level is shifted and the density of quasiparticles is changed due to the interaction. If we define $\rho(\theta)$ is the density then $\rho(\theta) = 0$ for $\theta > A$ with A is the shift of the Fermi level.

Without backscattering interaction, the current at zero temperature arises from the kinks moving to the left at the Fermi velocity

$$I_0(V) = ev_F\int_{-\infty}^{A} d\theta\rho(\theta) = \nu\frac{e^2}{2\pi}V \ . \tag{8.23}$$

The backscattering current is the rate at which the charge of the left-moving edge is depleted $I_B = \partial_t[e\Delta Q/2] = \partial_t[(e/\sqrt{2})Q^o]$. In the quasiparticle basis, tunneling corresponds to the process of a kink scattering off the contact into an antikink.

We consider the impurity S matrix element $S_{jk}(p/T_B)$ which describes a single quasiparticle of type j and momentum p scattering elastically of the point contact into a quasiparticle of type k. The energy T_B characterizes the contact $T_B \propto \lambda^{1/(1-\nu)}$ (perturbative argument of the renormalization group, see Ref. [127]) and the rapidity θ_B can be defined by the relation $T_B = Me^{\theta_B}/2$ so that the impurity S matrix elements are functions

of $\theta - \theta_B$. The Bethe-ansatz technique gives the tunneling probability as [124]

$$|S_{+-}(\theta - \theta_B)|^2 = \frac{1}{1 + \exp\left[2\frac{1-\nu}{\nu}(\theta - \theta_B)\right]} \tag{8.24}$$

and $|S_{++}|^2 = 1 - |S_{+-}|^2$. So that at zero temperature, we have

$$I_B(V, T_B) = -ev_F \int_{-\infty}^{A} d\theta \rho(\theta) |S_{+-}(\theta - \theta_B)|^2 \tag{8.25}$$

The total current I: $I(V, T_B) = I_0(V) + I_B(V, T_B)$ does not depend on time since the system is in a steady state. In fact, this current is $I = \langle j(t) \rangle$ where the current operator $j(t)$ includes the current with its fluctuations. The current fluctuations are characterized by the correlator

$$C(\omega) = \frac{1}{2} \int dt e^{i\omega t} \langle [j(t), j(0)] \rangle \ . \tag{8.26}$$

In this quasiparticle picture, the quasiparticles are correlated but at zero temperature, all the kink states with rapidity less than A are filled, and the remaining kink states, as well as all antikink states, are empty. Shot noise occurs when the backscattering is included. We can describe the dc shot noise from the quasiparticle approach because the scattering off the point contact is elastic and one by one. A left mover backscatters into a right mover corresponds to an odd-boson kink scattering into an antikink. If we define $f = 1$ when a kink of momentum p scatters into an antikink, and $f = 0$ if it scatters into a kink then the average over many events is $\langle f \rangle = |S_{+-}(p/T_B)|^2$. In the quasiparticle approach, the noise is then proportional to the fluctuation of f: $C(0) \propto (\langle f^2 \rangle - \langle f \rangle^2)$. Since f is either 0 or 1, $\langle f^2 \rangle = \langle f \rangle$ [53, 54], we have

$$C(0) = e^2 v_F \int_{-\infty}^{A} d\theta \rho(\theta) |S_{+-}(\theta - \theta_B)|^2 [1 - |S_{+-}(\theta - \theta_B)|^2] \ . \tag{8.27}$$

Following the form of the transmission amplitude in Eq. (8.24), we can write

$$|S_{+-}|^2 [1 - |S_{+-}|^2] = \frac{\nu}{2(1-\nu)} \frac{\partial |S_{+-}|^2}{\partial \theta_B} \ . \tag{8.28}$$

Since neither ρ nor A depends on θ_B, we can pull the ∂_{θ_B} out of the integral. Using the expressions (8.23) and (8.25) for $I(V, T_B)$ and noticing that $T_B \partial_{T_B} = \partial_{\theta_B}$, we have

$$C(0) = -\frac{e\nu}{2(1-\nu)} T_B \partial_{T_B} I(V, T_B) \ . \tag{8.29}$$

We notice that $I(V, T_B)/V$ is the function of only V/T_B (see Eqs. (9) and (10) of Ref. [115]), that means

$$V \frac{\partial}{\partial T_B} \frac{I(V, T_B)}{V} = -\frac{V^2}{T_B} \frac{\partial}{\partial V} \frac{I(V, T_B)}{V} \ , \tag{8.30}$$

then we find another formula for zero-frequency noise [115]

$$C(0) = \frac{e\nu}{2(1-\nu)} (V G_{diff} - I) \ , \tag{8.31}$$

where $G_{diff} = \partial_V I$ is the differential conductance.

We can therefore invoke current conservation at the point contact to derive a general formula for the decoherence rate, which describes the crossover from the weak to the strong backscattering regime,

$$(\tau_\varphi^{-1})^{(2)} = \frac{e^3\tau_0^2}{d^2}\frac{\nu}{1-\nu}(VG_{diff} - I) \ , \tag{8.32}$$

Equation (8.32) allows us to describe the crossover in the dephasing rate from the weak to the strong backscattering regime at zero temperature. It is more difficult to derive a general result at finite temperature because the current in the absence of backscattering fluctuates at finite temperature.

8.3.3 Dephasing rate in the case of arbitrary screening

We now consider again the pertubative calculation of the dephasing rate. Remarkably, for the weak and strong backscattering regimes, it is possible to go beyond the strong screening limit, and we can compute Eq. (8.12) for an arbitrary Coulomb kernel $f(x)$:

$$\begin{aligned}(\tau_\varphi^{-1})^{(2)} =& -\frac{\nu^2\Gamma_0^2}{4\beta^2\pi^2 v_F^2\alpha^2}\int dx \int dx' f(x)f(x') \\ \times&\sum_\eta \int_{-\infty}^{\infty} d\tau \cos[\omega_0\tau]\left[\frac{\sinh^{2\nu}\left(\frac{\pi}{\beta}i\tau_0\right)}{\sinh^{2\nu}\left[\frac{\pi}{\beta}(\eta\tau + i\tau_0)\right]} + \frac{\sinh^{2\nu}\left(\frac{\pi}{\beta}i\tau_0\right)}{\sinh^{2\nu}\left[\frac{\pi}{\beta}(-\eta\tau + i\tau_0)\right]}\right] \\ \times&\int_{-\infty}^{\infty} d\tau_1 \left[\mathrm{sgn}(\tau_1)\coth\left(\frac{\pi}{\beta}[-\eta\mathrm{sgn}(\tau_1)(x/v_F - \tau_1) + i\tau_0]\right) + \coth\left(\frac{\pi}{\beta}(-\eta(x/v_F - \tau_1) + i\tau_0)\right)\right] \\ \times&\int_{-\infty}^{\infty} d\tau_2 \left[-\mathrm{sgn}(\tau_2)\coth\left(\frac{\pi}{\beta}[\eta\mathrm{sgn}(\tau_2)(x' + \tau_2) + i\tau_0]\right) + \coth\left(\frac{\pi}{\beta}[\eta(x'/v_F + \tau_2) + i\tau_0]\right)\right] \ .\end{aligned} \tag{8.33}$$

The triple-time integral in the second order contribution to the dephasing rate is computed analytically as

$$\begin{aligned}(\tau_\varphi^{-1})^{(2)} =& -\frac{\Gamma_0^2}{4\beta\pi^3 v_F^2\alpha^2}\frac{\nu^2(-i)^{2\nu}2^{2\nu-2}}{\mathbf{\Gamma}(2\nu)}\sinh^{2\nu}\left(\frac{\pi}{\beta}i\tau_0\right)\cosh\left(\omega_0\tau_0 - \frac{\omega_0\beta}{2}\right)\left|\mathbf{\Gamma}\left(\nu + i\frac{\omega_0\beta}{2\pi}\right)\right|^2 \\ &\times\sum_\eta\left\{\int dx f(x)\left[i(2\tau_0 + \eta\beta) + \frac{\beta}{\eta\pi}\ln\left(\frac{\sinh\left[\frac{\pi}{\beta}(\eta x/v_F + i\tau_0)\right]}{\sinh\left[\frac{\pi}{\beta}(-\eta x/v_F + i\tau_0)\right]}\right)\right]\right\}^2 \ .\end{aligned} \tag{8.34}$$

We also consider the dephasing rate in Eq. (8.34) for $\tau_0 \ll \omega_0^{-1},\ \beta$ with regarding the properties of function $\ln\left(\sinh\left[\frac{\pi}{\beta}(\eta x/v_F + i\tau_0)\right]/\sinh\left[\frac{\pi}{\beta}(-\eta x/v_F + i\tau_0)\right]\right)$ and further simplifying that $f(x)$ even, we obtain

$$(\tau_\varphi^{-1})^{(2)} = \frac{4\Gamma_0^2}{\pi^2 v_F^4}\frac{\nu^2\tau_0^{2\nu-2}}{\mathbf{\Gamma}(2\nu)}\left(\frac{2\pi}{\beta}\right)^{2\nu-1}\cosh\left(\frac{\omega_0\beta}{2}\right)\left|\mathbf{\Gamma}\left(\nu + i\frac{\omega_0\beta}{2\pi}\right)\right|^2\left[\int_0^\infty dx f(x)\right]^2 \ . \tag{8.35}$$

The result can be displayed in terms of the ratio between the arbitrary screening dephasing rate and the strong screening dephasing rate (both nonequilibrium contributions):

$$F \equiv \frac{(\tau_\varphi^{-1})^{(2)}}{(\tau_\varphi^{-1})^{(2)}_{\lambda_s\to\alpha}} = \frac{d^2}{(e\alpha)^2}\left[\int_0^\infty dx f(x)\right]^2 \ , \tag{8.36}$$

where the integral is a function of d/λ_s and we recall that α is the spatial cutoff. If the Coulomb interaction kernel $f(x)$ is chosen as suggested before [see Eq. (8.5)], the dephasing rate at arbitrary λ_s has an analytical expression

$$F = \left(\frac{\pi d}{2\alpha}\right)^2 \left[E_0\left(\frac{d}{\lambda_s}\right) + N_0\left(\frac{d}{\lambda_s}\right)\right] , \tag{8.37}$$

where $E_0(d/\lambda_s)$ and $N_0(d/\lambda_s)$ are the Weber and Neumann functions[128], both of zero order. F is plotted in the inset of Figure 8.3, and $(\alpha/d)^2$ is taken to be a small constant. F is infinite in the absence of screening, but in practical situations, the presence of metallic gates always imposes a finite screening length. F decreases with d/λ_s and approaches 1 when λ_s is close to the spatial cutoff α (strong screening). The dephasing rate increases when the screening decreases.

8.4 Conclusion

To summarize, we have established a general formula for the dephasing rate of a quantum dot located in the proximity of a fluctuating fractional edge current. In the case where screening is strong, we have shown that the dephasing rate is given by the tunneling current noise, regardless of the regime (weak or strong backscattering) which is considered. For weaker screening, the spatial dependence of the density-density correlation function has to be taken into account, but we have shown explicitly that the long-range nature of the Coulomb interaction can be included as a trivial multiplicative factor.

We conjecture that in order to describe the crossover in the dephasing rate between weak and strong backscattering cases for arbitrary screening, it is sufficient to use the strong screening crossover result of Eq. (8.32) and to insert it into Eq. (8.36). We note that this is clear at zero temperature. However, our result is also applied for the finite temperature and because the continuity equation is general, we expect that we can also describe the dephasing rate (or noise) for the arbitrary backscattering at finite temperature by investigating noise (or dephasing rate) in the corresponding case. It turns out to suggest another way to measure noise at zero-frequency.

On the one hand, the fact that the dephasing rate decreases with increasing voltage can be reconciled with the fact that the charge noise is directly related to the backscattering current noise in the FQHE. There it is known, and seen experimentally, that when the bias voltage dominates over the temperature, both the tunneling current and noise bear a power-law dependence $\sim V^{2\nu-1}$ with a negative exponent. On the other hand, the fact that at low temperatures, the dephasing rate for filling factors can be lower than that of the integer quantum Hall effect comes as a surprise, which is contained in the temperature-voltage crossover formula of Eq. (8.18). It is yet another consequence of chiral Luttinger liquid theory.

The present results could be tested with gated heterostructures as in Ref. [129] (see Figure 4a of this work), provided that the electron mobility and the magnetic field are further increased in order to achieve the FQHE regime and provided that the quantum dot is placed next to the quantum point contact as in Figure 8.1.

Conclusion

In this thesis, we have described situations where two mesoscopic devices are coupled to each other. One of these constitutes the "detector" while the other one is the "source" – the device on which a measurement is performed. The source was subjected to an applied dc bias, resulting in a current which fluctuates in time. These fluctuations were characterized, in our work, the finite frequency noise (the Fourier transform of the current-current correlation). In the first part of the thesis, we focused on a system where the source of noise is arbitrary. In the second part, we used a known source of noise – a fluctuating current in the fractional quantum Hall regime.

We presented a review of noise and its detection at high frequencies in the first part. The concepts of noise were presented in chapter 2. So far, measurements of noise have been done mainly at low frequency (kHz range), which corresponds to the white noise regime of thermal and shot noise. Yet, while it is difficult to measure it, high frequency noise allows to further characterize the transport in mesoscopic devices. In nanotube transport for instance, we can probe frequency scales which corresponds to the size of the device [130] (which in practice can reach frequencies from the GHz to the THz regime). This has challenged physicists working in quantum nanophysics to construct methods to measure noise at high frequency, using novel electronic detection such as on chip devices coupled to the source of noise. In the recent years, measurement setups for detecting quantum noise have used capacitive coupling between two mesoscopic systems [20]. The detection then makes use of dynamical Coulomb blockade theory [64], which was presented in chapter 3 of this thesis, and has recently generated a lot of excitement [20, 21, 22, 23, 75]. Pursuing this current issue, we have studied a new capacitive coupling scheme based on hydrid normal metal-superconductor devices in order to study the high frequency spectral density of noise of a mesoscopic device. The original results of this work were explained in chapter 5.

In our model, the detector, which consists of a normal metal-superconductor junction, was capacitively coupled to a mesoscopic device where noise is to be measured. Because the junction contains a superconducting element, in the subgap regime, two electrons need to be transferred as the elementary charge tunneling process. "Photons" originating from the mesoscopic circuit can be provided to/from the constituent electrons of the Cooper pair in the tunneling process. We have computed the dc current in the detector circuit for two different situations. In a first step, we considered a single normal metal–superconductor junction, and we computed all lowest order elastic and inelastic charge transfer processes which can be involved in the measurement of noise: the photo-assisted transfer of single (and pairs of) electrons (with energies within the gap) into quasiparticle(s) above the gap, and photo-assisted Andreev transfer of electrons as a Cooper pair in the subgap regime. It was shown that when the detector voltage is smaller than (and not close to) the superconducting gap, the Andreev reflection contribution dominates in the photo-assisted tunneling current. This suggested to consider Andreev reflection to probe high frequency

noise in a more complex detector circuit where the normal metal and the superconductor are separated by a quantum dot. There, the dot acts as an additional energy filtering device. We found that it is possible to make such a distinction between photon emission and absorption processes. The NDS detection setup could therefore provide more information on the spectral density of noise than the NS setup. The central point of this study is to obtain the signature of noise via the measurement of dc photo-assisted tunneling current in the detector circuit, for both the NS and NDS setups, following one form (see text in chapter 5). We noticed that the sign of the frequency corresponding to the absorption/emission of a photon from/to the mesoscopic circuit lets us distinguish clearly these different processes in the asymmetrized noise.

This study has dealt only with the measurement of the lowest current moment, the noise. Yet in order to fully characterize transport in a mesoscopic device, all current moments, at all frequencies, need to be known. This constitutes a very exciting field of mesoscopic physics called full counting statistics [73]. While full counting statistics is a field where theoretical contributions dominate, recent experiments have started to address such challenges [74]. The third moment of the current has now been measured at relatively low frequencies, but its detection at high frequencies remains a challenge. It would be therefore be very useful to imagine detection schemes based on the above capacitive scenarios where the frequency spectrum of the third moment could be measured. This constitutes an interesting perspective for future work [131].

Another perspective deals with the detection of finite frequency noise correlations in mesoscopic conductors which contain many terminals. Specially, in Y shaped junctions, where electrons are injected from one lead, and collected in two other leads, we can for instance probe directly the statistics of the charge carriers by measuring noise cross correlations between the two branches [55, 132]. The dynamics of electron transfer at the junction could thus be studied by analyzing the spectrum of the cross correlations [133]. So far, there are no experiments which can address these issues at high frequencies, yet proposals for detecting quantum non locality effects (Bell inequalities) [134] or for detecting anomalous charges in carbon nanotubes [135] require such type of measurements. Given the success of two terminal high frequency noise measurements using capacitively coupled circuits, it is tempting to ask whether the same detection scenarios can be envisioned for the high frequency noise cross correlations.

For the second part of this study, our motivation was different, and we used a known source of noise: a point contact placed on a quantum Hall bar, placed at sufficiently high magnetic field so that one reaches the fractional quantum Hall regime [101, 102]. In this setup it is well established that electron interactions in the Hall fluid lead to dramatic behavior in the current and in the noise [31, 32, 33]. Indeed, besides non-interacting systems, it is more challenging to study a system with electron interaction effects as a noise source. In general, this constitutes a daunting problem, yet in one dimension, there are available tools (Luttinger liquid theory [111]) which allows to tackle such problems. The history and properties of FQHE were presented in chapter 6. If a fluctuating current originated from the quantum point contact is placed next to a quantum dot, strong charge fluctuations associated with the current noise will affect the quantum dot level. In chapter 7, we introduced the dephasing of electron propagation through a quantum dot embedded in one arm of a double-slit interference due to the effect of this environment (the quantum point contact).

Following the pioneering work of Y. Levinson [28], we established a general formula for

the dephasing rate of a quantum dot located in the proximity of a fluctuating fractional edge current, which was presented in chapter 8. The quantum dot can, as in the first part of this study, be considered as a detector: information about the line width (obtained for instance by placing the dot in an Aharonov-Bohm ring) is directly linked to charge noise. In the case where screening is strong, we showed that the dephasing rate is proportional to the backscattering current noise and therefore, in the weak backscattering regime, it decreases when voltage bias applied to the quantum point contact is increased. This result is counter intuitive when considering non interacting noise sources [28, 29], or noise sources consisting of normal metal-superconducting junctions [120], because there it is predicted that the dephasing always increases when the voltage bias of the noise source is increased. In our case, these results can nevertheless be reconciled with the fact that the charge noise is directly related to the backscattering current noise in the FQHE regardless of the regime (weak or strong backscattering). The decrease of the dephasing rate with an increasing voltage is a mere consequence of the anomalous behavior on the current voltage characteristics of fractional quantum Hall chiral edge states in the weak backscattering regime [31, 32, 33]. We also considered the case of arbitrary screening. For weaker screening, the spatial dependence of the density-density correlation function has to be taken into account, but we showed explicitly that the long range nature of the Coulomb interaction can be included as a trivial multiplicative factor. Next, we conjectured that it is possible to describe the crossover in the dephasing rate between weak and strong backscattering cases for arbitrary screening at zero temperature.

The results which have been presented could be tested using Gallium Arsenide two dimensional electron gases of high mobility under high magnetic fields. Experiments on dephasing in the integer quantum Hall regime have already been performed [129], confirming to some extent the predictions of Levinson. Yet from our point of view, it would be very stimulating to increase the magnetic field in order to probe the dephasing of the quantum dot next to a noise source which is placed in the fractional quantum Hall regime.

A perspective of this work would be to go beyond the Gaussian approximation of Levinson, which was used to derive the dephasing rate. In principle this dephasing rate should also include a dependence of the higher moments of charge, which are also related to the higher moments of currents from the full counting statistics. But this constitutes a very challenging task.

Bibliography

[1] B. L. Altshuler, P. A. Lee, and R. A. Webb, *Mesoscopic Phenomena in Solid* (North-Holland, Amsterdam, 1991).

[2] C. W. J. Beenakker and H. van Houten, *Quantum Transport in Semiconductor Nanostructures*, in *Solid State Physics*, edited by H. Ehrenreich and D. Turnbull (Academic Press, 1991).

[3] *Single Charge Tunneling*, edited by H. Grabert and M.H. Devoret (Plenum, New York 1992).

[4] *Mesoscopic Quantum Physics*, edited by E. Akkermans, G. Montambaux, J.-L. Pichard, and J. Zinn-Justin (Elsevier, Amsterdam,1995).

[5] *Mesoscopic Electron Transport*, edited by L. L. Sohn, L. P. Kouwenhoven, G. Schön (Kluwer Academic, Dordrecht, 1997).

[6] D. Ferry, S. M. Goodnick, D. K. Ferry, *Transport in Nanostructures* (Cambridge U. P., Cambridge, 1997).

[7] Y. Imry, *Introduction to Mesoscopic Physics* (Oxford U. P., Oxford, 1997).

[8] S. Datta, *Electronic Transport in Mesoscopic Systems* (Cambridge U. P., Cambridge, 1995).

[9] B. D. Josephson, Phys. Lett. **1**, 251 (1962).

[10] G Bergmann, Phys. Scr. **T 14**, 99 (1986).

[11] K. von Klizing, G. Dorda, and M. Pepper, Phys. Rev. Lett. **45**, 494 (1980).

[12] S. A. Washburn and R. A. Webb, Advance Physics **35**, 375 (1986).

[13] B. J. van Wees, H. van Houten, C. W. J. Beenakker, J. G. Williamson, L. P. Kouwenhoven, D. van der Marel, C. T. Foxon, Phys. Rev. Lett. **60**, 848 (1988); D. A. Wharam, T. J. Thornton, R. Newbury, M. Pepper, H. Ahmed, J. E. F. Frost, D. G. Hasko, D. C. Peacock, D. A. Ritchie, G. A. C. Jones, J. Phys. C **21**, L209 (1988).

[14] For a review, see Z. Phys. B **85**, 317 (1991); H. van Houten, C. W. J. Beenakker, and A. A. M. Staring*Coulomb blockade oscillations in semiconductor nanostructures* in *Single Charge Tunneling*, edited by H. Grabert and M.H. Devoret (Plenum, New York 1992); *Single Electron Tunneling and Mesoscopic Devices* edited by H. Koch, and H. Lübbig (Springer, 1991).

[15] For a recent review, see L. P. Kouwenhoven, C. M. Marcus, P. L. McEuen, S. Tarucha, R. M. Westervelt, and N. S. Wingreen, Proceedings of the Advanced Study Institute on *Mesoscopic Electron Transport* edited by L. L. Sohn, L. P. Kouwenhoven, G. Schön (Kluwer Academic, Dordrecht, 1997); R. C. Ashoori, Nature **379**, 413 (1996).

[16] M. J. M. de Jong and C. W. J. Beenakker, in *Mesoscopic Electron Transport*, ed. by L. L. Sohn, L. P. Kouwenhoven, and G. Schön, NATO ASI Series E, Vol. 345 (Kluwer Academic Publishing, Dordrecht, 1997) and the references therein.

[17] Y.M. Blanter and M. Büttiker, Phys. Rep. **336**, 1 (2000).

[18] G. B. Lesovik and R. Loosen, Pis'ma Zh. Éksp. Teor. Fiz. **65**, 280 (1997) [JETP Lett. **65**, 295, (1997)].

[19] U. Gavish, Y. Levinson, and Y. Imry, Phys. Rev. B. **62**, 637 (2000).

[20] R. Aguado and L. P. Kouwenhoven, Phys. Rev. Lett. **84**, 1986 (2000).

[21] R. Deblock, E. Onac, L. Gurevich, and L. P. Kouwenhoven, Science **301**, 203 (2003).

[22] P.-M. Billangeon, F.Pierre, H. Bouchiat, and R. Deblock, Phys. Rev. Lett. **96**, 136804 (2006).

[23] E. Onac, F. Balestro, B. Trauzettel, C. F.J. Lodewijk, and L. Kouwenhoven, Phys. Rev. Lett. **96**, 026803 (2006).

[24] A. Stern, Y. Aharonov, and Y. Imry, Phys. Rev. A **41**, 3436 (1990).

[25] A. Yacoby, M. Heiblum, D. Mahalu, and Hadas Shtrikman, Phys. Rev. Lett. **74**, 4047 (1995).

[26] A. Yacoby, R. Schuster, and M. Heiblum, Phys. Rev. B **53**, 9583 (1996).

[27] R. Schuster, E. Buks, M. Heiblum, D. Mahalu, V. Umansky, and H. Shtrikman, Nature **385**, 417 (1997).

[28] Y. Levinson, Europhys. Lett. **39**, 299 (1997).

[29] I. L. Aleiner, Ned S. Wingreen, and Y. Meir, Phy. Rev. Lett. **79**, 3740 (1997).

[30] X. G. Wen, Phys. Rev. B **43**, 11025 (1991); Phys. Rev. Lett. **64**, 2206 (1990); Int. J. Mod. Phys. B **6**, 1711 (1992); Adv. Phys. **44**, 405 (1995).

[31] C. L. Kane and M. P. A. Fisher, Phys. Rev. Lett. **68**, 1220 (1992).

[32] C. L. Kane, M. P. A. Fisher, Phys. Rev. Lett. **72**, 724 (1994).

[33] C. de C. Chamon, D. E. Freed, and X. G. Wen, Phys. Rev. B **51**, 2363 (1995).

[34] For an introduction see Sh. Kogan, *Electronic noise and fluctuations in solids*, Cambridge University Press (1996).

[35] N. Weiner, Acta Mathematica **55**, 117 (1930); A. Khintchine, Math. Ann. **109**, 604 (1934).

[36] J. B. Johnson, Phys. Rev. B **29**, 367 (1927).

[37] H. Nyquist, Phys. Rev. **32**, 110 (1928).

[38] W. Schottky, Ann. Phys. (Leipzig) **57**, 541 (1918).

[39] J. H. Davies, P. Hyldgaard, S. Hershfield, and J. W. Wilkins, Phys. Rev. B **46**, 9620 (1992).

[40] L. Saminadayar, Y. Jin, B. Etienne, and D. C. Glattli, Phys. Rev. Lett. **79**, 2526 (1997).

[41] R. de Picciotto, M. Reznikov, M. Heiblum, V. Umansky, G. Bunin, and D. Mahalu, Nature **389**, 162 (1997).

[42] M. Reznikov, R. de-Picciotto, T.G. Griffiths, M. Heiblum and V. Umansky, Nature **399**, 238 (1999).

[43] M. J. M. de Jong and C. W. J. Beenakker, Phys. Rev. B **49**, 16070 (1994); P. Dieleman, H. G. Bukkems, T. M. Klapwijk, M. Schicke and K. H. Gundlach, Phys. Rev. Lett. **79**, 3486 (1997).

[44] S. Oberholzer, E. V. Sukhorukov, C. Strunk, C. Schönenberger, T. Heinzel, and M. Holland, Phys. Rev. Lett. **86**, 2114 (2001).

[45] M. Henny, S. Oberholzer, C. Strunk, and C. Schönenberger, Phys. Rev. B **59**, 2871 (1999).

[46] R. H. Brown and R. Q. Twiss, Nature **178**, 1046 (1956).

[47] E. Purcell, Nature **178**, 1449 (1956).

[48] L. Van Hove, Phys. Rev. **95**, 249 (1954).

[49] R. J. Schoelkopf, A. A. Clerk, S. M. Girvin, K. W. Lehnert, and M. H. Devoret, *Quantum noise*, chapter *Qubits as Spectrometers of Quantum Noise*, Kluwer Academic, Dordrecht (2003), cond-mat/0210247.

[50] M. Büttiker, Phys. Rev. Lett. **65**, 2901 (1990); Phys. Rev. B **46**, 12485 (1992).

[51] R. Landauer, Z. Phys. B **68**, 217 (1987); M. Büttiker, Y. Imry, R. Landauer, and S. Pinhas, Phys. Rev. B **31**, 6207 (1985).

[52] M. Büttiker, Phys. Rev. Lett. **57**, 1761 (1986); Phys. Rev. B **38**, 9375 (1988).

[53] R. Landauer and Th. Martin, Physica **B 175**, 167 (1991); **182**, 288 (1992).

[54] R. Landauer, Physica **D 38**, 226 (1987).

[55] Th. Martin and R. Landauer, Phys. Rev. B **45**, 1742 (1992); M. Büttiker, Phys. Rev. B **45**, 3807 (1992).

[56] H. B. Callen and T. A. Welton, Phys. Rev. **83**, 34 (1951).

[57] G. B. Lesovik, JETP Lett. **49**, 594 (1989).

[58] S. R. Eric Yang, Solid State Commun. **81**, 375 (1992).

[59] D. V. Averin and K. K. Likharev, J. Low Temp. Phys. **62**, 345 (1986); D. V. Averin and K. K. Likharev, chapter 6 in: *Mesoscopic Phenomena in Solids*, edited by B. L. Altshuler, P. A. Lee, and R. A. Webb (Elsevier, Amsterdam, 1991).

[60] G. Schön and A. D. Zaikin, Phys. Rep. **198**, 237 (1990).

[61] Yu. V. Nazarov, Pis'ma Zh. Eksp. Teor. Fiz. **49**, 105 (1989) [JEPT Lett. **49**, 126 (1989)].

[62] M. H. Devoret, D. Esteve, H. Grabert, G.-L. Ingold, H. Pothier, and C. Urbina, Phys. Rev. Lett. **64**, 1824 (1990).

[63] S. M. Girvin, L. I. Glazman, M. Jonson, D. R. Penn, and M. D. Stiles, Phys. Rev. Lett. **64**, 3183 (1990).

[64] G. L. Ingold and Yu. V. Nazarov, in *Single Charge Tunneling*, edited by H. Grabert and M.H. Devoret (Plenum, New York, 1992).

[65] A. A. Odintsov, Zh. Eksp. Teor. Fiz. **94**, 312 (1988) [Sov. Phys. JEPT **67**, 1265 (1988)].

[66] D. V. Averin and A. A. Odintsov, Phys. Lett. A **140**, 251 (1989).

[67] M. Reznikov, M. Heiblum, H. Shtrikman, and D. Mahalu, Phys. Rev. Lett. **75**, 3340 (1995).

[68] A. Kumar, L. Saminadayar, D. C. Glattli, Y. Jin, and B. Etienne, Phys. Rev. Lett. **76**, 2778 (1996).

[69] T. G. Griffiths, E. Comforti, M. Heiblum, A. Stern, and V. Umansky, Phys. Rev. Lett. **85**, 3918 (2000).

[70] A. H. Steinbach, J. M. Martinis, and M. H. Devoret, Phys. Rev. Lett. **76**, 3806 (1996).

[71] R. J. Schoelkopf, P. J. Burke, A. A. Kozhevnikov, D. E. Prober, and M. J. Rooks, Phys. Rev. Lett. **78**, 3370 (1997).

[72] R. J. Schoelkopf, A. A. Kozhevnikov, D. E. Prober, and M. J. Rooks, Phys. Rev. Lett. **80**, 2437 (1998).

[73] L. S. Levitov, and G. B. Lesovik, JETP Lett.,**58**, 230 (1993); D. A. Ivanov and L. S. Levitov, JETP Lett.,**58**, 461 (1993); L.S. Levitov, H. Lee and G. B. Lesovik, J. Math. Phys. **37**, 4845 (1996). For more reviews, see part three in *Quantum Noise in Mesoscopic Physics*, edited by Yu. V. Nazarov (Kluwer Academic, Dordrecht, 2002).

[74] S. Gustavsson, R. Leturcq, B. Simovic, R. Schleser, T. Ihn, P. Studerus, K. Ensslin, D. C. Driscoll, and A. C. Gossard, Phys. Rev. Lett. **96**, 076605 (2006).

[75] E. Onac, F. Balestro, L. H. Willems van Beveren, U. Hartmann, Y. V. Nazarov, and L. P. Kouwenhoven, Phys. Rev. Lett. **96**, 176601 (2006).

[76] A. F. Andreev, Sov. Phys. JETP **19**, 1228 (1964) [Zh. Eksp. Teor. Fiz. **46**, 1823 (1964)].

[77] D. M. Pepper, Sci. Am. **254** (1), 56 (1986).

[78] M. Octavio, M. Tinkham, G. E. Blonder, and T. M. Klapwijk, Phys. Rev. B **27**, 6739 (1983).

[79] G. E. Blonder, M. Tinkham, and T. M. Klapwijk, Phys. Rev. B **25**, 4515 (1982).

[80] N. N. Bogolubov, V. V. Tolmachev, and D. V. Shirkov, *A New Method in the Theory of Superconductivity*, (Consultant Bureau, New York, 1959).

[81] P.-G. De Gennes, *Superconductivity of Metals and Alloys* (Addison-Wesley, 1989).

[82] C. W. J. Beenakker, Phys. Rev. B **46**, 12841 (1992).

[83] Y. Takane and H. Ebisawa, J. Phys. Soc. Jpn. **60**, 3130 (1991); and, **61**, 1685 (1992).

[84] C. J. Lambert, J. Phys. Condens. Matter **3**, 6579 (1991).

[85] A. L. Shelankov, Fiz. Tverd. Tela **26**, 1615 (1984).

[86] A. V. Zaitsev, Zh. Eksp. Teor. Fiz. **78**, 221 (1980) [Sov. Phys. JETP **51**, 111 (1980)]; **79**, 2016(E) (1980) [**52**, 1018(E) (1980)]; **86**, 1742 (1984) [**59**, 1015 (1984)].

[87] T. Martin in *Proceedings of Les Houches Summer School, Session LXXXI*, edited by E. Akkermans, H. Bouchiat, S. Gueron, and G. Montambaux (Elsevier, New York, 2005).

[88] G. Falci, R. Fazio, A. Tagliacozzo, and G. Giaquinta, Europhys. Lett. **30**, 169 (1995).

[89] P. Devillard, R. Guyon, T. Martin, I. Safi, and B. K. Chakraverty, Phys. Rev. B **66**, 165413 (2002).

[90] P. Recher, E. V. Sukhorukov, and D. Loss, Phys. Rev. B **63**, 165314 (2001).

[91] G. B. Lesovik, T. Martin, and G. Blatter, Eur. Phys. J. B **24**, 287 (2001).

[92] P. Recher and D. Loss, Phys. Rev. Lett. **91**, 267003 (2003).

[93] I. Safi, P. Devillard, and T. Martin, Phys. Rev. Lett. **86**, 4628 (2001).

[94] N. M. Chtchelkatchev, G. Blatter, G. B. Lesovik, and T. Martin, Phys. Rev. B **66**, 161320(R) (2002).

[95] E. Dupont and K. Le Hur, Phys. Rev. B **73**, 045325 (2006).

[96] R. Fazio and R. Raimondi, Phys. Rev. Lett. **80**, 2913 (1998); Q. F. Sun, H. Guo, and T. H. Lin, Phys. Rev. Lett. **87**, 176601 (2001); A. A. Clerk, V. Ambegaokar, and S. Hershfield, Phys. Rev. B **61**, 3555 (2000); J. C. Cuevas, A. L. Yeyati, and A. Martín-Rodero, Phys. Rev. B **63**, 094515, (2001).

[97] M. R. Gräber, T. Nussbaumer, W. Belzig, T. Kontos, and C. Schönenberger, in *Quantum Information and Decoherence in Nanosystems*, Proceedings of the "Rencontres de Moriond", D. C. Glattli, M. Sanquer, and J. Tran Thanh Van editors, (Thé Gioi Publishers, Hanoi, Vietnam 2004); M.R. Gräber, T. Nussbaumer, W. Belzig, and C. Schönenberger, Nanotechnology **15**, 479 (2004).

[98] C. de C. Chamon, D. E. Freed, and X. G. Wen, Phys. Rev. B **53**, 4033 (1996).

[99] J. B. Ketterson and S. N. Song, *Superconductivity* (Cambridge University Press, Cambridge, England, 1999).

[100] K. v. Klitzing, G. Dorda, and M. Pepper, Phys. Rev. Lett. **45**, 494 (1980).

[101] D. C. Tsui, H. L. Stormer, and A. C. Gossard, Phys. Rev. Lett. **48**, 1559 (1982).

[102] R. B. Laughlin, Phys. Rev. Lett. **50**, 1395 (1983).

[103] J. K. Jain, Phys. Rev. Lett. **63**, 199 (1989).

[104] S. -S. Chern and J. Simons, Annals Math. **99**, 48 (1974).

[105] B. I. Halperin, Phys.Rev. B **25**, 2185 (1982).

[106] M. Stone, Ann. Phys. (N.Y.) **207**, 38 (1991).

[107] M. Büttiker, Phys. Rev. Lett. **57**, 1761 (1986).

[108] M. Büttiker, Phys. Rev. B **38**, 9375 (1988).

[109] X. G. Wen, Phys. Rev. B **41**, 12838 (1990).

[110] S. Tomonaga, Prog. Theor. Phys. **5**, 544 (1950).

[111] J. M. Luttinger, J. Math. Phys. **4**, 1154 (1963).

[112] A. A. Abrikosov, L. P. Gorkov, and I. E. Dzyaloshinski, *Quantum field theoretical methods in statistical physics*, (Permagon, 1965).

[113] J. Rammer and H. Smith, Rev. Mod. Phys. **58**, 323 (1986).

[114] L. V. Keldysh, Zh. Eksp. Teor. Fiz. **47**, 1515 (1964) [Sov. Phys. JETP**20**, 1018 (1965)].

[115] P. Fendley, A. W. W. Ludwig, and H. Saleur, Phys. Rev. Lett. **75**, 2196 (1995).

[116] E. Buks, R. Schuster, M. Heiblum, D. Mahalu, V. Umansky, and H. Shtrikman, Phys. Rev. Lett. **77**, 4664 (1996).

[117] A. L. Yeyati and M. Büttiker, Phys. Rev. B **52**, 14360 (1995).

[118] E. Buks, R. Schuster, M. Heiblum, D. Mahalu, and V. Umansky, Nature **391**, 871 (1998).

[119] Y. Levinson, Phys. Rev. B **61**, 4748 (2000).

[120] R. Guyon, T. Martin, and G. B. Lesovik, Phys. Rev. B **64**, 035315 (2001).

[121] R. Guyon and T. Martin (unpublished).

[122] P. Fendley and H. Saleur, Phys. Rev. B **54**, 10845 (1996).

[123] P. Fendley, A. W. W. Ludwig, and H. Saleur, Phys. Rev. B **52**, 8934 (1995).

[124] S. Ghoshal and A. B. Zamolodchikov, Int. J. Mod. Phys. A **9**, 3841 (1994).

[125] A. B. Zamolodchikov and Al. B. Zamolodchikov, Ann. Phys. (N.Y.) **120**, 253 (1979).

[126] P. Fendley, H. Saleur, and N. P. Warner, Nucl. Phys. **B430**, 577 (1994).

[127] C. L. Kane and M. P. Fisher, Phys. Rev. B **46**, 15233 (1992).

[128] *Handbook of Mathematical Functions*, edited by M. Abramowitz and I. A. Stegun (Dover, New York, 1972).

[129] D. Sprinzak, E. Buks, M. Heiblum, and H. Shtrikman, Phys. Rev. Lett. **84**, 5820 (2000).

[130] B. Trauzettel, I. Safi, F. Dolcini, and H. Grabert, Phys. Rev. Lett. **92**, 226405, (2004).

[131] T. T. Heikkilä, P. Virtanen, G. Johansson, and F. K. Wilhelm, Phys. Rev. Lett. **93**, 247005 (2004).

[132] W. D. Oliver, J. Kim, R. C. Liu, and Y. Yamamoto, Science **284**, 299 (1999); M. Henny, S. Oberholzer, C. Strunk, T. Heinzel, K. Ensslin, M. Holland, and C. Schönenberger, Science **284**, 296 (1999); H. Kiesel, A. Renz, and F. Hasselbach, Nature **218**, 393 (2002).

[133] M. Creux, A. Crépieux, and T. Martin, Phys. Rev. B **74**, 115323 (2006).

[134] N. M. Chtchelkatchev, G. Blatter, G. B. Lesovik and T. Martin, Phys. Rev. B **66**, 161320(R) (2002).

[135] A. V. Lebedev, A. Crepieux, and T. Martin, Phys. Rev. B **71**, 075416 (2005).

CURRICULUM VITAE

NGUYEN Thi Kim Thanh

• 03/8/1979: born in Haiphong, Vietnam.

• 9/1997-7/2001: Bachelor of Science in Physics (excellent, 1st ranked of University in Physics) at Hanoi University of Education, Vietnam, with the thesis entitled: *Charge ordering in the extended Hubbard model in magnetic field.*

• 08/2001-09/2004: Junior Researcher at the Institute of Physics and Electronics, Hanoi, Vietnam.

• 9/2002-9/2004: Master of Science in Theoretical Physics (excellent) at the Institute of Physics and Electronics, Vietnam, with the thesis entitled: *Charge ordering in the two dimension pyrochlore lattice.*

• 10/2004-9/2007: Ph. D. study in Theoretical Physics, "cotutelle" between the Centre de Physique Théorique, Marseille, France and the Institute of Physics and Electronics, Hanoi, Vietnam.
Supervisors: Prof. Thierry MARTIN (France) and Prof. NGUYEN Ai Viet (Vietnam).
Thesis Project: *Electronic transport through nano-objects.*

• 10/2007-10/2009: Postdoctoral in The Condensed Matter and Statistical Physics Section of ICTP (International Centre for Theoretical Physics), Trieste, Italy.

List of publications

1 - *Photo-assisted Andreev reflection as a probe of quantum noise*,
T. K. T. Nguyen, T. Jonckheere, A. Crépieux, A. V. Nguyen, and T. Martin,
Phys. Rev. B. **76**, 035421 (2007), cond-mat/0602408.

2 - *Quantum dot dephasing by fractional quantum Hall edge states*,
T. K. T. Nguyen, A. Crépieux, T. Jonckheere, A. V. Nguyen, Y. Levinson, and T. Martin,
Phys. Rev. B **74**, 153303 (2006), cond-mat/0606218.

3 - *Measuring noise and cross correlations at high frequencies in nanophysics*,
M. Creux, T. K. T. Nguyen, A. Crépieux, and T. Martin,
Proceedings of the Mesoscopic Superconductivity and Spintronics conference, H. Takayanagi and J. Nitta, editors, NTT Basic Research Laboratories, Atsugi, 2006 (World Scientific 2007).

4 - *Dephasing due to a fluctuating fractional quantum Hall edge current*,
T. K. T. Nguyen, A. Crépieux, T. Jonckheere, A. V. Nguyen, Y. Levinson, and T. Martin,
Proceedings of the 6th Rencontres du Vietnam (2006), arXiv: 0704.1443